Simulation and characterisation of a concentrated solar power plant

Dissertation submitted in partial fulfilment of the requirements for the degree *Magister Ingeneriae of Engineering* in Computer and Electronic Engineering at the Potchefstroom Campus of the North-West University

CJ Nel
21132976

Supervisor: Prof. G van Schoor
Co-supervisor: Dr. KR Uren

December 2014

Declaration

I, Coenraad Josephus Nel, hereby declare that the dissertation entitled "**Simulation and characterisation of a concentrated solar power plant**" is my own original work and has not already been submitted to any other university or institution for examination.

_____.

Coenraad Josephus Nel

Student number: 21132976

Signed on the 5th day of December 2014 at Potchefstroom.

Acknowledgements

First and foremost, I would like to thank my loving wife Anrie for all the love and support that she has bestowed upon me so that I could successfully close this chapter of my life. I would like to thank my study leaders, Prof. George van Schoor and Dr. Kenny Uren for pushing me when I needed a push, and for allowing me to grow into the person who I am today. I would then also like to extend my gratitude; to M-Tech industrial for providing me with Flownex® simulation software and the technical support associated with it as well as to my fellow students for always being willing to offer a helping hand.

Finally, I must express my profound gratitude to the NRF and THRIP for the financial support that they have given me[1].

[1] This work is based on the research supported in part by the National Research Foundation of South Africa (UID: 80020); The grant holder acknowledges that opinions, findings and conclusions or recommendations expressed in any publication generated by the NRF supported research are that of the authors, and that the NRF accepts no liability whatsoever in this regard.

Abstract

Concentrated solar power (CSP) is an efficient means of renewable energy that makes use of solar radiation to produce electricity instead of making use of conventional fossil fuel techniques such as burning coal. The aim of this study is the simulation and characterisation of a CSP plant in order to gain a better understanding of the dominant plant dynamics. Due to the nature of the study, the dissertation is divided into two main parts namely the simulation of a CSP plant model and the characterisation of the plant model.

Modelling the CSP plant takes the form of developing an accurate Flownex® model of a 40 MW combined cycle CSP plant. The model includes thermal energy storage as well as making use of a duct burner. The Flownex® model is based on an existing TRNSYS model of the same plant. The Flownex® model is verified and validated, by making use of a bottom-up approach, to ensure that the developed model is in fact correct.

The characterisation part of this dissertation involves evaluating the dynamic responses unique to that of a CSP plant as stated in the literature. This involves evaluating the dominant dynamic behaviour, the presence of resonant and anti-resonant modes found within the control bandwidth, and the change in the dynamics of the plant as the plants' operating points change throughout the day.

Once the developed model is validated, characterisation in the form of evaluating the open loop local linear models of the plant is implemented. In order to do so, these models are developed based on model identification processes, which include the use of system identification software such as Matlab® SID Toolbox®.

The dominant dynamic behaviour of the plant model, obtained from the developed local linear models, represents that of an over damped second order system that changes as the operating points of the plant change; with the models' time responses and the bandwidth decreasing and increasing respectively as the thermal energy inputs to the plant increases. The frequency response of the developed local linear models also illustrates the presence of resonant and anti-resonant modes found within the control bandwidth of the solar collector field's temperature response. These modes however are not found to be present in the mechanical power output response of the plant.

The use of adaptive control, such as feedforward and gain-scheduled controllers, for the plant should be developed to compensate for the dynamic behaviours associated with that of a CSP plant.

Keywords: CSP, mathematical modelling, local linear models, system identification, resonant, anti-resonant, characterisation.

Contents

List of Figures

List of Tables

Nomenclature

Subscripts

min	Minimum value
max	Maximum value
HCE	Heat collecting element
CG	Combustion gasses
p	Proportional
I	Integral
u	Ultimate
GT1	Gas turbine 1
GT2	Gas turbine 2
TESin	Fluid entering TES
TESout	Fluid exiting TES
amb	Ambience
abs	Absolute value
f	Fluid
g	gas
s	Specific
b	Evaporator exit value

Symbols

Symbol	Unit	Description/Quantity
θ	rad	Radiation incident angle
δ	rad	Declination angle
ha	rad	Hour angle
θ_z	rad	Zenith angle
Ω	Hz	Bandwidth
ω	Hz	Frequency
$\dot{Q}$	kJ/s	Total heat/energy transfer rate
η	-	Efficiency
T	℃	Temperature

Symbols

c_p	kJ/kg.K	Specific heat
$\dot{m}$	kg/s	Mass flow rate
ΔT	℃	Temperature difference
k	-	Gain
t	sec	Time
P	W	Power
W	kJ/kg	Total work done
h	kJ/kg	Fluid enthalpy
pr	-	Pressure ratio
Υ	-	Specific heat ratio
p	bar	Pressure
ρ	$\mathrm{kg/m^3}$	Fluid density
V	$\mathrm{m^3}$	Tank volume
R	$\mathrm{Jkg^{-1}K^{-1}}$	Specific gas constant
x	-	Fluid to gas ratio
s	kJ	Fluid entropy
C	J/K	Heat capacitance
N	rpm	Speed
Q	$\mathrm{m^3/s}$	Volumetric flow rate
H	m	Head value
g	$\mathrm{m/s^2}$	Gravitational acceleration
w	m	Width

Abbreviations

CFD	Computational Fluid Dynamics
CSP	Concentrated Solar Power
DNI	Direct Normal Irradiance
HCE	Heat Collecting Element
HLoss	Heat Losses
HTF	Heat Transfer Fluid
IAM	Incident Angle Modifier

Abbreviations

NTU	Number of Transfer Units
OS	Operating Scenario
PI	Proportional Integral
PI	Proportional Integral
PRBS	Pseudo Random Binary Sequence
RHLoss	Receiver Heat Losses
RS	Row Shadowing
SAM	Solar Advisor Model
SCF	Solar Collector Field
SEGS	Solar Electric Generating System
SFA	Solar Field Aperture
SID	System Identification
TES	Thermal Energy Storage
TRNSYS	Transient Simulations

Chapter 1: Introduction

Chapter 1 outlines the proposed research problem with its associated objectives and the appropriate methodology that will be followed in order to complete the objectives of the study. Finally a chapter layout of the study will be given.

1.1 Background

Renewable energy by definition is an inexhaustible source of energy that originates from on-going natural processes. These natural resources include wind-, solar radiation-, hydro- and biogas energy, which form the various renewable energy sources [1]. Numerous questions have been raised about renewable energy. The most frequently asked question is whether renewable energy is the answer to global warming and the declining fossil fuel levels especially in South Africa [2].

According to Science Daily [3], the use of fossil fuels (oil, coal, and natural gasses) in the generation of electricity, has caused carbon dioxide (CO_2) emission levels to increase by 29 % from the year 2000 up to the year 2008 and it is still increasing by the day. The available amount of fossil fuels in the world is not precisely known, but experts predict that the fossil fuel reserves will reach critical levels in the near future. The use of renewable energy can help to both reduce the carbon footprint as well as the use of fossil fuels [3].

Eskom provides approximately 95 % of South Africa's electricity and since it is difficult to store large quantities of energy, it is mostly generated on demand. This demand for electricity grows each year due to the rapid growth of the economy. Due to this growth, Eskom is forced to start looking at alternative methods to keep up with the growing demand without increasing the usage of conventional fossil fuels. Eskom considers concentrated solar power (CSP) as key to the future energy mix in South Africa. In order to explore the viability of CSP, a pilot plant is planned in the Northern Cape.

This renewable energy plan is already in motion. According to Eskom's fact sheet, the construction of the CSP plant will start in 2016 [4].

Concentrated solar power is an efficient renewable energy source that makes use of solar radiation to produce electricity instead of making use of conventional fossil fuel techniques such as burning coal. CSP is highly effective due to its availability (solar radiation), and its adaptability (conventional fossil fuel plants can be integrated with CSP technologies) [5].

Figure 1.1 shows a schematic representation of a typical Rankine cycle CSP plant. With the addition of the source of thermal energy (solar) to the cycle being different, the Rankine cycle CSP plant resembles that of a conventional coal-fired power plant. The energy source is used to generate power during the day and at night by using stored thermal energy [5].

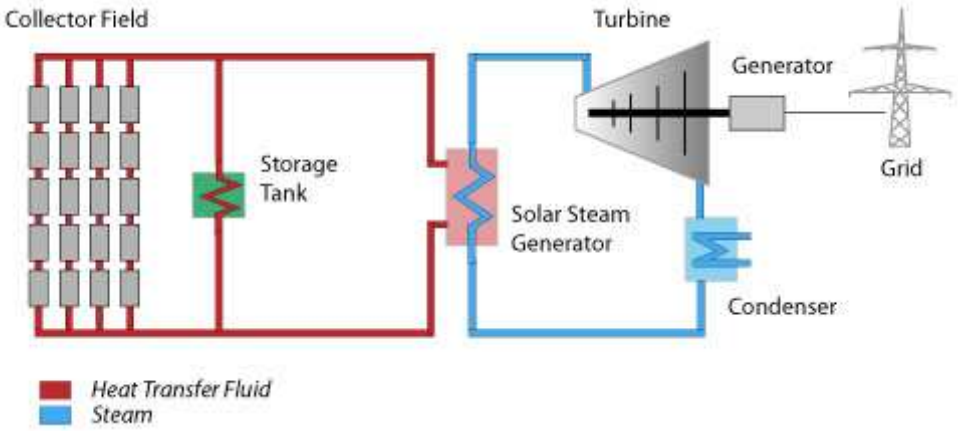

Figure 1.1: Basic schematic diagram of a Rankine cycle CSP plant [6]

1.2 Problem statement

This study addresses the need to develop a complete and accurate model of a concentrated solar power plant, with the intent of obtaining a deeper understanding of the dynamic responses characteristic to that of a CSP plant by performing simulations. The insight gained from the study will be used to gain knowledge on some of the design considerations for a controller for such a plant.

1.3 Research objectives

The research problem can be divided into three main objectives that need to be addressed.

CSP plant model development

A methodology is required to develop a simulation model of a CSP plant that produces the correct steady state as well as the dynamic responses of the plant. Parallel to the process of developing a model of the plant, a verification methodology is required as to ensure that the model behaves similarly to an actual CSP plant.

CSP plant model validation

Determining whether the model is accurate and correct, requires a method of validating the model.

Dynamic characterisation

The process of obtaining insights into the dynamic responses characteristic to that of a CSP plant, in order to give inputs into some of the design considerations of a controller for the plant, requires a methodology for identifying and evaluating these responses.

1.4 Research methodology

The objectives mentioned form an important part in the simulation and characterisation of such a plant, which would lead to insight gained regarding the influence of the CSP components' responses with respect to the dynamic responses of the system. The methodology of solving each of the above-mentioned objectives will now be discussed.

CSP plant model development

The development of a CSP plant simulation model can be implemented by following the steps shown in Figure 1.2.

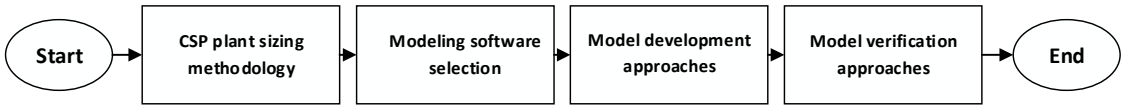

Figure 1.2: Model development

In order to develop a model of a CSP plant it is necessary to obtain an understanding of the structure and operation of such a plant. This is done by investigating existing CSP plant configurations to decide which configuration suits the study best. After the configuration is selected, the modelling software will be identified. In order do so the type of model and the physical domains involved must be determined. Once the modelling software has been selected, a component sizing methodology must be studied to specify the calculated parameters of the plant.

CSP plant model validation

Ensuring that the developed model is correct, all the different validation procedures available in the development of a simulation model must be studied to select the appropriate validation methodology that will be best suited for this study.

Dynamic characterisation

The characterisation process in order to obtain and evaluate the dynamic responses of the plant can be implemented by evaluating the local linear models of the plant. In order to do so the following steps shown in Figure 1.3 is implemented.

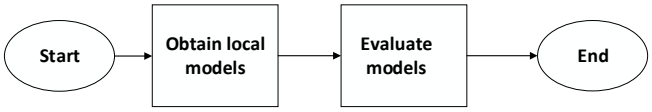

Figure 1.3: Characterisation process

Once the dynamic responses unique to that of a CSP plant are identified, the local linear models of the developed model can be obtained. In order to do so a methodology of obtaining each of the required local linear models, as done in the industry, needs to be identified. A methodology of evaluating these local models also needs to be identified in order to extract the information required to comment on the responses unique to that of a CSP plant.

1.5 Dissertation overview

The literature overview chapter (Chapter 2) firstly gives an overview of how solar energy is collected and stored. Thereafter an overview will be given on the different CSP power plant configurations. In order to obtain an understanding of what the dynamic responses of a CSP plant's components should resemble, when developing the model, some of the main components of the plant's dynamic responses will be discussed. After this is done the model development and the characterisation process will be discussed. Finally, a critical evaluation of all the literature studied in the chapter will be discussed. Here some form of decision-making will take place in terms of evaluating which technology will best suit this research problem.

The Brayton cycle model development chapter (Chapter 3) gives the processes followed to select and size each of the components of the Brayton cycle part of the combined cycle CSP plant. This includes the literature required to calculate the parametric values of each component used in the software. After the calculated parametric values have been substituted into each component, the component is simulated to determine whether the desired response is obtained serving the purpose of verification.

The Rankine cycle model development chapter (Chapter 4) gives the processes followed to select and size each of the components of the Rankine cycle part of the combined cycle CSP plant. This includes the same processes as described in the Brayton cycle model development chapter.

In the model integration chapter (Chapter 5) all the designed components of both the Brayton and Rankine cycle are integrated to form the complete combined cycle CSP plant. Once all the components are integrated, validation will take place in the form of a series of simulations where the developed model of the CSP plant is compared to a benchmark model, which will determine if the model is correct.

The characterisation chapter (Chapter 6) will discuss the dynamic responses, unique to a CSP plant, by evaluating the dynamic responses of the entire plant at each of the various operating points of the plant.

Chapter 2: Literature overview

The characterisation of a concentrated solar power (CSP) plant can be used to gain insight into some of the plant's dynamic responses through the use of a validated model. This chapter presents the process of developing and characterising a simulation model of a CSP plant with some theoretical background on the generation of electricity through the use of CSP. This chapter will be concluded with important modelling and characterisation decisions.

2.1 Concentrated solar power

Concentrated solar power (CSP) first came into existence around 200 BC when Archimedes made use of panels of mirrors to concentrate the sun's rays on the invading Roman fleet, in order to drive them back. In 1913, the first CSP station came into existence when Frank Schuman made use of parabolic troughs to power a 60-70 hp pump, which pumped water from the Nile River to cotton fields [7].

It was since the 1980's that CSP started booming, when California constructed nine CSP plants known as Solar Electric Generating Systems (SEGS), which totalled up to 354 MW, and made use of steam turbines to generate its power. From 2005 the growth in CSP plant construction is estimated at 40 % per year [7].

The technology used to concentrate solar energy and to convert it into electricity has remained the same, with some changes made to the configurations of the plants. To understand the process of generating electricity through the use of CSP, the process of concentrating solar radiation needs to be discussed first.

2.1.1 Solar energy collection

The process of collecting solar energy for the generation of electricity is illustrated in Figure 2.1. Solar rays of the sun are focussed on a receiver or a Heat Collecting Element (HCE) by means of mirrors angled towards the receiver. The focussed solar rays then heats up some type of Heat Transfer Fluid (HTF) flowing through the HCE. The heated HTF is then used either to drive a turbine or to heat up another fluid [8]. The combination of the mirrors and the HCE form the Solar Collector Field (SCF).

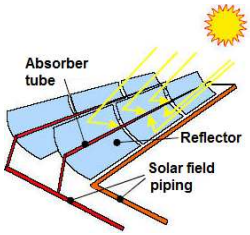

Figure 2.1: Solar Collector Field [2]

There are currently four different topologies of a SCF: Fresnel trough, dish/engine, solar tower and parabolic trough topology [2].

The energy balance of a HCE consists of energy being absorbed and radiated. Depending on the time of year, the magnitude of change in temperature of the HTF, from entering to exiting the HCE, varies. The temperature of the HTF exiting the HCE is not only a function of time, but also of the following: Direct Normal Irradiance, Radiation incident angle (θ), Declination angle (δ), Hour angle (ha), Zenith angle (θ_z), Incidence angle modifier (IAM), Row shadowing (RS), End losses (EL) and SCF efficiency [9].

The thermal energy gained from the SCF heating up the HTF can be used to generate electricity, as well as to store a portion of the thermal energy, which has advantages of its own. The next section will discuss the concept of storing thermal energy and the advantages associated with it.

2.1.2 Solar energy storage

The storage of solar energy takes the form of making use of Thermal Energy Storage (TES) tanks, where the solar energy is converted into thermal energy. The storage of thermal energy proves to have advantages that increase the effectiveness of CSP plants. Before discussing the advantages of thermal energy storage, the process of storing thermal energy will briefly be discussed. Two main concepts used to store thermal energy will now be discussed:

2.1.2.1 Passive heat storage

In passive heat storage, thermal energy is stored by making use of a fixed storage medium, normally bedrock or concrete, with the HTF flowing over it to transfer its thermal energy. The

charge/discharge process of the TES involves the hot/cold HTF flowing over the storage medium transferring its thermal energy to/from the medium through convection [10].

2.1.2.2 Active heat storage

Active heat storage can further be divided into two separate concepts including: direct active and indirect active heat storage.

Direct active heat storage: In this concept the HTF serves as the storage medium. The charge process of direct active TES involves the HTF inside the tank mixing with the hot HTF flowing into the tank, which results in an increase in the average temperature of the HTF inside the tank [10].

Indirect active heat storage: With indirect TES, the storage medium, which is also a fluid, is separated from the HTF through the use of a heat exchanger. The charge process of indirect active TES involves circulating both the hot HTF on the primary side and the cold storage medium through the secondary side of the heat exchanger, which results in the energy transferred from the HTF to the storage medium [10].

2.1.2.3 TES connection configuration

Depending on the configuration that the TES tank is connected to the SCF, series or parallel, the advantages of making use of TES differ.

Series connection: Connecting the TES in series with the SCF, as seen in Figure 2.2(a), has the advantage of damping fluctuations in the output temperature of the SCF which allows for a stable power generation. The fluctuations, caused by a number of factors including clouds moving past and reflective mirrors not functioning properly, can be seen in the yellow highlighted area of Figure 2.2(b). The use of TES to damp these fluctuations results in a temperature profile with some delay as seen in the “energy in storage” line of Figure 2.2(b) [11].

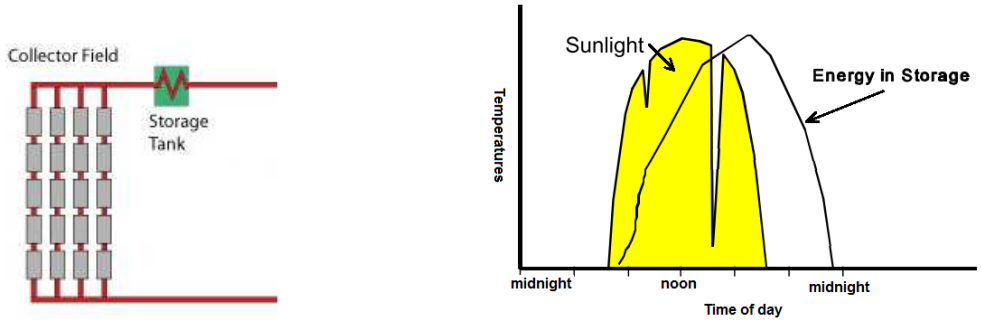

a) Series TES connection **b) Effect of series connection**

Figure 2.2: TES connected in series with the SCF [11]

Parallel connection: The parallel connection of TES, as seen in Figure 2.3, has the advantage of allowing the selection between the sources of thermal energy to the plant (SCF or TES). This is primarily implemented by controlling the flow of the HTF flowing through both the TES as well of

the SCF. The parallel connection also allows for the manipulation of the amount of energy transferred to both the TES as well as to the rest of the plant during the day by changing the ratio of the HTF flowing through the TES to the HTF flowing through to the rest of the plant [12].

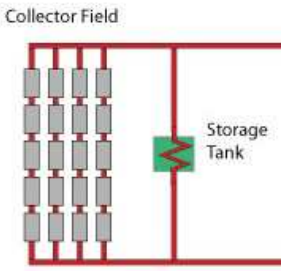

Figure 2.3: Parallel TES connection

2.2 Concentrated solar power plant configurations

Now that the process of both collecting and storing solar energy is discussed, the conversion of solar energy to electricity can be explained. The generation of electricity using solar energy, utilises the same three power generation cycle configurations used in normal coal-fired plants, with the exception of a few modifications made to their source of thermal energy and the use of TES.

A CSP plant can be configured using the Rankine cycle, the Brayton cycle or a hybrid of the two. Each one of these configurations proves to have its own unique advantages and disadvantages. The operation of the three configurations, together with its respective advantages and disadvantages are discussed next.

2.2.1 Rankine cycle CSP plant configuration

A Rankine cycle configured CSP plant, as seen in Figure 2.4(a), can be explained by discussing the Rankine cycle itself and the function of each component in the cycle, by making use of the ideal temperature vs. entropy curve of the Rankine cycle as seen in Figure 2.4(b).

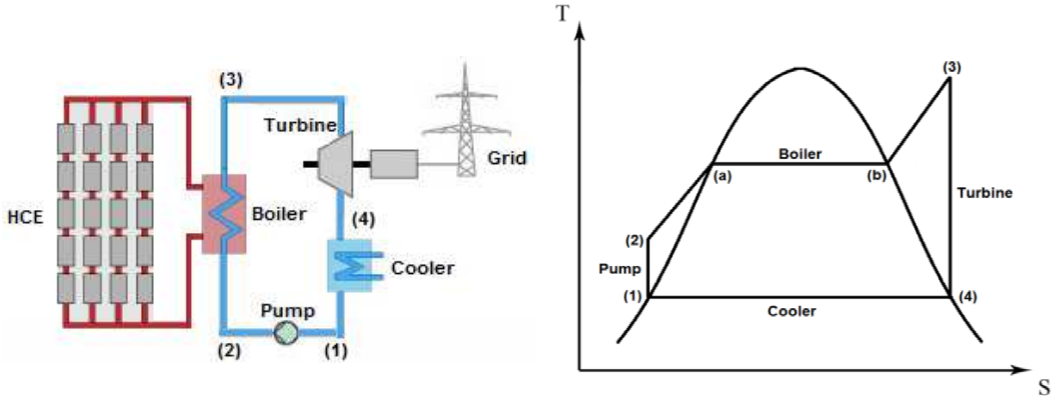

a) Simple Rankine cycle CSP plant **b) Ideal temperature vs. entropy curve**

Figure 2.4: The simple ideal Rankine cycle [13]

The operation of the Rankine cycle CSP plant is discussed by dividing the plant into its five main components namely the water pump, boiler, SCF, steam turbine, and the cooler; with a brief discussion on the function of each of these components in the cycle.

2.2.1.1 The water pump

The water pump of the Rankine cycle has the function of both circulating the water through the cycle as well as to increase the pressure and temperature of the water entering the boiler without changing the phase of the water. The increase in the temperature of the water can be seen in Figure 2.4(b) between points (1) and (2).

2.2.1.2 The boiler

The boiler of the Rankine cycle is responsible for changing the phase of the saturated water flowing through the cycle into superheated steam. Heating is generally done by making use of three heat exchangers connected in series, each with its own function [13].

The first heat exchanger, known as the economiser, has the purpose of heating up the water flowing through it without changing the phase of the water. This process can be seen in Figure 2.4(b) between points (2) and (a). The water is heated up to its maximum temperature before changing its phase [13].

The next heat exchanger, known as the evaporator, changes the phase of the water flowing through it from water to steam. This can be seen in Figure 2.4(b) between points (a) and (b). As the water, at point (a), flows through the evaporator it changes its phase to steam as it approaches point (b), whilst maintaining a constant temperature [13].

The third heat exchanger is the super-heater. It has the function of increasing the temperature of the steam flowing out of the evaporator up to such a value that the steam is considered to be "dry". Making use of “dry” steam to rotate the turbines has the advantage of both increasing the efficiency of the cycle as well as reducing the risk of fluid build-up on its blades, which causes problems such as rust [13].

2.2.1.3 The Solar Collector Field (SCF)

The primary side of the boiler forms the source of thermal energy to the Rankine cycle. Conventionally, in a coal-fired power plant, this source of thermal energy would be provided by a combustion chamber with coal particles burned and its thermal energy transferred to the water of the Rankine cycle through the boiler.

In the case of a Rankine cycle CSP plant the combustion chamber is replaced with the SCF with the heated HTF circulating through both the SCF and the boiler which in turn transfers the induced thermal energy from the SCF to the water circulating through the Rankine cycle.

2.2.1.4 The steam turbines

The turbines of the Rankine cycle have the purpose of converting the thermal energy of the superheated steam entering the turbine into rotational (mechanical) energy, which rotates the shaft connected to a generator [13]. This process results in a decrease in the pressure and temperature of the steam, without changing phase, which is due to the energy reduction of the steam. This can be seen in Figure 2.4(b) between points (3) and (4). At point (4) in Figure 2.4(b), any further decrease in pressure in the steam would result in turbine damage due to fluid build-up.

The efficiency of the cycle is increased by directly connecting the high-pressure turbine to an intermediate-pressure turbine and a low-pressure turbine. This ensures maximum energy transfer from the steam to the turbines [14].

2.2.1.5 The cooler

The cooler of the Rankine cycle converts the steam exiting the low-pressure turbine back to saturated water by transferring the remaining energy of the steam to another fluid by means of a condenser. The process can be seen in Figure 2.4(b) between points (4) and (1) where the steam entering the cooler, at point (4), changes phase, with the gas to fluid ratio decreasing as it moves towards point (1) where only fluid is present in the mixture [13].

The condenser of the cooler has a fluid flowing through its secondary side, which extracts thermal energy from the steam flowing through the primary side of the condenser. In order to cool down the cooling fluid flowing in the secondary side of the condenser, a cooling tower is used. The cooling tower has the function of transferring thermal energy from the cooling water to the air at ambient temperature [15].

2.2.2 Brayton cycle CSP plant configuration

The operation of a Brayton cycle configured CSP plant, as seen in Figure 2.5(a), is discussed by making use of both its ideal temperature vs. entropy curves, as seen in Figure 2.5(b), and the components constituting that of a Brayton cycle CSP plant.

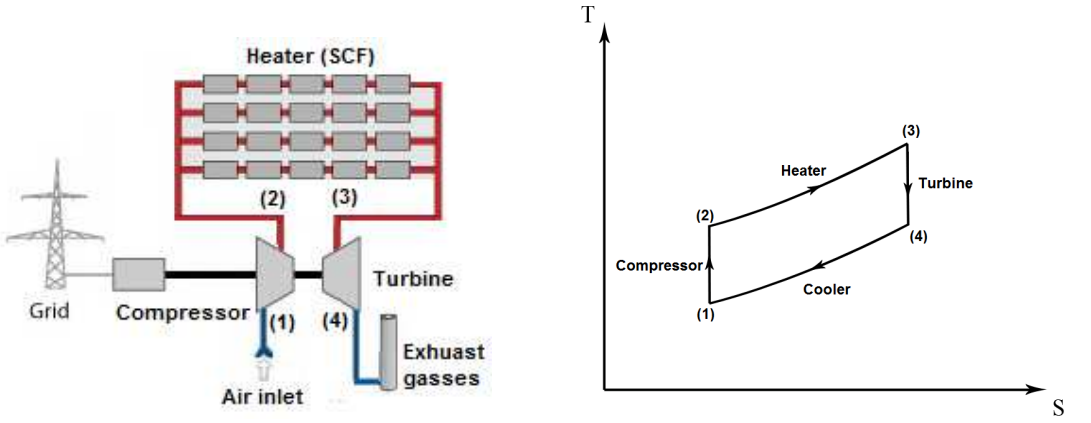

a) **Components of the Brayton cycle**

b) **Brayton cycles' temperature vs. entropy curve**

Figure 2.5: The simple ideal Brayton cycle [13]

The operation of the Brayton cycle CSP plant is discussed by dividing the plant into its four main components namely a compressor, heater, gas turbine, and a cooler; with a brief discussion on the function of each of these components in the cycle.

2.2.2.1 The compressor

The compressor of the Brayton cycle pressurises air, at ambient temperature, entering the compressor. This pressure increase results in a slight increase in the temperature of the air as seen in Figure 2.5(b) between points (1) and (2) [13].

2.2.2.2 The heater

The pressurised air exiting the compressor is then heated to an even higher temperature, as seen in Figure 2.5(b) between points (2) and (3), by making use of the heater. In a conventional coal-fired plant, the air is heated by making use of a combustion chamber where the energy from the burning coal is transferred to the air flowing through the chamber [16].

Heating in a Brayton cycle configured CSP plant on the other hand makes use of the HCEs of the SCF to raise the temperature of the air exiting the compressor by letting the compressed air flow through the HCEs, instead of making use of a combustion chamber. The air exiting the SCF is then heated to a temperature dependent on the amount of thermal energy transferred from the concentrated solar radiation to the compressed air [17].

2.2.2.3 The gas turbine

The gas turbine is responsible for producing the necessary mechanical work to drive both the compressor and the generator. The heated, compressed air exiting the heater then expands upon entering the gas turbine, transferring its thermal energy into mechanical energy, rotating the turbine shaft. The air then exits the gas turbine at a lower pressure and temperature due to the energy

transfer from the air to the turbine. This process can be seen in Figure 2.5(b) between points (3) and (4) [18].

2.2.2.4 The cooler

The cooler of the Brayton cycle has the function of cooling down the exhaust air exiting the gas turbine, which can be seen in Figure 2.5(b) between points (4) and (1). The methodology used to cool down the exhaust air depends on whether it is a closed or open cycle configured Brayton cycle. In an open cycle configuration, such as the one in Figure 2.5, the exhaust air is cooled by the atmosphere, whereas in a closed cycle, cooling is implemented by making use of a heat exchanger transferring thermal energy to another working fluid [19].

2.2.3 Combined cycle CSP plant configuration

The operation of a combined cycle configured CSP plant, as seen in Figure 2.6, forms a combination of the operation of both the Rankine and the Brayton cycle, which together forms a plant that combines the advantages of both cycles, and helps solve some of the shortcomings associated with each of these cycles.

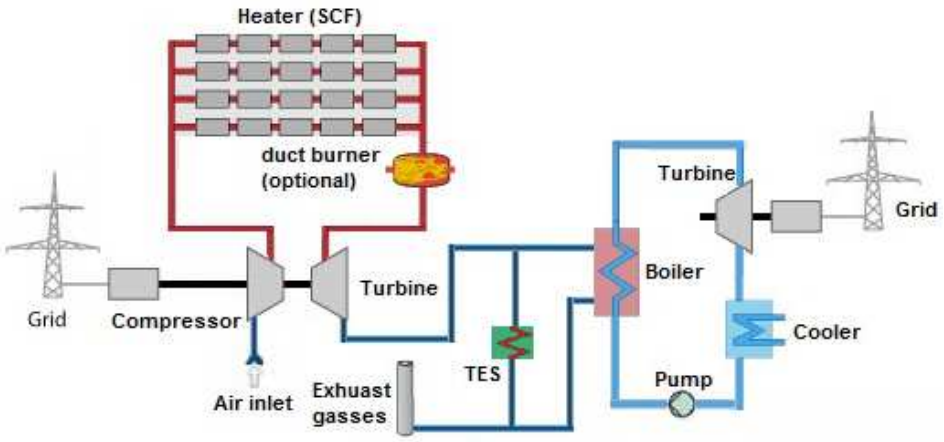

Figure 2.6: Basic schematic diagram of a combined cycle CSP plant [13]

The operation of the combined cycle CSP plant can be discussed by dividing the plant into two separate Operating Scenarios (OS) under which the plant functions. These operating scenarios include the operation of the plant during the day and at night. In both of these operating scenarios the configuration of the plant varies slightly. The configuration and working of the plant at each OS will now be discussed. Important to note is the additional use of a duct burner. Although it is not one of the essential components of the plant, it does however play an important role in the system itself.

2.2.3.1 Operating scenario 1 (daytime)

The sun supplies thermal energy to the plant through the SCF. Placed in series with the SCF is a duct burner, which has the function of providing additional thermal energy to the plant by injecting combustion gasses (burnt methane and oxygen mixture) into the system.

The additional thermal energy from the burner is introduced to optimise the operation of the plant by increasing the temperature of the air exiting the SCF. This is due to the fact that the Brayton cycle can function at temperatures that exceed those produced by the SCF. Since the energy produced by the SCF changes arbitrary due to external disturbances, the duct burner also serves the purpose of maintaining a constant power output by manipulating the amount of energy of the air entering the gas turbines.

The mixed gases (HTF mixed with combustion gasses) exiting the burner then enters the gas turbine which rotates the generator and the compressor as discussed in the Brayton cycle configured CSP plant. The exhaust gasses exiting the gas turbine is then divided between the parallel connection of both the boiler of the Rankine cycle and the TES tank with the ratio determined by the demand.

During this operating scenario the TES tank charges at a rate depending on the ratio of the mixed gasses divided between the TES and the boiler, which also supplies thermal energy to the Rankine cycle side of the plant.

2.2.3.2 Operating scenario 2 (night-time)

During operating scenario 2 the configuration of the plant changes slightly since the source of thermal energy from the SCF is unavailable, which results in the isolation of the SCF from the rest of the plant. This results in the further isolation of the rest of the components of the Brayton cycle, with exception of the parallel connection of the boiler as well as the TES. The configuration of the plant at operating scenario 2 is shown in Figure 2.7.

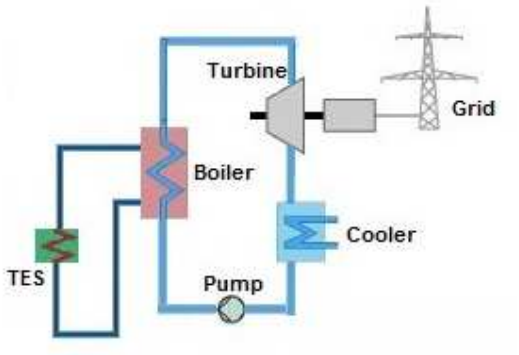

Figure 2.7: Combined cycle CSP plant configuration at OS 2

As seen in Figure 2.7, the TES tank forms the source of thermal energy to the rest of the plant with its gasses circulating through the boiler, which transfers thermal energy from the gasses to the water. This process results in the TES to discharge.

The combination of the two cycles provides more than just an increase in the overall efficiency of the plant. It also has the following benefits:

One major benefit of combining the two cycles includes the temperature limitations under which the two cycles can function. This is especially important in CSP plants since some of the solar collector technologies can produce working fluid temperatures of up to $1200\,℃$ such as the power tower technologies [2]. The Brayton cycle has no problem with functioning under temperatures such as that of the power tower since it can function at temperatures of up to $1500\,℃$. The Rankine cycle on the other hand has a much lower limit on its maximum operating temperatures, ranging between $500\,℃$ and $600\,℃$. Using the combined cycle eliminates this problem. This is since the output temperature of the gas turbine can easily be lowered to temperatures suitable for the Rankine cycle [20].

It is important to note that the duct burner is only used for supplementary and control purposes and that the SCF remains the main source of thermal energy to the plant.

With the process of generating electricity using solar energy explained above, the process of creating a simulation model of a CSP plant, so as to implement simulations for characterisation purposes, will be discussed. Before doing so, let us first consider some of the dynamic responses characteristic to that of a CSP plant and the importance of developing a transient model of the plant.

2.3 Concentrated solar power plant dynamics

The characterisation of any model requires a model to be developed which reflects all of the most important dynamics of that system. Evaluating the dynamic responses of each of the major components of the CSP plant can aid in obtaining a better understanding as to how the system should respond when altering some of its input signals. In the next section some of the major dynamic responses that will be used to aid in developing a model of the plant will be discussed:

2.3.1 Dynamic responses of power stations

It is a known phenomenon that the responses of components are not linear due to the physical nature of the components. This means that a sudden increase or decrease in the input signals to a component results in some type of delay before the response of the component settles around a static value. In power stations, the same type of dynamic responses can be expected from its components. These dynamic responses are due to a number of factors including the structure of

the components and the configuration that the components of the plant are connected in. These factors, including others, cause a delay in the response of the plant's components [21].

Two of the main factors influencing the dynamic responses of the components of a power plant include both the temperature and the mass flow rate of the fluid flowing through the components. Since it is not always easy to alter the temperature of the fluid entering a component, the mass flow rate of the fluid is usually altered [21].

Let us discuss the dynamic responses which should be reflected by the developed model of the SCF, TES, Brayton cycle and the Rankine cycle by investigating the influence the mass flow rate of the fluid has on its dynamic responses starting with the SCF.

2.3.1.1 Solar collector field dynamic behaviour

One of the main responses measured from a typical SCF is its temperature response. To simulate the dynamic behaviour of a SCF, the mass flow rate of the HTF flowing through it is altered. Figure 2.8 gives a typical temperature response of a SCF with a step response of the mass flow rate of the fluid flowing through the component simulated [22].

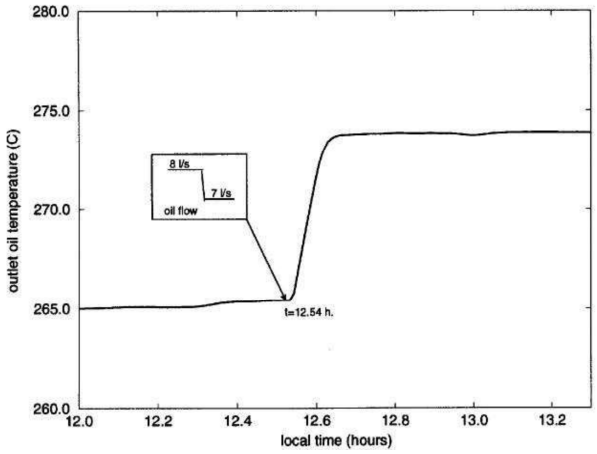

Figure 2.8: Solar collector field dynamic response [22]

From Figure 2.8 it can be seen that the response of a SCF can be modelled as an over damped second order system model with a negative gain, since an increase in the mass flow rate of the HTF flowing through the SCF would result in a decrease in the temperature of the HTF exiting the SCF. To improve the response of the cycle, a controller can be used to control the mass flow rate of the HTF.

2.3.1.2 Thermal energy storage dynamic behaviour

One of the main responses measured from a TES tank is its temperature response, more specifically, the rate at which it is charged. This rate is defined as the change in the average temperature of the fluid inside the tank over a period of time. To simulate the dynamic behaviour of

a TES tank, the temperature of the fluid inside the tank is simulated with a step response of the mass flow rate of the HTF flowing through the tank. This can be seen in Figure 2.9 where a passive heat storage system with a HTF flowing over pebbles, which in turn melt the pebbles' content at a certain temperature, is simulated [23].

The measurements taken from the simulation includes the duration it takes for the content of the pebbles to start melting. The TES is fully charged when the fluid inside the tank is fully melted. This represents the idea of a TES tank charging (melting of the content of the pebbles) and discharging (content of the pebbles returning to its solid state).

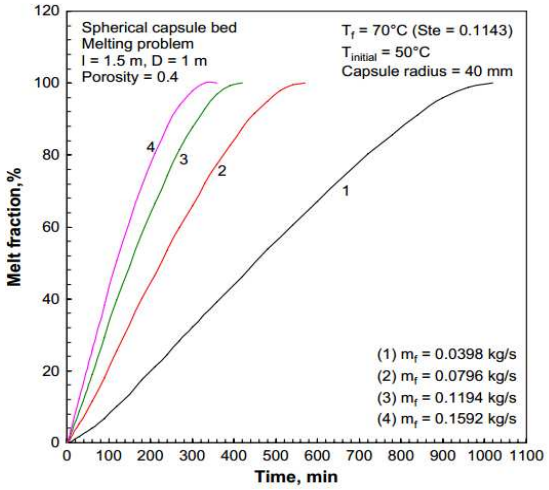

Figure 2.9: TES dynamic response [23]

From Figure 2.9 it can be seen that the response of a TES can also be modelled as an over damped second order system. To improve the response of the cycle, a controller can be used which alters the mass flow rate of the HTF.

2.3.1.3 Brayton cycle dynamic behaviour

The main measured response of the Brayton cycle includes the power output of the gas turbine and compressor combination. To simulate the dynamic behaviour of the Brayton cycle, the mass flow rate of the fluid flowing through the turbines is altered by changing the position of the air control valve. Figure 2.10 gives a typical open loop mechanical power output response of the Brayton cycle with a step response simulated of the mass flow rate of the fluid flowing through the cycle.

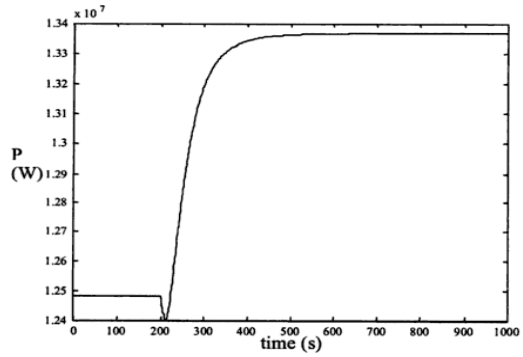

Figure 2.10: Brayton cycle power output step response [21]

From Figure 2.10 it is noted that the power output response of the Brayton cycle generates non-minimum phase behaviour with a step response in the mass flow rate of the air flowing through the cycle. To improve the response of the cycle, a controller can be used to alter the mass flow rate of the fluid.

2.3.1.4 Rankine cycle dynamic behaviour

The main measured response of the Rankine cycle includes the power output of the steam turbines. To simulate the dynamic behaviour of the Rankine cycle, the mass flow rate of the fluid flowing through it is altered by changing the speed at which the boiler feed pump rotates. Figure 2.11 illustrates a typical open loop mechanical power output response of the Rankine cycle with a step response of the mass flow rate, of the fluid flowing through the cycle, simulated.

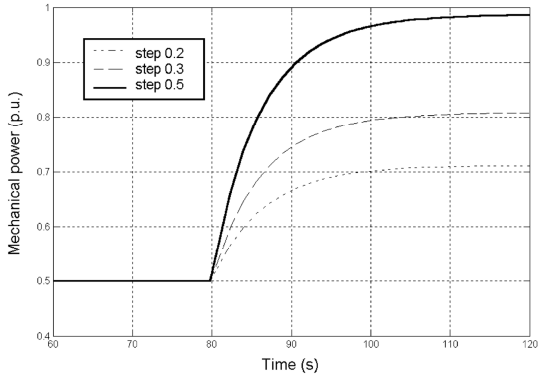

Figure 2.11: Rankine cycle power output step response [24]

From Figure 2.11 it can be seen that the power output of the steam turbines forms that of an over damped second order system when introducing a step response in the speed of the boiler feed pump. To improve the response of the cycle, a controller can be used to alter the mass flow rate of the fluid.

Changing the magnitude of the input signals to the components, results in the plant operating at different controlled conditions (operating points), which alters the dynamic response of the components. This can be seen in the TES simulation example (Figure 2.9), where the TES was simulated at different mass flow rate levels, which resulted in the settling time of the component to

change accordingly [25]. To optimize the efficiency of the components of the plant, the two critical parameters of the cycle, which include the temperature and the mass flow rate input, must be controlled [26].

The development of a simulation model of a CSP plant, which conforms to the responses mentioned, requires a transient model, capable of producing the same dynamic responses, to be developed. This is since constructing a steady state model would leave out important information concerning the dynamics of the model, whereas a dynamic model can be used to extract information concerning the dynamic behaviour of the plant [26].

The next section will discuss the details on how to develop a model that produces the same type of responses as mentioned.

2.4 CSP plant modelling

The development of a simulation model can be implemented by first obtaining a simulation platform capable of modelling the required responses mentioned in section 2.3. Once a suitable simulation platform is selected, a methodology for developing the model must be selected. After this is done, the model needs to be validated by the appropriate validation methodology. The next three sections will discuss some of the available selections used in the industry that can be used for the purpose of this study.

2.4.1 Model sizing techniques

The sizing of the CSP plant model can be implemented by making use of a number of methodologies; each dependent on both the type of data as well as the simulation platform available. This usually results in an approach where parameter values need to be determined for components of a model. To produce accurate results of the plant, some simulation software types require detailed information which is not always readily available to simply substitute into the model [28].

2.4.1.1 Model sizing through the use of baseline specifications

The sizing of a model can be implemented by the use of plant specifications, if all the specifications required for the plant are given. This can be information such as the size of the plant (power output) and the energy storage requirements (in hours) [29]. Table 2.1 shows an example of such specifications:

Table 2.1: Baseline plant specifications

Baseline Plant Conditions	
Nameplate Capacity	100 MW_e
Thermal Storage (operating time at nameplate capacity)	6 hours
Solar Multiple	2.0
Heat Transfer Fluid	Synthetic oil
Storage Fluid	Binary Na/K nitrate salt
Thermal Storage System	Indirect "2-tank" system [6]
Power Cycle	Superheated steam Rankine cycle with wet cooling
Location	Daggett, CA
Variation (1)	Air-cooled system of same nominal capacity & storage

Sizing a model of the plant in such a way proves to be difficult to validate, if an existing model/plant is unavailable to compare the resulting responses with one another.

2.4.1.2 Model sizing through assisting software

A model of a plant can also be sized by making use of the general knowledge of the components that can be expected to be in a CSP plant and make use of a program such as Solar Advisor Model (SAM), which allows for designs at a schematic level during the development of a potential project [30]. Here it is difficult to design the plant since there is no actual model that can be used to validate the developed model, but it does however allow for the model to be verified in terms of the type of responses expected of the model.

2.4.2 Model development approaches

The development of a model can be implemented by making use of one of three approaches. These approaches include: developing a model from first principles, making use of system identification techniques and by making use of pre-programmed models. A brief discussion of each approach will now be given:

2.4.2.1 First principle models

A first principle model is developed by using the laws of physics. This may result in a set of differential-algebraic equations. Modelling from first principles ensures a deeper understanding of the system dynamics. However, modelling from first principles is time consuming due to the fact that it takes longer to derive the differential equations of the system by hand [30]. This is especially the case if the system is of a complex nature and/or if the person who is deriving the model is inexperienced where the model can also be prone to human error.

Some examples of simulation platforms, which enable the user to simulate a model from first principles, include: Matlab®, Mathcad®, Symscape, and EES.

2.4.2.2 System identification models

A model can also be derived based on a grey box model approach, with the function of each of the components in the plant known, except for the mathematical expression describing the various components. System identification can be used to derive a model by measuring the responses of an existing model with certain input signals simulated, and by making use of sophisticated signal processing software to develop the same model [31].

Some examples of system identification software to develop a model include: Matlab® and LabVIEW™.

2.4.2.3 Pre-programmed models

One can also make use of pre-programmed models to develop a system containing a number of pre-programmed models, all interconnected to form a system of models. The use of conventional Computational Fluid Dynamic (CFD) models explains the principle of pre-programmed models best:

CFD analysis: CFD software components can be simulated without developing the mathematical model of the component since it has built-in model libraries. This allows for a detailed analysis of specific components, with the user only having to specify the parameters of the component [32]. The use of CFD software however is very limited to the number of components it can simulate simultaneously since it is very simulation intensive.

Some examples of simulation platforms which enable the user to simulate a model by making use of CFD software include: FlowTHERM™, and Trelis CFD™.

Simulating an entire CSP plant however, can result in large computational power required since an entire network of interconnected components needs to be simulated simultaneously. This can more easily be implemented by making use of systems CFD software.

Some examples of simulation platforms which enable the user to develop a model by making use of systems CFD analysis software include: Flownex®, TRNSYS, and GSE.

2.4.3 Model verification approaches

The verification of a model can be seen as a form of debugging; checking to see if the model developed is performing as it is intended to. The verification of a plant is usually used in parallel with the development of each of the components of the plant where the response of each

component is compared to the response theoretically expected from the component. There are several different types of techniques in existence today to verify a model. Some of these techniques will now be discussed:

Seed independence: The verification of a model, based on seed independence, involves simulating the model with random input values, which are within the limits of the model. If the model responds incorrectly to the specific random values used, then the model is incorrect. Different seed values must also be used [33].

Continuity testing: Verification through continuity testing, involves simulating the model continuously with slight changes made to its parametric values. If the model responds as expected, then the model is verified, but if the small changes made in the input to the model results in abnormal deviations in the responses of the model, then the model needs to be revised [33].

Structured walk-through/one-step analysis: This involves explaining the development of the model to peer persons in terms of its function and the aspects of the model. By doing so, the developer will become aware of the mistakes that he or she has made by simply revising the model itself [33].

2.5 Model validation

For a plant to be considered accurate and correct, the model must be validated. As mentioned above, the first step in validating the model is to determine if the model produces the correct type of response as is expected. The next step in the validation of the model is to determine whether the results obtained from the model represents the reality [34]. The validation of a model can constitute a number of techniques, including:

Model comparison: Here a series of simulations of the model is implemented to extract the system responses, which are compared to the results of another validated model's results [35].

Face validity: Here the validation of the plant is based on the knowledge of experts in the field. The expert will examine the model and its responses and decide whether the model is valid [35].

Historical data validation: Historical data validation involves making use of historical data of a plant that was specifically selected for the testing and building of the plant model and dividing it into two parts of data. One part of the plant data is used to develop the model, with the other part used to validate the model [35].

The validation procedure of each of the above mentioned techniques can be implemented by making use of either a top down or bottom-up implementation. This method is used since the internal components of the plant must also be verified and validated. The plant itself may be able to

produce the correct responses at system level, but some important responses at component level may not be correct which will also cause the model not to be valid.

Validating the plant with a bottom-up methodology can be implemented by first simulating each of the components of the plant separately in order to verify that the correct responses are obtained from each of the components. Once this is done, the plant is simulated with all the components integrated, to verify that the correct responses are obtained.

Validating the plant with a top down methodology is the exact opposite in terms of where the validation is started. Here the simulations to validate the system are made first, followed by simulations to facilitate validation of the model's components.

2.6 CSP plant model characterization process

The characterisation of a plant in order to obtain insights into some of its dynamic responses that are characteristic to the plant can be implemented by evaluating local linear models of the plant, which accurately describes the dynamics of the plant. To obtain a deeper insight into the dynamic responses of a CSP plant requires a study on the various dynamics characteristic to that of a CSP plant.

2.6.1 CSP plant characteristic responses

The construction of a CSP plant is of such a nature that there exists certain dynamic responses which influences the design considerations for a controller of the plant. Some of these responses include:

2.6.1.1 Change in dynamic behaviour

Research indicates that the dynamic responses of a CSP plant changes throughout the day as the thermal energy input to the plant changes. As the thermal energy input to the plant increases, the plant responds faster to changes made to its control variables, which increases the performance of the plant. This is due to the increase in temperature as well as the pressure of the fluids flowing through the system, which ultimately then leads to the components responding faster [36, 37].

2.6.1.2 Resonant and anti-resonant modes

It is shown in the literature that nonlinearities exist in the dynamic responses of a CSP plant. Occurrences known as resonant and anti-resonant modes, from the frequency response of distributed solar collector field CSP plants, are found situated at frequencies within the control bandwidth of these models. These modes influence the performance of the entire plant since it causes the responses of the system to change abruptly [36, 37].

The design of a controller for the plant should thus include the possibility of controlling the plant with changing dynamics as the thermal energy input changes throughout the day, as well as be able to control the plant with the presence of resonant and anti-resonant modes found within its control bandwidth [36, 37]. The next section will discuss some of the controllers used in the industry:

2.6.2 CSP plant controller evaluation

Due to the dynamic responses of the plant including nonlinearities in its responses as mentioned above, most of these types of power plants are controlled by making use of adaptive controllers to optimise the performance of the plant. Two of the most common controllers used in the industry include:

2.6.2.1 Gain-scheduled control

The use of a gain-scheduled controller can optimise the operation of the plant by changing the controlled variables as the operating point of the plant changes. Figure 2.12 illustrates a schematic design of a closed loop gain-scheduled controller for the plant [36].

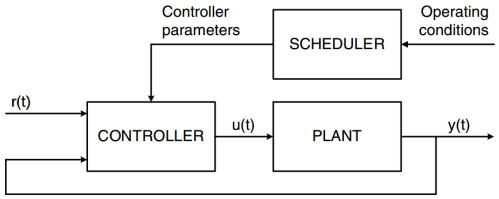

Figure 2.12: Basic gain scheduled controller scheme [36]

From Figure 2.12 it can be seen that the different operating points to the plant, which includes the thermal energy input to the plant, is used to calculate the control parameters of the plant for each operating point.

2.6.2.2 Feedforward control

Some CSP plants also make use of feedforward controllers to control its responses. The responses of a feedforward-controlled plant are controlled by measuring the disturbance signals of the plant, and by calculating the value that the controlled variable should be specified at to produce the required response according to the setpoint. The closed loop control configuration of a typical feedforward-configured controller for a CSP plant can be seen in Figures 2.13(a) and 2.13(b)

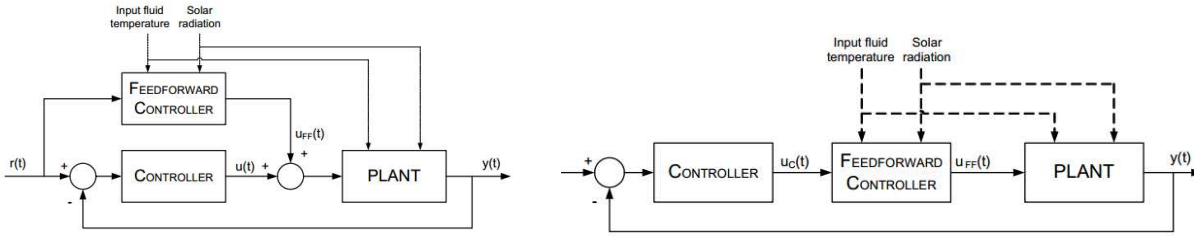

(a) Parallel configuration **(b) Series configuration**

Figure 2.13: Basic feedforward control schemes [36]

From Figure 2.13(a) and 2.13(b) it can be seen that the solar radiation as well the temperature of the fluid entering the SCF both form an input to the plant as well as to the feedforward controller. Although the temperature input of the SCF is considered as a disturbance input, in most cases it is ignored due to its influence being significantly small.

The process of characterising the plant by evaluating its open loop local linear models with the intent of identifying the dynamic responses unique to that of a CSP plant will now be discussed.

2.6.3 CSP plant model characterisation approach

To obtain open loop local linear models of the plant, there are two possible methodologies, which both depend on the approach followed during the development phase of the plant model. The next sections will discuss these two approaches:

2.6.3.1 Characterisation based on a first principle model approach

Making use of the modelling approach discussed in 2.4.2.1, where the model is developed from first principles, allows for an accurate model to be characterised. The characterisation of a first principle model would involve making use of the defined models of the entire plant and evaluating only the models relevant to the study.

2.6.3.2 Characterisation based on model extraction approach

Characterising a model based on a pre-programmed model development approach, as discussed in 2.4.2.2, involves the use of system identification procedures where the desired components are characterised by perturbing each of the relevant input signals of the components/plant with an excitation signal and measuring the resultant responses.

System identification software packages, such as Matlab® system identification toolbox™, uses the input/output data of a plant to further develop the local linear models to extract useful information concerning the dynamics of the plant [38]. Selecting the correct input data, to simulate the plant with, is important in the development of local linear models of the plant.

Excitation signal selection

Several different types of excitation signals could be used for system identification purposes. In order for the optimal signal, which has the highest possibility of capturing all the dynamics, to be selected, the following conditions must be met by the signals [39]:

i. The signal must excite the entire frequency band $\Omega = [\omega_{\min}, \omega_{\max}]$ where $\omega_{\min}$ and $\omega_{\max}$ is the minimum and maximum operating frequencies of the plant.

ii. The signal must be sufficiently rich to excite frequencies on a discrete grid with spacing less than or equal to η where $0 < \eta \leq \omega_{\min}$.

iii. No leakage in the Fourier Transform of the excitation signal and output signal should exist.

iv. The base tone response of the plant must be distinguishable from nonlinear distortions caused by subharmonics and superharmonics.

v. The crest factor of the signal, which is the ratio of the peak to rms value in the frequency band (Ω) of interest, should be as small as possible.

Some of the excitation signals that could be used to develop local linear models are shown in Figures 14(a)-14(f) [39]:

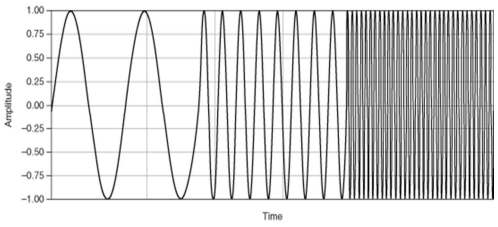

(a) Chirp signal

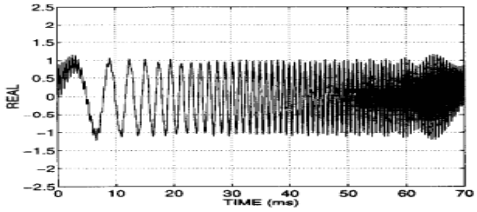

(b) Schroeder signal

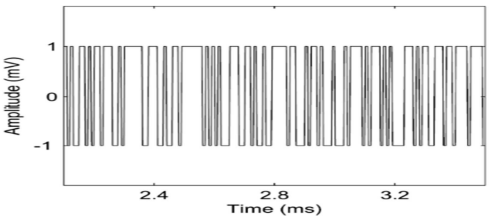

(c) Pseudorandom Binary Sequence (PRBS)

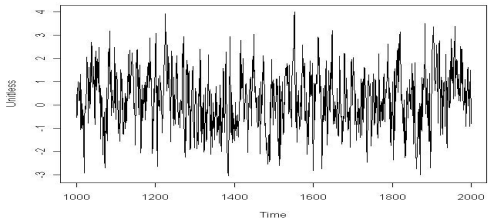

(d) Random noise signal

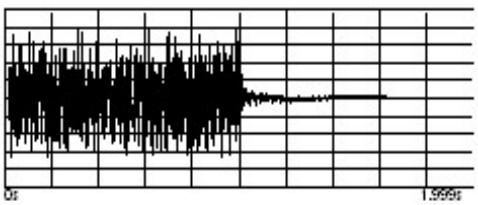

(e) Random burst signal

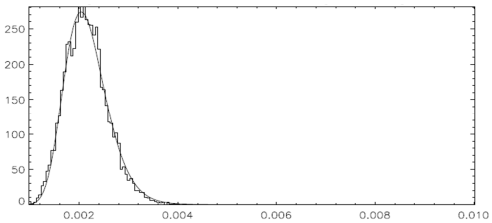

(f) Pulse-impact signal

Figure 2.14: Various excitation signals

Let us now discuss these signals by discussing how each signal conforms to conditions (i) to (v) listed above:

Table 2.2: Properties of the different excitation signals [39]

Excitation signal	Description	Excites Ω	Frequency spacing η	No leakage	Distortion removed	Crest factor	Time factor
Chirp	Chirp excitation signals are signals in which its frequency increases (up-chirp) or decreases (down-chirp) with time.	Yes	Yes	Yes	Yes	1.44	1.5 - 4
Schroeder	Schroeder or multisine signals are signals with varying frequencies and phases. It consists of a sum of several sinusoidal signals.	Yes	Yes	No	No	1.7	1.5
PRBS	Psuedorandom binary sequence excitation signals are periodic deterministic signals that oscilate between two levels, normally +1 and -1.	Yes	Yes	Yes	Yes	1	1.5
Random Noise	Random noise of excitation signals are noise sequences whose power spectrum can be altered by making use of digital filters.	Yes	$t >> \frac{1}{\omega_{\min}}$	Requires windowing	No	2 - 3	4.5
Random Burst	Random burst excitation signals are also a type of noise sequence, but the signal is divided in two stages. During the first stage, the excitation signal is the same as the random noise signal. The difference comes in during the second stage of the signal where a zero input is applied for the remainder of the excitation signal.	Yes	$t >> \frac{1}{\omega_{\min}}$	Requires $t >> \frac{1}{\omega_{\min}}$ or windowing	No	$3(\sqrt{\frac{t}{t_1}})$	$4.5(\frac{T}{T_1})$
Pulse-Impact Testing	The excitation signal of a pulse-impact signal is a short single pulse, measured directly in the time domain.	Yes	$t >> \frac{1}{\omega_{\min}}$	Requires $t >> \frac{1}{\omega_{\min}}$ or windowing	No	$\sqrt{\frac{t}{t_1}}$	$\frac{t}{t_1}$

The input signal used to excite the plant models with, is not the only important aspect considered. The order, at which the open loop local linear models are specified, also plays an important part in the characterisation of the plant, based on a model extraction approach. The next section will discuss the possibilities for specifying the orders of the models.

Model order selection: Reactive vs. high order models

In order for a robust controller, capable of achieving the highest bandwidth possible, to be derived, it is important not to only make use of low-order linear models. This is since important dynamics such as anti-resonant modes, found at frequencies around the plants' bandwidth, are neglected by making use of low-order linear models. The use of nonlinear models, or linear models with a sufficiently high order, can help to obtain a robust controller with a high bandwidth [38].

The use of low-order models does however have its own advantages. By making use of low-order models, the dominant poles and subsequently the dominant dynamic responses of these models can be evaluated. The use of the reaction curve method, which involves the simulation of a step response of a model, can be used to illustrate the dominant dynamic behaviour of the plant [36].

The order of the models is selected by making use of validation procedures where the resultant signal from the perturbed input signals are compared to that of the derived model. If the model produces a high enough fit to the selected order of the model, then the model is validated. This is done for both the high- and low-order models [38].

2.7 Critical evaluation

The critical evaluation of all the literature above, allows some form of decision-making to take place in terms of what technology is best suited for the purpose of this study. Some of the methodologies that will be followed throughout the study will now be discussed.

2.7.1 SCF evaluation

From the literature of the solar collector fields, mentioned at the beginning of the chapter, including the type of SCF structure and the factors influencing the efficiency of the amount of thermal energy absorbed by the collectors, it is noted that the model development of the SCF is of a complex nature. For this reason, the SCF will be modelled as a single pipe with a certain thermal energy input, in watts, which is determined by the solar radiation profile. This way the most important dynamics of the SCF including the temperature response of the SCF is still included into the design of the model.

2.7.2 CSP plant model development and validation evaluation

The selected configuration of the plant includes that of the combined cycle configured CSP plant as discussed. This is since the advantages of using this type of configuration, allow not only for any type of SCF topology to be used as the source of the thermal energy to the plant, but also for a more efficient plant to be developed that makes use of less water due to its configuration which is beneficial for the environment.

The selected model sizing technique of the plant will not include using either one of the two techniques mentioned. This is due to the fact that both of the sizing techniques only provide a limited amount of information supporting the total responses of the system, which makes it difficult to develop, verify and validate the model.

Instead, an alternative methodology will be followed which involves sizing the model based on well-documented results of a validated model. The responses of the model along with supporting literature will be used to specify the sizing of the components.

As discussed earlier, the modelling of the CSP plant starts by first determining which simulation platform to use. The use of first principle modelling can quickly become too complicated and nested, especially for a combined cycle CSP plant, which constitutes several different components. For each of the components to be accurately modelled, a large number of mathematical expressions must be derived to include all of the major dynamics of each component.

The use of normal CFD analysis tools can produce valuable information, which can be used in the characterisation process of such a plant since it provides a wide range of useful information surrounding the simulated components. The problem still is that an entire plant must be simulated, and since normal CFD software makes it difficult to simulate such a large number of interconnected components at the same time, due to the large amount of resources needed to simulate the system, an alternative is needed.

The use of systems CFD simulation platform would be best suited for this study. This is since it has the capabilities of representing all of the dynamics of the components used without developing mathematical expressions of each of the components in the software. This type of simulation platform also suits the study better, since the simulations made include a larger number of components that can be simulated at the same time, which normal CFD analysis platforms suffer in. Due to both the industrial partnership with M-Tech industrial, as well as its alignment to the specifications required of the simulation platform, Flownex is selected.

The methodology that will be followed to develop the model of the combined cycle CSP plant is shown in Figure 2.15.

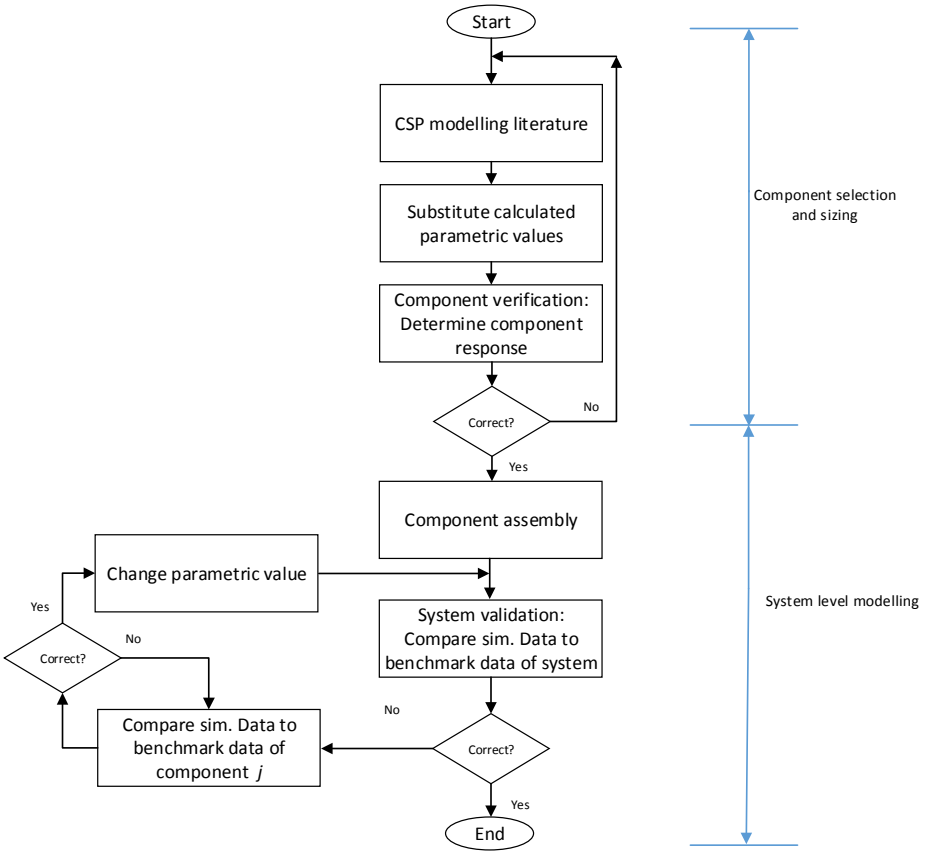

Figure 2.15: Model development methodology

The development of the model is divided into two levels of implementation. First is the component selection and sizing, which is followed by the model development at system level. Each of these two levels will now be discussed:

Component selection and sizing

The selection and sizing of each of the components that makes up the plant will be implemented by first obtaining a list of all the components existing in the selected plant technology. Further literature including mathematical expressions describing each of the components will then be researched to be able to specify the correct sizing of each component's parameters from the design specifications of the plant. After the mathematical expressions for each of the components are obtained, the known parametric values from the specifications are substituted into the equations in order to obtain the unknown parameters to complete the sizing of the components.

Once the calculated parametric values of each of the components are substituted, verification in the form of simulations can be conducted to verify that the resultant responses of each component are correct. If the response obtained from the simulation matches the response expected from the literature of the component, then the verification of the next component can start.

If the response of the component does not match the desired response according to the literature, then the component is revised by examining the calculated parameters of the component, to

determine whether a calculation error was made or if the wrong mathematical expression was used to describe the component.

System level modelling

Modelling at system level entails the integration of all the components to form an integrated system model. Once all of the components are interconnected correctly, the model is simulated with certain input signals to measure the response of the system as a whole. Validation of the developed model involves making use of the model comparison technique.

If the responses obtained from the developed model do not match the responses of the bench mark models with n amount of components, then the first component in the model ($j=1$) is compared to the same component of the benchmark model. If the results of the component matches that of the benchmark model then the next component ($j=j+1$) is checked again until all the components ($j=n$) have been checked. Once the components that produced the incorrect output have been identified, the model components will be improved.

2.7.3 CSP plant characterisation evaluation

The study of the dynamic responses characteristic to that of a CSP plant, illustrated both a change in the dynamic responses of the plant, as well as the presence of resonant and anti-resonant modes within the control bandwidth of a CSP plant. For this reason, the characterisation of the plant will include evaluating the presence of these phenomenons.

Although the study of the presence of these modes was conducted on distributed solar collector field topology CSP plants and not on solar power tower topology CSP plants, as is the case for this study, the presence of these modes will still be investigated, but for solar power tower topology CSP plants.

Selecting between either making use of a first principle model approach and a model extraction approach for the development of the local linear models of the plant to obtain a deeper understanding of the dynamic responses of the plant, result in selecting the model extraction approach. This is since the model development approach of the plant is based on a pre-programmed modelling approach.

Pseudo random binary sequence excitation signals will be used to simulate the plant. This is since these signals satisfy all the conditions for a model to produce all the important dynamics.

The order at which the open loop local linear models are to be specified at, includes the use of both high- and low-order models. This is since both these models each have separate advantages to identify all the dynamic responses unique to that of a CSP plant.

2.8 Conclusions

The model development of a CSP plant, with the intent of obtaining deeper insight into some of the responses characteristic to that of such a plant, along with the various methodologies to do so were discussed in this chapter. Due to its advantages, a combined cycle CSP plant will be developed and characterised, by making use of a Flownex® Simulation Environment. The verification of the model is done in parallel with the model development whereas model validation will only be performed when all the components of the model are integrated. Characterisation of the plant will involve a number of simulations to obtain an understanding of how the input signals of the plant influence the dynamic responses of the entire plant.

Chapter 3: Brayton cycle component selection and sizing

The use of a model producing responses close to that of the actual model is necessary during the characterisation process of any model. The following three chapters will discuss the model development of a combined cycle Concentrated Solar Power (CSP) plant in full. Chapter 3 discusses the selection and sizing of each component of the Brayton cycle. This includes all the needed literature, implementation procedures as well as the required simulations to verify that the correct components are selected for the simulation design. The same is done for the Rankine cycle in Chapter 4. The Brayton and Rankine cycle will then be combined in Chapter 5 in order to form the complete model of the combined cycle CSP plant. Chapter 5 will also discuss the validation of the model to ensure that the results obtained are correct.

3.1 Model discussion

The development of the Flownex combined cycle CSP model is guided by the use of documented responses of a validated model, along with the supporting literature on each of the components used in the model. The literature obtained is then used to translate the responses into useful information so as to specify the sizing of the components. The model is developed to produce the same responses as the validated model with the same operational input signals substituted into the model.

The next section will give an overview of the construction of the validated model, which includes an elaboration as to what information is available from the model that will be used to size each of the components of the Flownex model.

3.1.1 Description of validated model

The validated model, which the Flownex model is based on, is a 40 MW plant that was simulated by Stellenbosch's renewable energy division (Solar Thermal Energy Research Group) on a simulation platform known as Transient Simulations, or TRNSYS for short. The TRNSYS CSP plant is a combined cycle CSP plant with thermal energy storage and a duct burner for additional thermal energy. The Heat Transfer Fluid (HTF) used for the Brayton cycle is mixed gasses (air mixed with combustion gasses) and the fluid used for the Rankine cycle part of the plant is water.

The Solar Collector Field (SCF) makes use of solar power tower technology and the radiation profile input to the collectors is that of the Upington area. A duct burner is added to the system to increase and control the temperature of the mixed gasses up to a desired value. Thermal Energy Storage (TES) is used to ensure that energy transfer exists at the Rankine cycle part of the plant for a certain period through the night. The TES tank used by the TRNSYS model is made of concrete.

The model makes use of a three-stage boiler that constitutes three counter flow heat exchangers to transfer thermal energy from the Brayton cycle to the Rankine cycle. One of which is the pre-heater, the others being the evaporator and the super heater. The cooling strategy used to cool down the steam exiting the steam turbines in this model includes the use of a water type condenser.

The Rankine cycle also makes use of a three-stage turbine (high-pressure, intermediate-pressure and low-pressure) system to increase the efficiency of the system.

Since the Flownex model cannot be developed from only knowing what components are used in the TRNSYS model, additional information is required for each component of the model to be sized correctly. The additional information that is available from the TRNSYS model documentation includes information such as temperature responses as well as power outputs of the system.

Information concerning the input signals to the system is also included in the TRNSYS model documentation. This includes the mass flow rates of the fluids flowing through the major components of the system. As mentioned above, one of the responses also included in the documentation is the temperature profile of the SCF, as well as the controlled temperature response of the mixed gasses exiting the duct burner.

With an overview of the TRNSYS model's component layout and responses given, the process of developing the Flownex model from these specifications can now be discussed. Section 3.1.2 along with the rest of Chapter 3 will discuss how the Brayton cycle part of the model and its associated components are selected and sized to produce the same responses as that of the TRNSYS model.

3.1.2 Brayton cycle component selection and sizing

The Brayton cycle constitutes four main components including a heater, turbine, cooler and a compressor as seen in Figure 3.1. The selection of these components is based on both the type of components typically used in a Brayton cycle as well as the specific components used in the TRNSYS model to keep the Flownex model in line with the TRNSYS model.

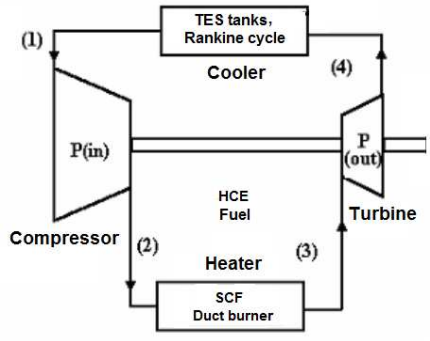

Figure 3.1: Brayton cycle component diagram

The process of sizing these components to produce the correct responses involves a three-phase process. The first phase of this process is to obtain literature on both the working principle as well as the model construction of the component being sized. Once the appropriate literature has been obtained, the implementation phase (second phase) can commence. The implementation phase involves using the model construction of the component along with the documented responses of the TRNSYS model to calculate the parametric values of the component. Verification of the component (third phase) takes the form of simulating each component and comparing the responses of the component to what is expected of the model.

An important size specification that needs to be considered is that of the pipes, used to connect each of the components in the model, should have the least effect on the dynamics of the plant, since the TRNSYS model, does not specify any pipes in its design. With Flownex not capable of interconnecting components without the use of pipes, they are sized in such a way to represent an ideal pipe which has little or no effect on the dynamics of the system. This is implemented by specifying the pipes to be 1 meter in length and 1 meter in diameter.

The size specification of each of the mentioned components of the Brayton cycle will now be discussed, starting with the sizing of the SCF and the duct burner of the heater.

3.2 Brayton cycle component sizing: Heater

The heater of this CSP plant configuration constitutes two components that supply thermal energy to the rest of the system as seen in Figure 3.1. These two components include the SCF and the duct burner, which introduces supplementary thermal energy to the system. The sizing of each of these two components will be discussed next.

3.2.1 Literature on solar collector fields

As mentioned in Chapter 2, the energy balance of a SCF constitutes energy being absorbed and energy being radiated. One of the largest factors influencing the amount of energy being absorbed is the Direct Normal Irradiance (DNI) levels, which by definition is the amount of solar radiation that is exposed perpendicularly on a surface area and is expressed in watts per square meter [$\mathrm{W/m^2}$]. The DNI forms a parabolic shaped curve that changes in magnitude throughout the day as well as throughout the year as seen in Figure 3.2 [40].

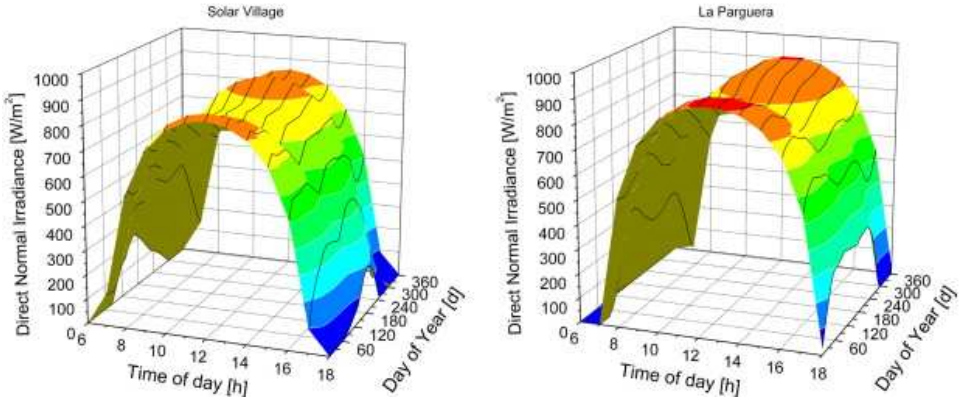

Figure 3.2: DNI profiles of both Solar Village as well as La Parguera areas [40]

The thermal energy gain of the air flowing through the SCF also resembles that of the parabolic shaped profile seen in Figure 3.2. This is due to the fact that the energy absorbed by the collector from the solar rays is transferred to the HTF in the form of thermal energy, which changes as the solar radiation intensity changes.

Model construction of a SCF

The model construction of a SCF constitutes energy being absorbed and energy lost. The total energy collected ($\dot{Q}_{Collected}$) by the SCF is given by the total amount of energy absorbed by the collector ($\dot{Q}_{Absorbed}$) subtracted by the total amount of energy lost due to receiver losses ($RHLoss$) [41]:

$$\dot{Q}_{Collected} = \dot{Q}_{Absorbed} - RHLoss \tag{3.1}$$

The amount of energy absorbed $\dot{Q}_{Absorbed}$ is given by:

$$\dot{Q}_{Absorbed} = DNI \times \cos(\theta) \times IAM \times RS \times EL \times \eta_{field} \times \eta_{HCE} \times SFA \tag{3.2}$$

where DNI is the direct normal irradiance, θ is the radiation incident angle, IAM is the Incident Angle Modifier, RS is the Row Shadowing, EL is the End Losses, η_{field} is the collector field efficiency, SFA is the Solar Field Aperture, and η_{HCE} is the HCE efficiency.

The total receiver losses of the collectors are given by:

$$RHLoss = \sum_{i=1}^{No.HCETypes} HCEFrac_i \times \frac{HLoss_{collector,i}}{w} \tag{3.3}$$

where $RHLoss$ is the total Receiver Heat Loss, w is the width of the collector aperture and $HCEFrac$ is the fraction of the HCE to the total number of HCE's used in the plant. The Heat Losses $HLoss_{collector}$ of the collector is given by:

$$HLoss_{collector} = \frac{a_0(T_0 - T_1) + \frac{a_1}{2}(T_0^2 - T_1^2) + \frac{a_2}{3}(T_0^3 - T_1^3) + \frac{a_3}{3}(T_0^4 - T_1^4) + DNI[b_0(T_0 - T_1) + \frac{b_1}{3}(T_0^3 - T_1^3)]}{(T_0 - T_1)} \tag{3.4}$$

where

a, b: are coefficients, T_1 is the inlet temperature of the solar collector field and T_0 is the outlet temperature of the solar collector field.

A simplified version of the model mentioned above, in terms of the models' inputs and outputs can be seen in Figure 3.3. The DNI levels, ambient temperature, temperature of the HTF entering the SCF and the mass flow rate of the air flowing through the SCF mainly influence the temperature of the HTF exiting the collectors [42].

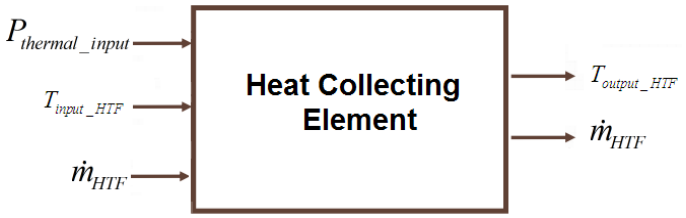

Figure 3.3: Input/output diagram of the heat collecting element

3.2.2 Sizing of the solar collector field

Since Flownex does not have a SCF as one of its library components, a replacement has to be derived. The model of the SCF is developed in Flownex by making use of a single pipe with its properties set to enable a heat input to the pipe to be specified, which represents the thermal energy absorbed from the solar radiation. Adjusting the thermal energy input to the pipe thus alters the temperature of the HTF exiting the SCF accordingly.

The sizing specification of the TRNSYS SCF model specifies the temperature response of the SCF to resemble that of the DNI profile, with the temperatures changing throughout the day from $600\ ^\circ C$ in the morning to $1100\ ^\circ C$ at noon, and back to $600\ ^\circ C$ during the afternoon. At night the temperature of the HTF exiting the SCF is to be at ambient temperature ($25\ ^\circ C$).

3.2.3 Simulation/Verification of the solar collector filed

The simulation setup of the SCF is implemented in Flownex by making use of a single pipe with air, which represents the HTF, flowing through it. Connected to the one side of the pipe is a boundary condition specifying the temperature of the fluid entering the pipe, which is set at a fixed temperature of $35\,°C$, and another boundary condition at the other end, specifying the mass flow rate of the fluid flowing through the pipe.

The simulation of the SCF is divided into two parts. The first part is the simulation of the temperature response of the SCF with changes made to the mass flow rate of the fluid flowing through it, whilst maintaining a fixed thermal energy input to the pipe. Figure 3.4 illustrates the resultant temperature response of the SCF with a step response in the mass flow rate simulated (from 6.186 kg/s to 8.41 kg/s).

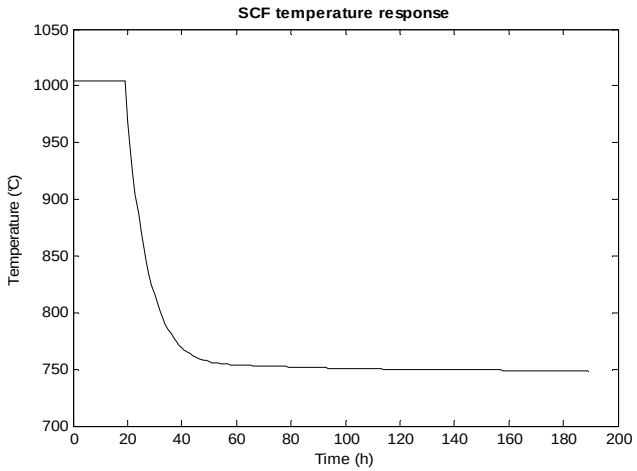

Figure 3.4: SCF temperature response.

From Figure 3.4 it can be seen that the temperature response of the SCF forms that of a over damped second order system with a negative gain, which is as expected.

The next part includes simulating the temperature response of the SCF, with the thermal energy input from the TRNSYS model used as the input to this model, using Matlab®. This is done whilst maintaining a constant mass flow rate of the air flowing through the pipe. Figure 3.5 illustrates the temperature response of the SCF with 12 hours of day simulated.

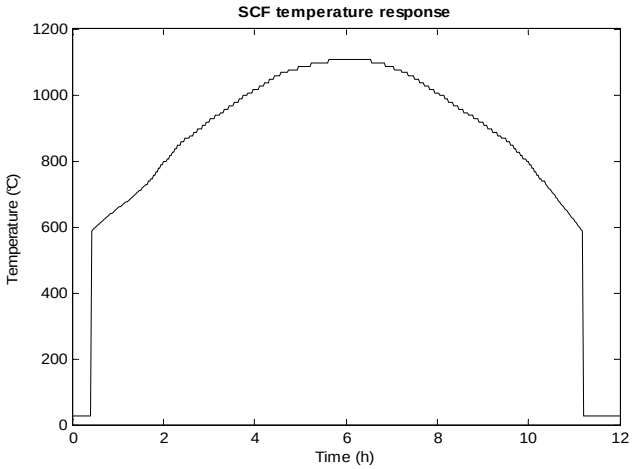

Figure 3.5: SCF temperature response.

As seen in Figure 3.5 the temperature of the HTF exiting the SCF starts at $600\ ℃$ during sunrise, until it reaches a maximum of $1100\ ℃$ at noon, where it then returns to $600\ ℃$ by sunset. During night time the temperatures of the collector returns to ambient temperature ($25\ ℃$) due to the mass flow rate stopping and no sun heating up the collectors.

3.2.4 Literature on the duct burner

As mentioned in Chapter 2, the duct burner is used to increase and control the temperature of the fluid entering the gas turbine in order to optimise the efficiency of the plant. The duct burner increases the temperature by injecting the combustion gasses of burnt fuel into the cycle. These combustion gasses mix with the HTF (air) exiting the SCF, which results in an increase in the temperature of the HTF due to the high temperature of the combustion gasses. Changing the amount of fuel added to the system alters the temperature of the mixed gasses entering the gas turbine due to the ratio of combustion gasses to air being altered. The more fuel added to the system the higher the ratio, which results in a higher average temperature to be obtained [43].

Model construction of the duct burner:

The process of heat transfer from one fluid to another, due to a difference in temperature between the two fluids in a mixed fluid system, forms the function of a heat exchanger. For this reason the model construction of the duct burner resembles that of a heat exchanger, more specifically, a direct contact heat exchanger where heat is transferred between two fluids which are mixed. The model construction of a duct burner can basically be represented by the following equations which represents the heat transfer rate of both fluids:

$$\dot{Q}_{fluid1} = \dot{m}_{fluid1} c_{p\ fluid1} \Delta T_{fluid1} \tag{3.5}$$

and

$$\dot{Q}_{fluid\,2} = \dot{m}_{fluid\,2} c_{p\ fluid\,2} \Delta T_{fluid\,2} \tag{3.6}$$

where $\dot{Q}$ is the heat transfer rate, $\dot{m}$ is the mass flow rate, c_p is the specific heat and ΔT is the difference between the initial and final temperature of the fluid. Subscripts $fluid\,1$ and $fluid\,2$ represents the two mixed fluids.

Assuming that no losses in the energy transfer between fluid 1 and fluid 2 exist, then it can further be assumed that the heat transfer rates of both fluids are the same:

$$\dot{Q}_{fluid\,1} = \dot{Q}_{fluid\,2} \tag{3.7}$$

This is possible since direct contact heat exchangers do not have a medium separating the two fluids, which result in a decrease in the losses associated with the transfer of thermal energy [44].

The input/output diagram of the duct burner is shown in Figure 3.6:

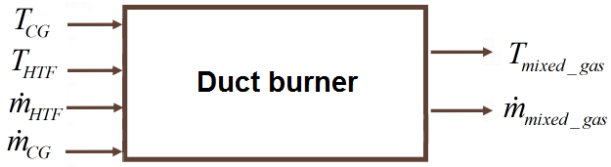

Figure 3.6: Input/Output diagram of the duct burner

3.2.5 Sizing of the duct burner

The duct burner is modelled in Flownex by making use of an adiabatic flame with two boundary conditions connected to the input of the flame. Each of these boundary conditions specifies a mass fraction, one of which is the fuel (CH_4) and the other being oxygen (O_2) which is both fed into the flame. The combination of the fuel, the oxygen and the adiabatic flame results in combustion to take place.

The output of the adiabatic flame is connected to the output of the SCF by using a T-junction. This results in both fluids (combustion gasses and air) mixing, which ultimately causes thermal energy transfer from the combustion gasses to the air. The T-junction is connected to the gas turbine.

The temperature of the mixed gasses exiting the T-junction, as specified from the TRNSYS model, is to be fixed at $1500\ °C$. This temperature has to be maintained for the first 12 hours of each day whilst solar radiation is available to the system. In order to maintain a fixed temperature of the mixed gasses, the rate of fuel added to the system has to be determined.

Due to the temperature of the air exiting the SCF not being constant, the amount of fuel added to the system changes as the temperature of the air changes. By making use of a controller controlling the amount of fuel added, the temperature of the mixed gasses can be manipulated. The use of Proportional Integral (PI) control meets the control requirements for this problem. This

is the case since it is one of the most used control schemes in the industry, and since the problem is a single loop problem with only one measured variable (temperature) and one control variable (mass flow rate) [45].

The Ziegler-Nichols method is one of the most commonly used methods of obtaining the controller gains without the use of the systems transfer functions. This is because it makes use of empirical values to derive its gain values [45]. Appendix A discusses the procedures of obtaining each of the resultant gains of the PI controller.

Before using the Ziegler-Nichols method to determine the gains of the controller, it is important to first obtain the control boundaries of the controller. That is, the maximum and minimum amount of fuel that is to be added to the system from the temperature range of the SCF. From Figure 3.5 it can be seen that the most amount of fuel is added to the system in the mornings and in the afternoon when the temperature of the air exiting the SCF is $600\,°C$. This is due to the large temperature difference between the desired set point and the actual value, and for this reason the most amount of fuel needs to be added to the system in order to maintain the $1500\,°C$.

With this in mind the mass flow rate of the fuel flowing through the burner is calculated with the minimum and maximum temperature of the air exiting the collector selected to determine the maximum and minimum mass flow rates of the fuel added. With the heat transfer rates of both fluids assumed to be equal, (3.7) can be rewritten as follows:

$$\dot{m}_{air} c_{p\ air} \Delta T_{air} = \dot{m}_{CG} c_{p\ \ CG} \Delta T_{CG} \tag{3.8}$$

where subscript "*air*" and "*CG*" represents the air and combustion gasses respectively.

Determining the rate of fuel that is added to the system involves making use of the documented results of the TRNSYS model so as to calculate the rest of the parameters to solve for the mass flow rate of the fuel added by using (3.8).

From the TRNSYS model the mass flow rate of the air flowing through the SCF is set at 6.555 kg/s. The temperature of the combustion gasses, which is not stated in the TRNSYS documentation, is calculated from the Flownex combustion model to average around $2500\,°C$. The specific heat of both the air as well as the combustion gasses are $1.006\ \text{kJ/kg.°C}$ and $1.99\ \text{kJ/kg.°C}$ respectively.

With the temperature response of the air exiting the SCF and the temperature of the combustion gasses known, the maximum mass flow rate (at $600\,°C$) and the minimum mass flow rate (at $1100\,°C$) of the fuel can be calculated.

The maximum mass flow rate of the fuel added to the plant is calculated by rewriting (3.8):

$$\dot{m}_{CG\_\max} = \frac{\dot{m}_{air} c_{p\ air} \Delta T_{air\_\max}}{c_{p\ CG} \Delta T_{CG}}$$

$$\dot{m}_{CG\_\max} = \frac{6.18 \times 1.006 \times (1500 - 500)}{1.99 \times (2500 - 1500)}$$

$$= 3.1 \text{ kg/s}$$

The minimum mass flow rate of the fuel added to the plant is again calculated by using (3.8):

$$\dot{m}_{CG\_\min} = \frac{\dot{m}_{air} c_{p\ air} \Delta T_{air\_\min}}{c_{p\ CG} \Delta T_{CG}}$$

$$\dot{m}_{CG\_\min} = \frac{6.18 \times 1.006 \times (1500 - 1100)}{1.99 \times (2500 - 1500)}$$

$$= 1.8633 \text{ kg/s}$$

PI controller design/implementation:

Control is implemented by making use of Flownex's build in PI controllers, where the temperature of the mixed gasses exiting the T-junction was measured and compared with a specific set temperature ($1500\ ^\circ\text{C}$) that the controller must maintain by controlling the mass flow rate of the fuel.

Calculating the different gains of the controller is done by making use of the Ziegler-Nichols tuning method, which is explained fully in appendix A. To summarise: the system must first be introduced with a step input with all the gains of the controller set to zero, and then gradually increasing the proportional gain until the system reaches its ultimate value with the temperature of the mixed gasses oscillating. This can be seen in Figure 3.7:

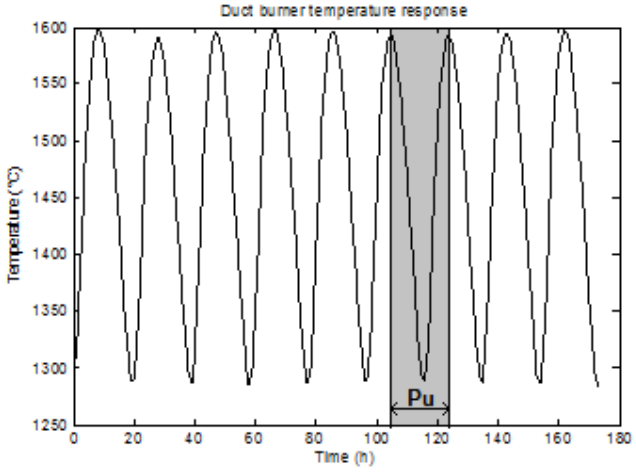

Figure 3.7: Neutrally stable system

As seen in Figure 3.7 the ultimate period is equal to 20 sec. The ultimate gain k_u, as determined from the simulation where the proportional gain was used, is equal to 200. From Table A.1 in Appendix A and from the values derived from the simulation, the PI gain values can be calculated.

The gain k_p is calculated as follows:

$$\begin{aligned} k_p &= 0.45k_u \\ &= 0.45\times 200 \\ &= 90 \end{aligned}$$

The gain k_I is determined by first calculating the time constant:

$$t_I = \frac{P_u}{1.2} = \frac{20}{1.2} = 24\,\text{sec} \qquad k_I = \frac{1}{t_I} = \frac{1}{24} = 41.6\times 10^{-3}$$

3.2.6 Simulation/Verification of the duct burner

The simulation of the duct burner involves simulating the temperature response of the mixed gasses exiting the T-junction. Connected to the T-junction is the duct burner and two pipes, one for the air coming into the burner at a temperature of $600\,°\text{C}$, and one for the mixed gasses exiting the T-junction. The temperature of the air entering the junction is set fixed by the use of a boundary condition, and the mass flow rate to control the temperature of the mixed gasses is controlled by the PI controller with the calculated gains used. A step response was simulated for the flow rate of the fuel by switching on the controller during simulation. Figure 3.8 shows the resultant temperature response (dash-dotted line) of the mixed gasses exiting the T-junction:

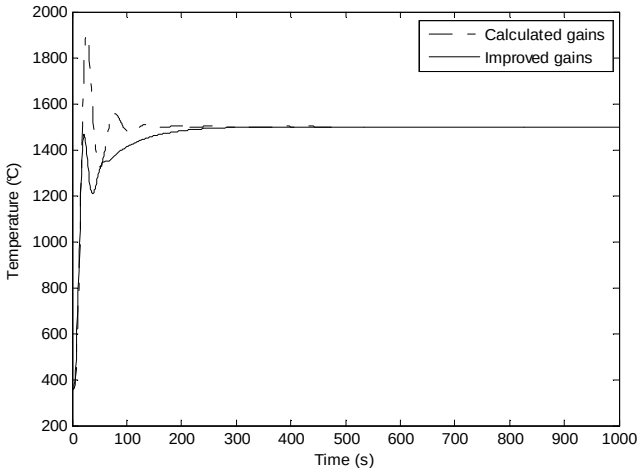

Figure 3.8: Derived PI controller step response

As seen in Figure 3.8 the temperature of the mixed gasses which is controlled by the PI controller. It can also be seen that there exists a large overshoot when using the calculated gains. To improve on the large overshoot, the gains of the controller must be adapted until the temperature response is at a satisfactory level. The resultant response after adapting the gains can be seen by the solid line in Figure 3.8. What can also be noted from the new response obtained, is the fact that the settling time has now increased due to the overshoot being decreased.

3.3 Brayton cycle component sizing: Turbine and compressor

The combination of the turbine with the compressor converts thermal energy, of the mixed gasses exiting the duct burner T-junction, into mechanical energy. The sizing of the gas turbine and compressor will be discussed in full in the following section:

3.3.1 Literature on gas turbines and compressors

Turbines are energy converters that convert thermal energy into rotational (mechanical) energy. The process of generating power with a turbine can be seen in Figure 3.9, where a high pressure and high temperature gas enters the nozzles of the turbine at a certain mass flow rate. Upon entering the turbine, the gas expands due to the change in the area of the turbine, which causes the pressure and temperature of the gas to decrease due to both the energy transfer and the change in area. Placed inside the turbine are stationary and rotating blades, angled in opposite directions to one another. The stationary blades forces the gas into one direction, which causes the rotating blades to rotate due to the direction of the force that the gas is exerts on the rotating blades [46].

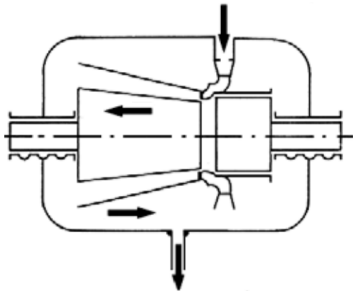

Figure 3.9: Steam flow in a turbine [46]

The turbine and compressor of the Brayton cycle continuously exchanges energy during operation. This is due to the fact that the turbine generates rotational energy in the shaft, connecting the two, which causes the compressor to rotate. The rotation of the compressor in turn increases both the pressure as well as the temperature of the mixed gasses flowing into the turbine.

Model construction of the turbine and compressor:

The power output or work transferred over one second of a turbine or compressor is given by (3.9) [41, 46]:

$$\frac{\partial W}{\partial t} = P = \dot{m}W \tag{3.9}$$

where $\dot{m}$ is the mass flow rate of the fluid flowing through the turbine and W is the sum of the work done, by either the turbine or by the compressor, and is given by (3.10) which is the difference in the enthalpy of the fluid entering and exiting the turbine/compressor:

$$W = h_1 - h_2 \tag{3.10}$$

where h is the enthalpy of the fluid.

By rewriting (3.10), to include the change in temperature of the fluid entering and exiting the turbine, the power output of a turbine can be given by (3.11):

$$\frac{\partial W}{\partial t} = \dot{m} c_p \Delta T \tag{3.11}$$

where c_p is the specific heat of the fluid and ΔT is the temperature difference of the fluid entering and exiting the turbine/compressor.

The temperature of the fluid exiting a turbine is influenced by both the pressure ratio (pr) of the turbine, which is given by the pressure of the gas entering the turbine divided by the pressure of the gas exiting the turbine, as well as the specific heat ratio (Υ) of the gas used [16].

$$T_2 = T_1 \times (\frac{1}{pr^{1-\frac{1}{\Upsilon}}}) \tag{3.12}$$

The resultant input/output diagram of a turbine is shown in Figure 3.10:

Figure 3.10: Input/output diagram of the turbine

The input/output diagram of the compressor forms the exact opposite to that of the turbine in terms of the work done, the pressure as well as the temperature input and output of the model.

3.3.2 Sizing of gas turbines and compressors

The development of the gas turbine and compressor is implemented in Flownex by making use of Flownex's standard turbine, compressor, and connecting shaft found in its component library. The sizing specification of both the turbine as well as the compressor is based on the documented TRNSYS model results. This requires that the temperature of the mixed gas exiting the gas turbine should be stepped down from $1500\ ^\circ C$ to $620\ ^\circ C$, with the mixed gas flowing through the turbine at a mass flow rate of 14 kg/s at maximum power delivery. In terms of the pressure increase due to the compressor, the pressure has to increase from ambient pressure (1 bar) to 10 bar.

Sizing of both the turbine as well as the compressor involves specifying the pressure ratios of both components. This is to ensure that the correct pressure and temperature change is obtained. With the input and output temperatures of the gas turbine known, (3.12) can be rewritten in order to determine the pressure ratio of the turbine:

$$pr = \left(\frac{T_3}{T_4}\right)^{\frac{\Upsilon}{\Upsilon-1}} \tag{3.13}$$

where pr is the pressure ratio, T_3 the input temperature of the turbine seen in Figure 3.1, T_4 the output temperature of the turbine and Υ the specific heat ratio of the fluid used.

The specific heat ratio of the mixed gasses, for temperatures ranging between $600\,°C$ and $1500\,°C$, averages around 1.35 and substituting it along with the input and output temperatures into (3.13) would result in the pressure ratio of the turbine to be equal to:

$$\begin{aligned} pr_{total} &= \left(\frac{1500}{620}\right)^{\frac{1.35}{1.35-1}} \\ &= 30.198 \end{aligned}$$

The total pressure ratio of the turbine should thus be 30.198. A number of factors influence the limitations on how high the pressure ratio of the turbine/compressor can be. Typically, a turbine/compressor is specified with a pressure ratio ranging between 4 and 20. Since the calculated pressure ratio of the gas turbine is so high, two gas turbines and compressors are connected in series to obtain the desired temperature decrease from $1500\,°C$ to $620\,°C$.

In order to do so the decrease in temperature of the mixed gas exiting the first gas turbine is selected to be at $1060\,°C$ which is half the required temperature drop. Calculating the pressure ratio of the first turbine is as follows:

$$\begin{aligned} pr_{GT1} &= \left(\frac{1500}{1060}\right)^{\frac{1.35}{1.35-1}} \\ &= 3.816 \end{aligned}$$

Calculating the pressure ratio of the second gas turbine is done by making use of (3.13), where the input temperature of the turbine is $1060\,°C$ and the temperature of the fluid exiting the turbine is $620\,°C$:

$$\begin{aligned} pr_{GT2} &= \left(\frac{1060}{620}\right)^{\frac{1.35}{1.35-1}} \\ &= 7.914 \end{aligned}$$

Calculating the pressure ratios of both the compressors in order to increase the pressure of the air exiting the compressors is achieved by dividing the total pressure ratio in two:

$$\begin{aligned} pr_{total} &= \frac{p_{out}}{p_{in}} \\ &= \frac{10}{1} \\ &= 10 \end{aligned}$$

Since two compressors are used, the square root of the total pressure ratio can be taken in order to specify each compressor's pressure ratio. The pressure ratio of each compressor is thus equal to $\sqrt{10}$.

3.3.3 Simulation/Verification of the gas turbines and compressors

The simulation setup of the gas turbine and compressor is implemented in Flownex by making use of an open Brayton cycle configuration. Both the heater as well as the cooler used in the model is modelled by making use of boundary conditions specifying the input temperature of the turbine as well as the input temperature and pressure of the compressor. The mass flow rate of the air flowing through the cycle is manipulated by changing the diameter of the control valve placed at the inlet of the compressor.

The compressor and turbine is simulated with the temperature of the fluid entering both the turbine and compressor specified by boundary conditions set fixed at $1500\,℃$ and $25\,℃$ respectively. The mass flow rate of the air flowing through the cycle is set to 14 kg/s at maximum power delivery and 0 kg/s at minimum power delivery. Since the time response of the cycle is not very long, the turbines and compressors are simulated over a short time interval. The simulated responses of the compressor and turbine combination include both the mechanical power generated as well as the temperature response of the turbines. Figure 3.11 shows the resultant power output of the system.

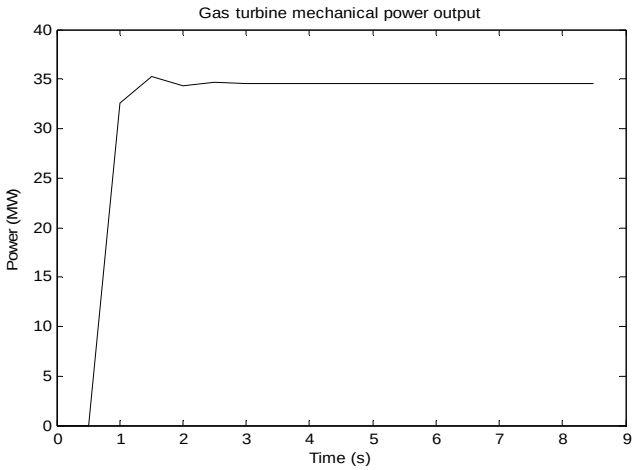

Figure 3.11: Gas turbine power output

From Figure 3.11 it can be noted that the generated power of the turbine and compressor combination produces a constant power output of 35 MW once the turbine/compressors reached steady state. Important to note is the overshoot of the power generated being quite high, reaching up to 36 MW which could be unhealthy for the inline components of the cycle.

In the second simulation, the temperature of the mixed gasses exiting the gas turbines is simulated.

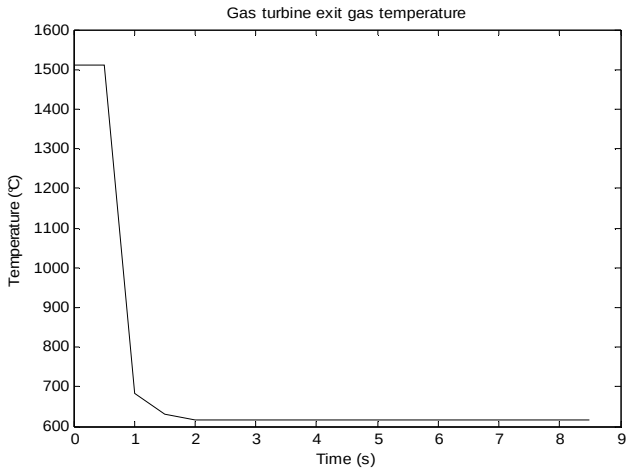

Figure 3.12: Downstream gas turbine temperature response

From Figure 3.12 it is noted that while the mass flow rate of the fluid flowing through the cycle is set to 0 kg/s the turbine exhaust gasses reaches a temperature close to that of the mixed gasses entering the turbine ($1500\ ^{\circ}C$). As a result thereof there exists only a small amount of thermal losses in the turbines due to no energy being transferred to rotate the turbine blades. As soon as the mass flow rate of the fluid flowing through the turbine is stepped up to 14 kg/s, the temperature of the exhaust gasses of the second turbine reaches $620\ ^{\circ}C$ which is due to the energy transfer to the turbines.

3.4 Brayton cycle component sizing: Cooler

The components of the Brayton cycle's cooler can be divided into the thermal energy storage (TES) tank and the boiler. Both these components extract the remainder of the energy of the exhaust gasses exiting the turbines, where it is then used to either charge the TES tanks or to heat up the water of the Rankine cycle. The model development of the boiler will be discussed in Chapter 4 with the design of the Rankine cycle components. The model development of the TES tanks will now be discussed:

3.4.1 Literature on thermal energy storage tanks

With the operating principle of the TES discussed in Chapter 2, the model construction of a TES tank will only be discussed.

Model construction of a TES tank

The mathematical model of a TES tank is developed by making use of both mass balance and the energy balance equations [12].

Mass balance equation:

According to the mass balance equation of any volumetric tank, the product of the fluid density and the change in volume over the change in time is equal to the difference in the flow rates of the fluid entering and exiting the tank. Applying this equation to a TES tank gives (3.14) [12]:

$$\rho \frac{dV_t}{dt} = \dot{m}_{TESin} - \dot{m}_{TESout} \tag{3.14}$$

where ρ is the density of the fluid, dV/dt is the change in the total volume of the fluid inside the tank; $\dot{m}_{TESin}$ and $\dot{m}_{TESout}$ are the mass flow rates of the fluid entering and exiting the TES tank.

Energy balance equation:

The energy balance equation can be determined by rewriting (3.14) with the heat capacity and the temperature of the fluid multiplied into (3.14). Added to the manipulation of (3.14) is the effect of the losses that needs to be included, which is introduced due to the walls of the tank as well as the temperature of the air surrounding the tank absorbing some of the energy [12].

The new derived mass energy balance equation is given by [12]:

$$\rho Q c_p T_{in} = \rho V_t \frac{dT}{dt} + \rho Q c_p T_{out} - AU_{loss}(T_{out} - T_{amb}) \tag{3.15}$$

where T_{in}, T_{out}, T_{amb} is the temperature of the fluid entering the tank, exiting the tank, and the ambient temperature respectively. cp is the specific heat of the fluid, AU_{loss} is the product of the area of the tank wall multiplied by the heat transfer coefficient of the tank wall; and Q is the flow rate of the fluid.

In order to calculate the volume of the tank, the fluid flow rate as well as the density of the fluid inside the tank needs to be calculated. The flow rate is calculated with (3.16) [47]:

$$Q = \frac{\dot{m}_{fluid}}{\rho} \tag{3.16}$$

where $\dot{m}_{fluid}$ is the mass flow rate of the fluid. The density of the fluid ρ is calculated with (3.17) [47]:

$$\rho = \frac{p_{abs}}{RT_{abs}} \tag{3.17}$$

where p_{abs} is the absolute pressure of the fluid in the tank, R is the specific gas constant of the fluid, and T_{abs} is the absolute temperature of the fluid in Kelvin.

The input/output diagram of a TES tank is shown in Figure 3.13. Basically it constitutes the mass flow rate of the fluid entering and exiting the tank as well as the ambient temperature surrounding the tank.

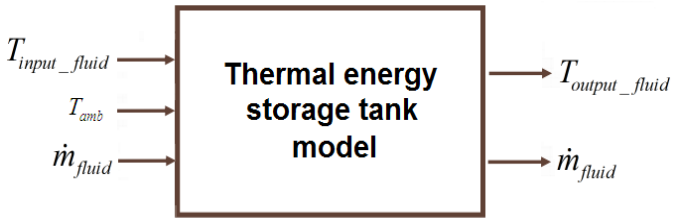

Figure 3.13: Input/output diagram of the TES tank

3.4.2 Sizing of the thermal energy storage tank

The model development of the thermal energy storage was implemented in Flownex by making use of Flownex's standard reservoir component. The specifications of the TES tank obtained from the TRNSYS model requires that while the gas turbines are running, the exhaust gasses of the turbines should flow through the tank at a desired mass flow rate of 13.88 kg/s whilst charging and 0.12 kg/s when fully charged. As soon as the gas turbines stop, the direction of the gasses flowing through the tank reverses in direction, flowing at a mass flow rate of 13.888 kg/s in the opposite direction. This mass flow rate is maintained as long as the temperature of the gasses inside the tank is above a set value. The second specification is that the tank should be charged fully within 8 hours during the day.

The size specification of the reservoir is implemented by making use of both the mass balance equation as well as the energy balance equation mentioned above. In order to decrease the complexity of the calculations a few assumptions, in terms of the properties of the model, has to be made. These assumptions include:

Since the mass flow rates of the exhaust gasses flowing into and out of the tank eventually becomes the same once the tank reaches steady state, it will be assumed that the mass flow rates are equal from the start ($\dot{m}_{TESin} = \dot{m}_{TESout}$). With the mass flow rates of the gasses flowing into and out of the tank assumed to be the same, it can further be assumed that the volume of the gasses in the tank stays the same. With the volume of the tank being at a constant value, the mass balance equation can be ruled out.

An important property that the Flownex reservoir component conforms to, and should be mentioned, is the fact that the fluids inside the tank are completely mixed. In other words, the temperature of the fluid inside the tank is equal to the fluid exiting the tank. This is an important property since unmixed fluids would result in additional calculations that will have to be made.

With all the assumptions included into the design, the mass energy equation can be used to determine the volume at which the tank has to be specified at by rewriting (3.15):

$$V = \frac{Q(T_{in} - T_{out})dt}{dT} \tag{3.18}$$

The volume of the tank is calculated by first obtaining the flow rate and the density of the fluid inside the tank by making use of (3.16) and (3.17). To calculate the density of the fluid, the input pressure of the TES tank is chosen to be at 2 bar which is due to a pressure drop of the turbines from 10 bar. The specific gas constant of the mixed gasses used is obtained from the properties of air in Flownex. The temperature range of the fluid inside the TES tank, as specified by TRNSYS documentation, ranges between $400\ ℃$ and $620\ ℃$:

$$\begin{aligned}\rho &= \frac{P}{RT} \\ &= \frac{2000}{1.2\times(620+274)} \\ &= 1.8621\ \text{kg/m}^3\end{aligned}$$

The flow rate of the exhaust gasses with a mass flow rate of 13.888 kg/s is given by:

$$\begin{aligned}Q &= \frac{\dot{m}}{\rho} \\ &= \frac{13.888}{1.8621} \\ &= 7.458\ \text{m}^3/\text{s}\end{aligned}$$

Finally, the volume of the tank can be calculated by substituting the calculated flow rate of the mixed gasses into (3.18):

$$\begin{aligned}V &= \frac{Q(T_{in} - T_{out})dt}{dT} \\ &= 7.458\times 28800 \\ &= 214786.253\ \text{m}^3\end{aligned}$$

3.4.3 Simulation/Verification of the thermal energy storage tank

The simulation setup of the TES tank is implemented by connecting two pipes, one at the input and one at the output of the tank, with a boundary condition connected to the input of the tank which specifies the temperature of the gasses entering the tank. The duration of the simulation was set at 12 hours to represent the full 12 hours of the day. The simulation of the discharge phase of the tank is not included in the simulation since the amount of thermal energy that is extracted from the tank is determined by the amount of energy used by the Rankine cycle. Figure 3.14 shows the resultant charge rate of the TES tank.

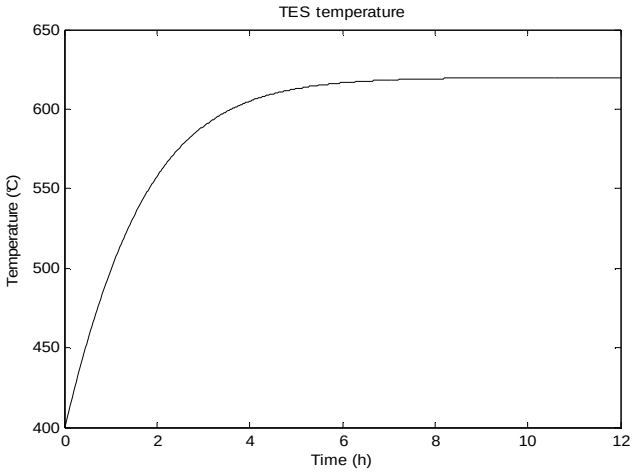

Figure 3.14: TES tank charging cycle

From Figure 3.14 it can be seen that the temperature response of the TES conforms to that expected from the model, which is a over damped second order response. This can be seen in Figure 3.14 with the temperature of the gasses inside the tank increasing from the initial $400\ ^{\circ}C$ as the time continues. After 8 hours of the simulation, it can be seen that the temperature of the gasses inside the tank reaches its steady state temperature of $620\ ^{\circ}C$ as expected.

3.5 Conclusion

The methodology for successfully selecting and specifying the size of each component of the Brayton cycle, so as to produce the same responses as that of the validated model, was implemented by: first obtaining the literature surrounding each component, followed by the implementation of the sizing of the component from the specifications. Finally, the components were simulated to verify that the components are correctly selected and sized.

Chapter 4: Rankine cycle component selection and sizing

As mentioned in chapter 3, the use of a model producing responses close to that of an actual model is necessary during the characterisation process of any model. Chapter 4 will continue with the process of developing a Flownex simulation model of a combined cycle Concentrated Solar Power CSP plant by discussing the selection and sizing of all the components that constitute that of the Rankine cycle part of the plant. In order to do so, all the needed literature, implementation procedures as well as the needed simulations to verify that the correct components are selected for the simulation design will be included, starting with a discussion on the process of developing the model of the Rankine cycle.

4.1 Rankine cycle model development

The same process followed in chapter 3 guides the development of the Rankine cycle model: Documented responses of the validated Transient Simulations (TRNSYS) model along with supporting literature on each of the components used in the model is used to "translate" the responses into useful information to specify the sizing of each component. The model is developed to modulate the same responses as that of the TRNYS model with the same operational input signals substituted into the model. The next section will explain the process of selecting and sizing each of the components of the cycle.

4.1.1 Rankine cycle component selection and sizing

The Rankine cycle constitutes four main components which include: a boiler, steam turbine, condenser and a boiler feed pump as seen in Figure 4.1. The selection of these components is based on both the type of components typically used in a Rankine cycle as well as the specific

components used in the TRNSYS model to keep the Flownex model in line with the TRNSYS model.

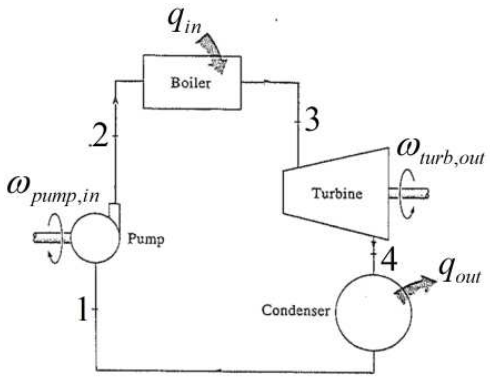

Figure 4.1: Rankine cycle component diagram

The process of sizing these components to produce the correct responses involves a three-phase process. The first phase of this process is to obtain literature on both the working principle as well as the model construction of the component being sized. Once the appropriate literature is obtained, the implementation phase (second phase) can commence. The implementation phase involves using the model construction of the component along with the documented responses of the TRNSYS model to calculate the parametric values of the component. Verification of the component (third phase) takes the form of simulating each component and comparing the responses of the component to the theoretically expected results of the model based on supporting literature.

Once again, as discussed in chapter 3, it is important to note that the pipes of the model being constructed should be sized as close as possible to an ideal pipe to have little or no influence on the dynamic response of the system. The size specification of each of the mentioned components of the Rankine cycle will now be discussed, starting with the sizing of the steam turbines.

4.2 Rankine cycle component sizing: Steam turbines

The function of the steam turbines of the Rankine cycle is to convert the thermal energy of the superheated steam exiting the boiler into rotational (mechanical) energy, which is used to drive a generator in order to generate electricity [46].

4.2.1 Literature on steam turbines

Due to the structure of a steam turbine being more or less the same as that of the gas turbine, and due to the fact that Flownex only has one generic model for both turbine types, the literature of the steam turbines is the same as that of the gas turbines discussed in 3.3.1.

Model construction of the steam turbines:

The model construction used to modulate the pressure ratios of steam turbines does however differ from that of gas turbines. This is due to the difference in the properties of both fluids, with the fluid of the Brayton cycle remaining in one phase (gas), while the fluid of the Rankine cycle alternates between two phases (fluid and gas) as it circulates through the cycle. The model construction of the components of the Rankine cycle can be obtained by making use of the principles of the temperature vs. entropy curve of the cycle, as seen in Figure 4.2, where points 1 to 4 represent the temperature and entropy of the fluid flowing through each component of the cycle.

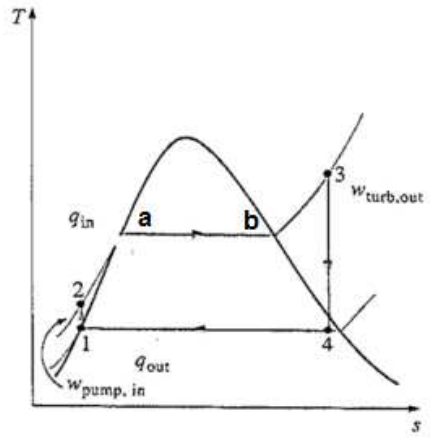

Figure 4.2: Rankine temperature vs. entropy curve [13]

The temperature and entropy of the superheated steam entering the steam turbines can be represented at point 3 in Figure 4.2, and the steam exiting the steam turbines, after most of its thermal energy has been transferred, can be represented at point 4 [13]. To decrease the complexity of the model, it is assumed that the turbines function under ideal circumstances. This includes the entropy of the steam assumed to be constant as it flows through the turbines, whilst the pressure and temperature of the steam exiting the turbines decreases due to the transfer of thermal energy to the turbines.

The model construction of the steam turbines is still represented by (3.9), but in order to calculate the amount of work done by the steam turbines the entropy and enthalpy of the steam entering and exiting the turbines need to be determined. To do so the temperature vs. entropy curve can be used.

Due to the difference in the properties of the steam at point 3, with the steam only containing dry superheated steam, and the steam at point 4, which contains a mixture of water and steam with a certain fluid to gas ratio, the approach of deriving the entropy and enthalpy of the steam can differ. The entropy and enthalpy of the dry steam at point 3 can be obtained from lookup tables known as superheated steam tables, whereas the entropy and enthalpy of the wet steam can be derived

from making use of a combination of saturated steam tables and (4.1) and (4.2) where the entropy of the wet steam is given by [48]:

$$s_4 = s_f + x(s_g - s_f) \tag{4.1}$$

where subscript *f* is for a fluid state and *g* is for a gas state. x is the fluid to gas ratio.

The enthalpy of steam at point 4 is given by:

$$h_4 = h_f + x(h_g - h_f) \tag{4.2}$$

The resultant input/output diagram of the different parameters of the turbine is shown in Figure 4.3:

Figure 4.3: Input/output diagram of a turbine

4.2.2 Sizing of the steam turbines

The development of the steam turbines are implemented in Flownex by making use of Flownex's standard turbine model found in its component library. The size specification of the high pressure, intermediate pressure, and low pressure turbines are based on the documented TRNSYS model results which requires that the temperature of the steam entering the high pressure turbine should be $500\,°C$ with the steam flowing through the turbines at a mass flow rate of 5 kg/s, whilst producing a combined power output of 6.5 MW.

With the intention of decreasing the complexity of calculating the pressure ratios of each turbine, due to the fact that all three turbines of the cycle perform the same function at different temperatures and pressures, all three of the turbines will first be considered as one combined turbine model. After the combined pressure ratio has been calculated, the pressure ratios of each turbine will be derived from this pressure ratio.

Due to the type of information made available from the TRNSYS documentation, calculating the pressure ratio of the combined turbine model involves calculating the pressure of the fluid entering and exiting the model. In order to do so, the enthalpy of the steam needs to be calculated first. This is since the pressure of the fluid can be obtained from the steam tables once the temperature and enthalpy of the fluid is known.

The enthalpy of the steam exiting the steam turbine is calculated by finding a suitable gas to fluid ratio that is not specified too low, since it would result in larger amounts of fluid build-up on the turbine blades, and too high which would result in a reduction of the amount of the thermal energy being transferred to the turbines. By making use of the saturated steam table (Table 4.1), the ratio can be obtained by selecting an entropy value, that is between the boundaries of the fluid at its gas

(8.331 kJ) and fluid state (0.521 kJ), as well as a pressure value for the steam. Let us select the entropy and pressure of the fluid to be equal to 7 kJ and 0.06 bar respectively.

Table 4.1: Saturated steam table

SATURATED STEAM - PRESSURE TABLE									
		Spec. vol. m^3=kg		Int. Ener. kJ/kg		Enthalpy kJ/kg		Entropy kJ=(kg°K)	
P bar	T °C	Sat. liq. v_f X1000	Sat. vap. v_g	Sat. liq. u_f	Sat. vap. u_g	Sat. liq. h_f	Sat. vap. h_g	Sat. liq. s_f	Sat. vap. s_g
0.06	36.15	1.006	23.75	151.5	2425	151.5	2567	0.521	8.331

By rewriting (4.1) the gas to fluid ratio will be:

$$\begin{aligned} x &= \frac{s_4 - s_f}{s_g - s_f} \\ &= \frac{7 - 0.521}{8.331 - 0.521} \\ &= 0.82 \end{aligned}$$

Selecting the pressure of the steam exiting the turbine to be at 0.06 bar, and the entropy of the fluid to be equal to 7 kJ results in a gas to fluid ratio of 82 % which is adequate for the design.

The enthalpy of the steam exiting the turbines at a pressure of 0.06 bar which will be used for the design of the condenser is calculated by making use of both (4.2) as well as Table 4.1:

$$\begin{aligned} h_4 &= h_f + x(h_g - h_f) \\ &= 151.5 + 0.83(2567 - 151.5) \\ &= 2132.21 \text{ kJ/kg} \end{aligned}$$

where h_4 is the enthalpy of the steam exiting the low pressure turbine, as seen at point 4 in Figure 4.2.

By rewriting (3.9), the total work done by the combined turbine model can be calculated. This is done to calculate the enthalpy of the fluid entering the model:

$$\begin{aligned} W &= \frac{P}{\dot{m}} \\ &= \frac{6.5 \times 10^6}{5} \\ &= 1300 \text{ kJ/kg} \end{aligned}$$

The total work done by the turbine model is thus equal to 1300 kJ/kg. With the total amount of work done by the turbines known, (3.10) can be used to calculate the enthalpy of the fluid entering the turbine model.

$$\begin{aligned} h_3 &= W + h_4 \\ &= 1300 + 2180.52 \\ &= 3432.21 \text{ kJ/kg} \end{aligned}$$

With the enthalpy of the fluid entering the turbine calculated, the fluid pressure can also be determined by reading the pressure value from the super-heated steam tables (Table 4.2) where the enthalpy of the fluid is more or less the same as h_3 at a temperature of $500\ °\text{C}$.

Table 4.2: Superheated steam table

SUPERHEATED STEAM

v in m^3=kg, u in kJ/kg, h in kJ/kg, s in kJ=(kg°K)

P= 40 bar

T	v	u	h	s
500	0.0864	3100	3445	7.090

From Table 4.2 it is noted that the pressure of the fluid entering the steam turbine is around 40 bar. What can also be noted is that the entropy of the superheated steam also averages around 7 kJ which is the same as the entropy of the steam exiting the turbine, which is as expected.

With the input pressure as well as the output pressure of the turbine model obtained, the pressure ratio of the model can be calculated by dividing the pressure of the steam entering the turbine by the pressure of the steam exiting the model:

$$\begin{aligned} pr &= \frac{p_{in}}{p_{out}} \\ &= \frac{40}{0.06} \\ &= 667 \end{aligned}$$

The pressure ratio of the combined turbine model is much too large to be practically implemented into a single turbine since the maximum pressure ratio that a turbine can be specified at is about 50 times smaller than the value calculated. An additional amount of turbines added to the system reduces the pressure ratio of each turbine.

The pressure ratio of each of the three turbines is determined in such a way as to have the largest pressure fall at the low-pressure turbine. This is since the turbines must be designed to have the least amount of fluid to build up, since at lower pressures the steam starts forming droplets. For this reason the pressure ratios of the turbines are selected to be 3.5, 6.5 and 29.3 respectively to produce a 59.94 bar pressure drop in the steam pressure.

4.2.3 Simulation/Verification of steam turbines

The simulation setup of the steam turbines is implemented in Flownex by making use of Flownex's standard turbines with superheated steam flowing through each turbine. All three turbines are connected in series to represent the three different stages (high pressure, intermediate pressure and low pressure). The boiler, which heats up the water into steam, is modelled by making use of a

boundary condition specifying the temperature of the fluid entering the high pressure turbine. The mass flow rate of the steam flowing through the turbines is altered by manipulating the pressure input of the steam entering the high pressure turbine.

The simulation of the steam turbine is implemented in Flownex by setting the temperature input of the boundary condition connected to the turbine at a fixed temperature of $500\ °C$, with the mass flow rate of the steam flowing through the cycle set to 5 kg/s at maximum power delivery and 0 kg/s at minimum power delivery. The simulated step response in the power output of the turbines is shown in Figure 4.4 with the pressure input of the turbines altered.

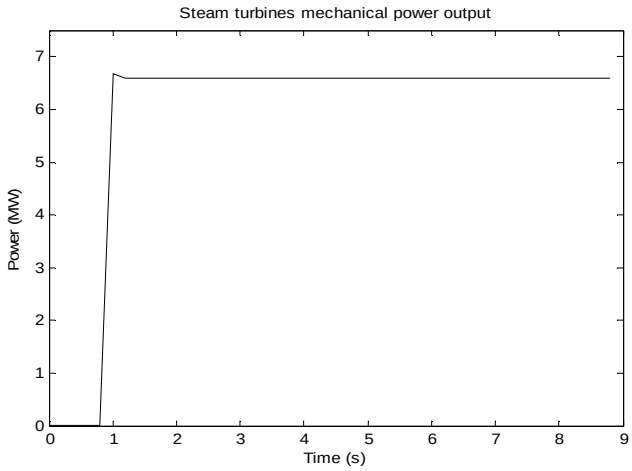

Figure 4.4: Steam turbine power output

From Figure 4.4 it can be noted that the combined power generated by the turbines produces a constant power output of 6.5 MW once the turbines reached steady state.

4.3 Rankine cycle component sizing: Condenser

The function of the condenser is to remove the remainder of the thermal energy from the steam exiting the low pressure turbine up to an enthalpy where the fluid returns to its liquid form, in order for the boiler feed pump to be able to circulate the water through the cycle. The next section will discuss the process of sizing the condenser of the cycle by first discussing some supporting literature on condensers.

4.3.1 Literature on condensers

The cooling of the induced steam exiting the steam turbines plays an important part in a plant when ensuring stable control of the amount of steam generated by the boilers. Cooling involves making use of either two heat exchangers, namely a condenser and a cooling tower, which is used in indirect cooling condensers, or a single heat exchanger, namely an air-cooled condenser which is used in direct cooling condensers. Figure 4.5 illustrates the concept of a condenser as a heat

exchanger where cool water flows from the cooling tower (cooling water inlet) through the condenser and back to the cooling tower (cooling water outlet) [15].

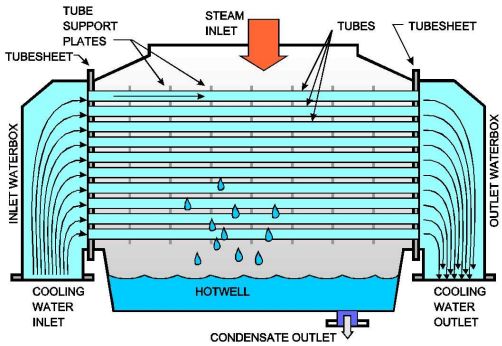

Figure 4.5: Steam condenser model [15]

Cooling towers are responsible for extracting the heat introduced to the cooling water from the condenser by transferring the induced heat of the cooling water to another medium. The medium can either be air, which is known as dry cooling, water cooling, which is known as wet cooling, or a combination of both, which is known as hybrid cooling [49]. Figure 4.6 illustrates a hybrid-cooling tower, where the cooling water circulates through a heat exchanger coil while a combination of air and water is passed over the coil to cool down the cooling water.

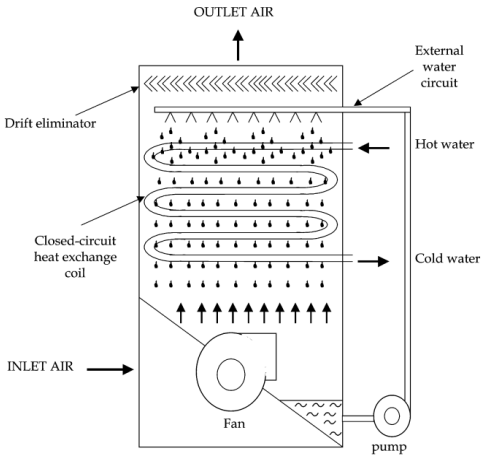

Figure 4.6: Hybrid cooling tower

Model construction of a condenser:

The model construction of a condenser is developed by making use of a specially designed method called the effectiveness Number of Transfer Units (NTU) method. This method can be used since the condenser is a heat exchanger. This method was developed specifically for the purpose of determining the different temperatures of the heat exchanger, without the use of trial and error. This method utilises an effectiveness equation to solve the responses of a heat exchanger [50]. The model construction of a condenser is thus an efficiency equation, which is given by (4.3).

$$\varepsilon = \frac{\dot{Q}}{\dot{Q}_{\max}} \tag{4.3}$$

where $\dot{Q}$ is the heat transfer rate and $\dot{Q}_{\max}$ is the maximum heat transfer rate of the heat exchanger. Both these two values can be calculated by making use of (4.4) and (4.5). The value of $\dot{Q}$ is given by:

$$\dot{Q} = \dot{m}_{fluid}(h_{in} - h_{out}) \tag{4.4}$$

where h_{in} is the enthalpy of the steam entering the primary side of the heat exchanger, h_{out} is the enthalpy of the water exiting the heat exchanger and $\dot{m}_{fluid}$ is the mass flow rate of the fluid flowing through the exchanger.

$\dot{Q}_{\max}$ is given by:

$$\dot{Q}_{\max} = C_{\min}\Delta T_{\max} \tag{4.5}$$

where $C_{\min}$ is the minimum heat capacitance of the fluid and $\Delta T_{\max}$ is the maximum temperature difference. Both these values are given by equations (4.6) and (4.7):

$\Delta T_{\max}$ is given by:

$$\Delta T_{\max} = (T_{\max} - T_{\min}) \tag{4.6}$$

where $T_{\max}$ is the maximum temperature input or output to the heat exchanger and $T_{\min}$ is the minimum temperature input or output to the heat exchanger.

$C_{\min}$ is given by:

$$C_{\min} = \min(C_{cool\_water}, C_{steam}) \tag{4.7}$$

where C_{cool_water} is the heat capacitance of the cooling water flowing through the secondary side of the condenser and C_{steam} is the heat capacitance of the steam flowing at the primary side of the heat exchanger.

The input/output diagram of a condenser is shown in Figure 4.7, which forms that of a heat exchanger.

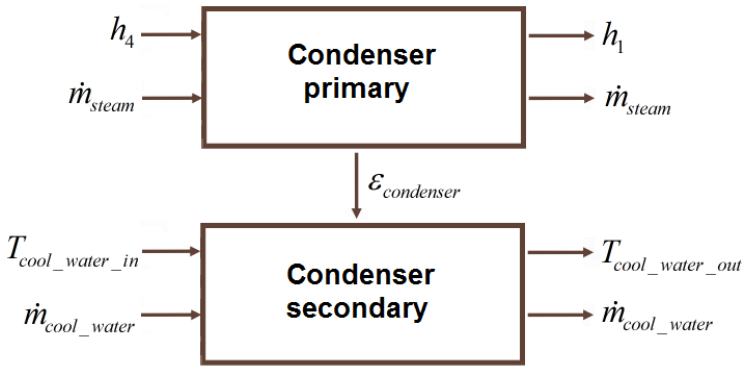

Figure 4.7: Input/output diagram of the condenser

4.3.2 Sizing of the condensers

The development of the condenser is implemented in Flownex by making use of Flownex's standard heat exchangers found in its component library. The sizing specification of the condenser is based on the documented TRNSYS model results for which no specifications are documented from the TRNSYS model in terms of the responses of the condenser, except for the mass flow rate of the steam flowing through the cycle. The only guideline available for the sizing of the condenser is the fact that the remainder of the energy in the steam should be extracted in order for the steam to change its phase back to water again. Thus the gas to fluid ratio should be zero for only water to be present.

In order to simplify calculations it will be assumed that the condenser functions under ideal conditions. This involves the pressure and temperature of the steam entering and exiting the condenser to be considered the same. With this in mind the pressure of the steam entering and the water exiting the condenser is at 0.06 bar, from the turbine calculations. The temperature of the fluid entering and exiting the condenser will be maintained at a temperature of $36.2\ ^{\circ}\mathrm{C}$ from Table 4.1.

The sizing of the condenser is implemented by making use of both the effective-NTU method as well as the temperature vs. entropy curve, where points 4 and 1 in Figure 4.2 represent the enthalpy of the steam entering and exiting the condenser, to serve as a guideline for calculating the efficiency of the heat exchanger. The efficiency of the heat exchanger is calculated by obtaining the actual heat transfer rate ($\dot{Q}$) and the maximum heat transfer rate ($\dot{Q}_{\max}$). In order to do so the enthalpy of the fluid entering and exiting the condenser need to be calculated first.

The mass flow rate of the steam flowing through the primary side of the heat exchanger is set to $\dot{m}_{steam} = 5\ \mathrm{kg/s}$ which is obtained from the results of the TRNSYS model.

The enthalpy of the steam entering the condenser, calculated in section 4.3.1, is equal to $h_4 = 2030.759\ \mathrm{J/kg}$. The only unknown variable is the enthalpy h_1 of the fluid exiting the primary

side of the condenser. Since both the temperature as well as the pressure of the fluid entering and exiting the condenser is known, and the fluid to gas ratio is equal to 0 %, the enthalpy h_1 can be calculated by making use of (4.2):

$$\begin{aligned} h_1 &= h_f + x(h_g - h_f) \\ &= 151.5 + 0(2567 - 151.5) \\ &= 151.5 \text{ kJ/kg} \end{aligned}$$

With the value of h_1 now known the value of $\dot{Q}$ can now be calculated:

$$\begin{aligned} \dot{Q} &= \dot{m}_{steam}(h_4 - h_1) \\ &= 5(2030.759 - 151.5) \\ &= 9.396 \text{ kW} \end{aligned}$$

By making use of (4.5) the value of $\dot{Q}_{\max}$ can be calculated. In order to do so the values of $\Delta T_{\max}$ and $C_{\min}$ must first be calculated by using (4.6) and (4.7):

$$\begin{aligned} \Delta T_{\max} &= (T_{\max} - T_{\min}) \\ &= (36.2 - 28) \\ &= 8.2 \text{ °C} \end{aligned}$$

In order to determine the value of $C_{\min}$, the smallest heat capacitance value between both the steam as well as the cooling water must be obtained. The heat capacitance of the cooling water with a specific heat of $cp_{cool\_water} = 4.184 \text{ kJ/kg} \cdot \text{K}$ and the mass flow rate of $\dot{m}_{cooling\_water} = 1 \text{ kg/s}$ is given by:

$$\begin{aligned} C_{cool\_water} &= \dot{m}_{cool\_water} cp_{cool\_water} \\ &= 1 \times 4.184 \\ &= 4.184 \text{ J/K} \end{aligned}$$

The heat capacitance of the steam with a specific heat of $cp_{steam} = 4.184 \text{ kJ/kg} \cdot \text{K}$ and a mass flow rate of $\dot{m}_{steam} = 5 \text{ kg/s}$ is given by:

$$\begin{aligned} C_{steam} &= \dot{m}_{steam} cp_{steam} \\ &= 5 \times 4.184 \\ &= 20.92 \text{ J/K} \end{aligned}$$

The value of $C_{\min}$ used to calculate $\dot{Q}_{\max}$ is thus the heat capacity value of the cooling water since it has the smallest value. The value of $\dot{Q}_{\max}$ is thus equal to:

$$\begin{aligned}\dot{Q}_{\max} &= C_{\min}\Delta T_{\max} \\ &= 4.184 \times 8.2 \\ &= 34.3088 \text{ kW}\end{aligned}$$

The efficiency of the heat exchanger can thus be calculated by making use of (4.3):

$$\begin{aligned}\varepsilon &= \frac{\dot{Q}}{\dot{Q}_{\max}} \\ &= \frac{9.396}{34.3088} \\ &= 0.2738\end{aligned}$$

The resultant efficiency of the condenser heat exchanger used is thus 27.38 %.

4.3.3 Simulation/verification of the condensers

The simulation setup of the condenser in Flownex proves to be a challenge on its own due to the fact that Flownex's evaporator cannot simulate phase changing fluids as it is supposed to. The standard heat exchangers of Flownex also cannot simulate a phase change which is a required function due to the fact that it is required for the condenser. In order to simulate the phase of the steam changing into water an alternative approach is used. Making use of a two phase tank placed before a heat exchanger with an efficiency equal to that calculated in 4.3.2 seems to solve the problem.

The implementation of the condenser further constitutes making use of a boundary condition specifying the enthalpy and pressure of the steam flowing into the condenser model, which now constitutes a two phase tank and a heat exchanger. The secondary side of the heat exchanger has two boundary conditions, one specifying the temperature and the other specifying the mass flow rate of the cooling water flowing through the condenser.

The simulation of the condenser is implemented by setting the boundary condition of the steam entering the condenser to have an enthalpy of 2030.759 kJ/kg at a pressure of 0.06 bar. The boundary conditions of the cooling water side of the heat exchanger is set to have a temperature of 28 °C at a pressure of 1 bar, whilst maintaining a mass flow rate of 1 kg/s. The enthalpy of the water exiting the condenser is simulated by simulating a step response in the mass flow rate of the steam flowing through the primary side of the condenser, from 5 kg/s to 7 kg/s. Figure 4.8 shows the enthalpy of the water exiting the condenser.

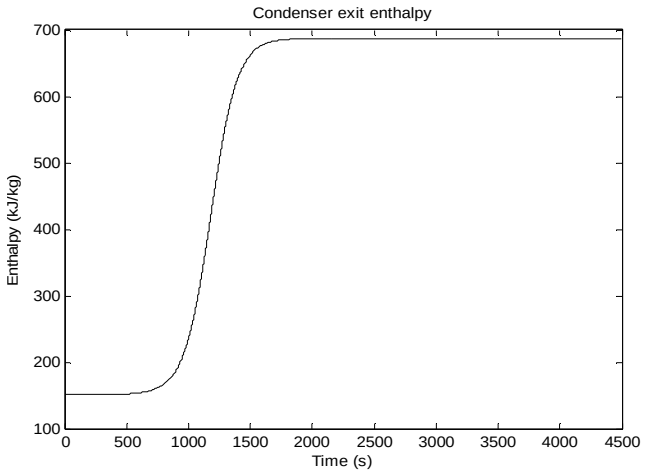

Figure 4.8: Condenser downstream water enthalpy

From Figure 4.8 it can be seen that the enthalpy of the water exiting the condenser, at a mass flow rate of 5 kg/s, settles at 151 kJ/kg as is required from the condenser. It can also be noted that an increase in the mass flow rate of the steam flowing through the condenser results in an increase in the enthalpy of the water exiting the condenser. The same applies for a decrease in the mass flow rate. This is due to the residence time changing, which influences the heat transfer rate, as the mass flow rate changes.

4.4 Rankine cycle component sizing: Boiler feed pump

The function of the boiler feed pump is to circulate the water flowing through the cycle, and specifically to provide high-pressure water for the boiler which feeds the turbines with steam. As the boiler feed pump circulates water through the cycle, it increases the temperature and pressure of the water exiting the pump. The next section will discuss the process of sizing the boiler feed pump of the cycle by first discussing some supporting literature on a boiler feed pump.

4.4.1 Literature on boiler feed pumps

The use of a pump to circulate and increase the pressure of the water flowing through the cycle has several advantages. One of these advantages includes being capable of altering the mass flow rate of the fluid flowing through the entire cycle. This ultimately alters the power output of the turbines due to the change in pressure of the steam entering the turbines. Another advantage is the power consumption of the boiler feed pump compared to that of the compressor of the gas turbines. Due to the fact that saturated water is denser compared to that of gas in gas turbines, less power is required to pump the water through the cycle.

The typical power consumption of the boiler feed pump ranges between 2 % to 5 % of the total power generated whereas the power consumption of the compressor of the Brayton cycle can consume up to 20 % of the generated power. Let us now discuss the model construction of a boiler feed pump.

Model construction of the pump:

The sizing of the boiler feed pump involves calculating the speed that the pump rotates at, and for this reason the model construction of the boiler feed pump should be constructed in such a way that the model contains the speed of a pump. The model construction of a pump is given by (4.8):

$$N = \frac{N_s (H)^{\frac{3}{4}}}{\sqrt{Q}} \tag{4.8}$$

where N_s is the specific speed, Q is the volume flow rate and H is the head of the pump which is given by (4.9):

$$H = \frac{W_{pump}}{g} \tag{4.9}$$

where g is the gravitational acceleration and W_{pump} is the total work done by the pump which is given by the difference in the enthalpy of the fluid exiting (h_2) and entering (h_1) the pump:

$$W_{pump} = h_2 - h_1 \tag{4.10}$$

The volume flow rate of the pump is calculated using (4.11):

$$Q = \frac{3960 \times P}{H} \tag{4.11}$$

where P is the power consumed by the pump, which is given by (4.12):

$$P = \dot{m} W_{pump} \tag{4.12}$$

where $\dot{m}$ is the mass flow rate of the water flowing through the pump.

The input/output diagram of the boiler feed pump constitutes three input parameters and two output parameters including the pressure and enthalpy of the fluid entering and exiting the pump along with the work done on the fluid. Figure 4.9 illustrates the model construction of a pump:

Figure 4.9: Input/output diagram of the pump

4.4.2 Sizing of the boiler feed pump

The development of the boiler feed pump is implemented in Flownex by making use of Flownex's standard variable speed pumps found in its component library. The sizing specification of the pump is based on the documented TRNSYS model results for which the following: no specifications are

documented from the TRNSYS model in terms of the responses of the pump, is included. The only guideline available for the sizing of the pump is the fact that the pump must increase the pressure of the water flowing though it from 0.06 bar up to 40 bar which is the pressure of the steam entering the steam turbines.

Calculating the speed of the pump involves calculating each of the parameters discussed above. Before doing so, the pressure and temperature of the water exiting the pump needs to be selected to determine the enthalpy of the water exiting the pump. Selecting the water to be at a pressure of 40 bar and a temperature of $46\ ^{\circ}\mathrm{C}$ results in the enthalpy of the water to be 196.09 kJ/kg when reading the values from the water tables.

Now that the enthalpy of the water entering the pump, from the condenser calculations, and the enthalpy of the water exiting the pump is known, the total work done by the pump can be calculated:

$$\begin{aligned} W_{pump} &= h_2 - h_1 \\ &= 196.09 - 151.5 \\ &= 44.59\ \mathrm{kJ/kg} \end{aligned}$$

Next the power consumption, and the head of the pump can be calculated by using (4.12) and (4.9). Power consumption:

$$\begin{aligned} P &= \dot{m} W_{pump} \\ &= 5 \times 44.59 \\ &= 222.95\ \mathrm{W} \end{aligned}$$

Pump head:

$$\begin{aligned} H &= \frac{W_{pump}}{g} \\ &= \frac{44.95}{9.81} \\ &= 4.582\ \mathrm{m} \end{aligned}$$

The volume flow rate of the pump is given by:

$$\begin{aligned} Q &= \frac{3960 \times P}{H} \\ &= \frac{3960 \times 222.95}{4.582} \\ &= 4.931 \times 10^{-3}\ \mathrm{m^3/s} \end{aligned}$$

Finally the speed of the pump can be calculated, with the specific speed of the pump of 1450 obtained from properties of the variable speed pump in Flownex. In order to calculate the speed of the pump, the values should first be converted into standard units.

$$N = \frac{N_s (H)^{\frac{3}{4}}}{\sqrt{Q}}$$
$$= \frac{1450 \times 47^{\frac{3}{4}}}{\sqrt{78.154}}$$
$$= 2926.887 \text{ rpm}$$

The speed of the pump is thus equal to 2926.887 rpm.

4.4.3 Simulation/Verification of the boiler feed pump

The simulation setup of the boiler feed pump is implemented in Flownex by making use of Flownex's standard variable speed pump with water flowing through the pump at a mass flow rate set by specifying the rpm value of the pump. In order to specify the properties of the water entering the pump, a boundary condition is used. The head of the pump is specified by setting the elevation of one of the upstream pipes to the calculated value.

The simulation of the boiler feed pump is implemented in Flownex by simulating the change in pressure of the water exiting the pump by altering the speed of the pump. Figure 4.10 illustrates the change in the pressure of the water flowing through the pump as the mass flow rate of the pump increases from 0 kg/s to 5kg/s.

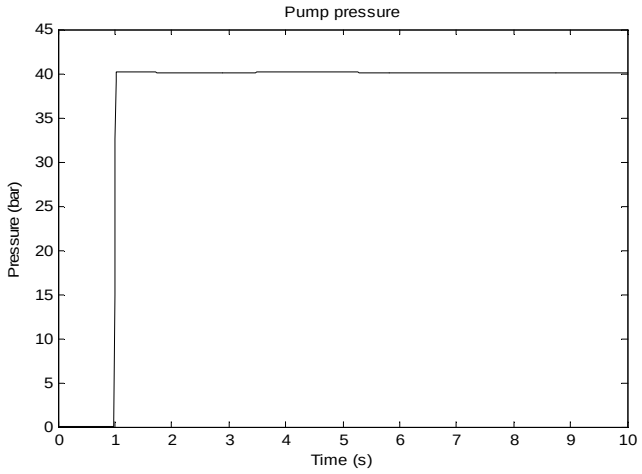

Figure 4.10: Pump pressure response

From Figure 4.10 it can be noted that the pressure output of the boiler feed pump settles around 40 bar at its maximum speed as expected.

4.5 Rankine cycle component sizing: Boiler

The boiler of the Rankine cycle, which constituted an economiser, evaporator and a super heater, has the function of generating the steam required to drive the turbines from the water exiting the boiler feed pump. Heating is implemented by transferring thermal energy to the water by means of

heat exchangers. The next section will discuss the process of sizing the heat exchangers of the boiler by first discussing some supporting literature.

4.5.1 Literature on boiler heat exchangers

Heat exchangers can be categorised into three types of thermal energy transfer components including: direct contact type, storage type and direct transfer type. The differences in the function of these types will now be discussed:

Direct contact type: Direct contact type heat exchangers are usually used when the two heat exchange mediums are normally one of a gas type medium, and one of a liquid type medium. The use of two different fluids results in a decrease in the mixture of the two fluids [51].

Storage type: Storage type heat exchangers work more or less the same as that of a thermal energy storage (TES) tank where two fluids flows through the heat exchanger at separate time intervals. Its operation consists of one fluid first being pumped through the heat exchanger, where the heat of the fluid is then transferred to the storage medium. Once enough energy is transferred to the storage medium, the flow of the fluid is stopped and the remaining fluid is then drained. After all the liquid is drained, the next fluid is pumped through the exchanger where the energy from the storage medium is then transferred to the fluid through convection. This process is repeated several times [51].

Direct transfer type: The direct transfer type heat exchangers are the most common types of heat exchangers used in power station applications. Unlike the first two types of heat exchangers, a direct transfer type heat exchanger completely isolates the different fluids from one another. There are three shapes of direct transfer heat exchangers namely a tubular shape, plate shape, and an extended surface shape direct transfer heat exchanger [51].

The heat exchangers of a boiler is not only categorised by its structure, but also by the direction in which the fluid flows through the exchanger, which has an influence on the temperature response of the exchanger, can also be categorised.

Direction of working fluid paths

There are three types of flow path arrangements for the working fluids used in heat exchanger design. These arrangements include: parallel flow, counter flow and cross flow.

A parallel flow heat exchanger has its working fluids flowing in the same direction, whilst counter flow heat exchangers have their working fluids flowing in opposite directions. Cross flow heat exchangers have their fluid paths crossing each other [51]. Figure 4.9 gives a representation of parallel and counter flow heat exchangers.

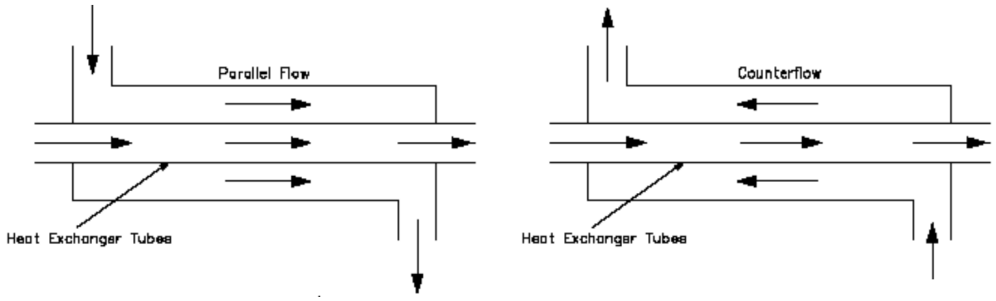

Figure 4.11: Parallel flow vs. counter flow heat exchangers [51]

Parallel flow heat exchangers are less efficient due to its disadvantages which include: due to the larger difference in the temperature between the two inlet points of the working fluids, larger thermal stresses can result in the exchanger. Secondly, the parallel flow exchanger is less efficient due to the fact that the output temperature of the secondary working fluid can never exceed the temperature of the output temperature of the primary working fluid, due to its arrangement. This results in less energy capable of being transferred to the secondary working fluid [51]. Figure 4.12 gives the temperature profile of both arrangements of the heat exchangers:

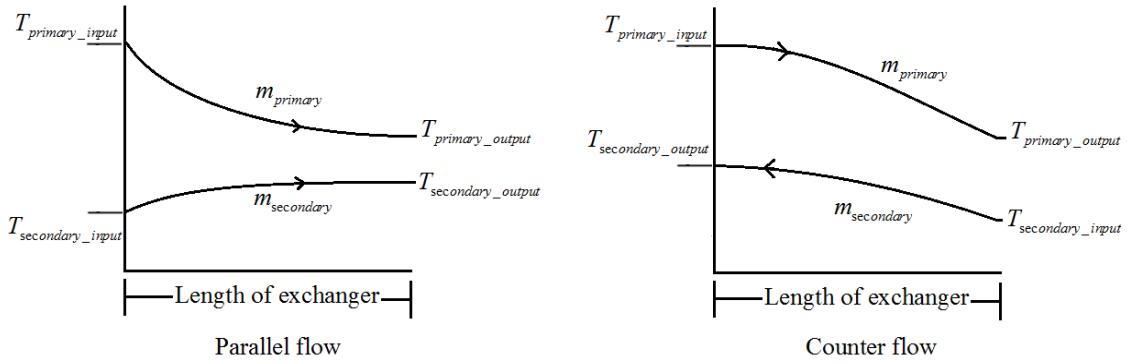

Figure 4.12: Counter flow vs. parallel flow thermal profiles

The boilers of a combined cycle plant transfers most of the remaining thermal energy from the mixed gasses exiting both the gas turbines as well as of the TES tanks to all the components of the Rankine cycle without mixing the two fluids [51]. The boiler can be divided into three heat exchangers which in combination increases the efficiency of the boiler since heat exchangers have a maximum value at which its efficiency can be specified. By connecting these heat exchangers in a counter flow arrangement also increases the efficiency of the boiler.

The mathematical model construction of the boiler heat exchangers used is the same as that of the condenser, where the effectiveness NTU method can again be used to derive the effectiveness specifications of the heat exchangers used.

Model construction of a boiler:

The same model construction used for the condenser can be used to model each of the heat exchangers of the boiler. This is since the exact same heat exchanger construction is used for the

boiler and the condenser. This also results in the same efficiency expression used to calculate the efficiency specification of each of the heat exchangers of the boiler.

The input/output diagram used to illustrate the inputs and outputs of the boiler is seen in Figure 4.13.

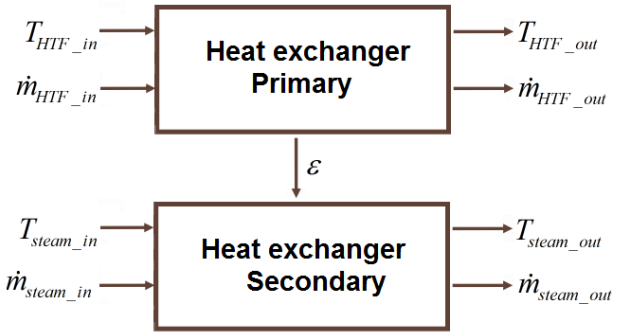

Figure 4.13: Input/output diagram of each heat exchanger of the boiler

4.5.2 Sizing of the boiler heat exchangers

The development of the boiler's heat exchangers is implemented in Flownex by making use of Flownex's standard heat exchangers found in its component library. The sizing specification of each of the three heat exchangers is based on the documented TRNSYS model results which requires that the super-heated steam at a pressure of 40 bar should be at a temperature of 500 ℃ while the steam flows through the heat exchangers at a mass flow rate of 5 kg/s.

The sizing of the heat exchangers will constitute calculating the efficiency of each heat exchanger. In order to do so the efficiency equations discussed in 4.3, along with the temperature vs. entropy curve in Figure 4.2 will be used to determine the efficiency of each heat exchanger. Point (2) in Figure 4.2 represents the fluid exiting the water pump, point (a) represents the steam exiting the economizer and entering the evaporator, point (b) represents the steam exiting the evaporator and entering the super heater, and point (3) represents the super heated steam exiting the super heater.

To calculate the efficiency of each heat exchanger, some assumptions must first be made in order to simplify the calculations:

It will be assumed that the model of each heat exchanger will function under ideal circumstances. As a result hereof the pressure and temperature of the fluids entering and exiting the evaporator are assumed to be constant ($T_{evaporator\_in} = T_{evaporator\_out}$ and $p_{evaporator\_in} = p_{evaporator\_out}$). In addition, the mass flow rates of the fluids entering and exiting all the heat exchangers are also assumed to be the same ($\dot{m}_{fluid,in} = \dot{m}_{fluid,out}$).

With both the pressure and temperature of the steam exiting the super heater known, the efficiency of the super heater can be calculated by making use of (4.3). In order to do so the $\dot{Q}_{super-heater}$ value must be calculated first by making use of (4.4), where $h_3 = 3374\ \text{kJ/kg}$ from the superheated steam tables (Table 4.1), and the mass flow rate of the steam flowing through the heat exchangers is set at 5 kg/s from the TRNSYS results.

The enthalpy h_b of the steam entering the super-heater is determined from the saturated steam tables (Table 4.3) where the pressure of the steam is set at 40 bar.

Table 4.3: saturated steam table 2

SATURATED STEAM - PRESSURE TABLE									
		Spec. vol. m^3=kg		Int. Ener. kJ/kg		Enthalpy kJ/kg		Entropy kJ=(kg°K)	
P bar	T °C	Sat. liq. v_f X1000	Sat. vap. v_g	Sat. liq. u_f	Sat. vap. u_g	Sat. liq. h_f	Sat. vap. h_g	Sat. liq. s_f	Sat. vap. s_g
40	250.4	1.252	0.050	1082	2602	1087	2801	2.796	6.070

From Table 4.3 it can be seen that the enthalpy of the steam entering the super heater is equal to $h_b = 2801\ \text{kJ/kg}$ with no fluid in the mixture.

The value of $\dot{Q}_{super-heater}$ is thus equal to:

$$\begin{aligned}\dot{Q}_{super\_heater} &= \dot{m}_{steam}(h_3 - h_b)\\ &= 5\times(3374-2801)\\ &= 2870\ \text{kW}\end{aligned}$$

The value of $\dot{Q}_{super-heater\_\max}$ can be calculated by first obtaining the minimum heat capacitance value $C_{super-heater\_\min}$ which is given by (4.7). The value of $C_{super\_heater\_steam}$ at a temperature of $500\ °\text{C}$ is calculated as follows:

$$\begin{aligned}C_{super-heated\_steam} &= \dot{m}_{steam}c_{p\ steam}\\ &= 5\times 2.8\\ &= 14\ \text{J/K}\end{aligned}$$

The value of C_{mixed_gasses}, which is the heat capacitance of the mixed gasses of the Brayton cycle with a mass flow rate of 14 kg/s and a specific heat of 2.1 kJ/kg.K, is calculated as follows:

$$\begin{aligned}C_{mixed\_gasses} &= \dot{m}_{mixed\_gasses}c_{p\ mixed\_gasses}\\ &= 14\times 2.1\\ &= 29.4\ \text{J/K}\end{aligned}$$

Since the heat capacitance of the steam is the smallest, it will be used to calculate the value of $\dot{Q}_{super-heater\_max}$:

$$\begin{aligned}\dot{Q}_{super-heater\,max} &= C_{super-heated\_steam}\Delta T_{super-heater\_max}\\ &= 14\times(500-212.4)\\ &= 4026.4\ \text{kW}\end{aligned}$$

The efficiency of the super-heater can thus be calculated by making use of (4.3):

$$\begin{aligned}\varepsilon_{super\_heater} &= \frac{\dot{Q}_{super-heater}}{\dot{Q}_{super-heater\_max}}\\ &= \frac{2870}{4026.4}\\ &= 71.28\%\end{aligned}$$

The temperature of the mixed gasses exiting the super heater is calculated by rewriting (4.4):

$$\begin{aligned}T_{MG\_SH\_exit} &= T_{MG\_SH\_input} - \frac{\dot{Q}_{super-heater}}{\dot{m}_{mixed\_gasses}cp_{mixed\_gasses}}\\ &= 500-\frac{2870}{14\times 2.1}\\ &= 426.785\ ^{\circ}\text{C}\end{aligned}$$

The efficiency of both the economiser as well as the evaporator is calculated by following the same process used to calculate the efficiency of the super-heater. Table 4.4 gives all the calculated data for all three heat exchangers:

Table 4.4: Boiler heat exchanger parameters

	Super heater	Evaporator	Economiser
$c_{p\ steam}$	2.8 kJ / kg.K	5.9 kJ / kg.K	4.41 kJ / kg.K
$c_{p\ mixed\_gasses}$	2.1 kJ / kg.K	2.1 kJ / kg.K	2.1 kJ / kg.K
C_{steam}	14 J/K	29.5 J/K	22.03 J/K
C_{mixed_gasses}	29.4 J/K	29.4 J/K	29.4 J/K
$C_{\min}$	14 J/K	29.4 J/K	22.03 J/K
$h_{in(steam)}$	2800 kJ/kg	1087.42 kJ/kg	193.99 kJ/kg
$h_{out(steam)}$	3374 kJ/kg	2800 kJ/kg	908.8 kJ/kg
$T_{in(steam)}$	212.4 °C	250.4 °C	46 °C

$T_{out(steam)}$	500 °C	250.4 °C	250.4 °C
$T_{in(mixed\_gasses)}$	500 °C	426.79 °C	80.75 °C
$T_{out(mixed\_gasses)}$	426.79 °C	80.75 °C	22.73 °C
$\dot{m}_{steam}$	5 kg/s	5 kg/s	5 kg/s
$\dot{m}_{mixed\_gasses}$	14 kg/s	14 kg/s	14 kg/s
$\dot{Q}$	2870 kW	9456 kW	3574.05 kW
$\dot{Q}_{\max}$	4026.4 kW	10173.49 kW	4177.48 kW
ε	71.28 %	92.9 %	92.74 %

Now that the sizing of each of the heat exchangers of the boiler has been calculated, the simulations to verify the response of the boiler can be implemented.

4.5.3 Simulation/Verification of the boiler heat exchangers

The simulation setup of the boiler heat exchanger is implemented in Flownex by making use of the same components used in the simulation of the condenser with the addition of two extra heat exchangers to resemble that of the economiser, evaporator, and the super-heater. In order to specify the properties of the water entering the boiler, a boundary condition will be used to specify both the temperature as well as the pressure of the water entering the boiler. The mass flow rate of the water/steam flowing through the boiler is set by specifying the mass flow rate of the water flowing through one of the upstream pipes. Each of the heat exchangers used are specified the efficiencies calculated in 4.5.2.

The simulation of the boiler is implemented in Flownex by simulating the change in the temperature of the water exiting the super-heater with changes made to the mass flow rate of the water/steam flowing through the boiler. Figure 4.14 illustrates the change in the temperature of the water flowing through the boiler as the mass flow rate of the water increases from 0.1 kg/s to 5 kg/s.

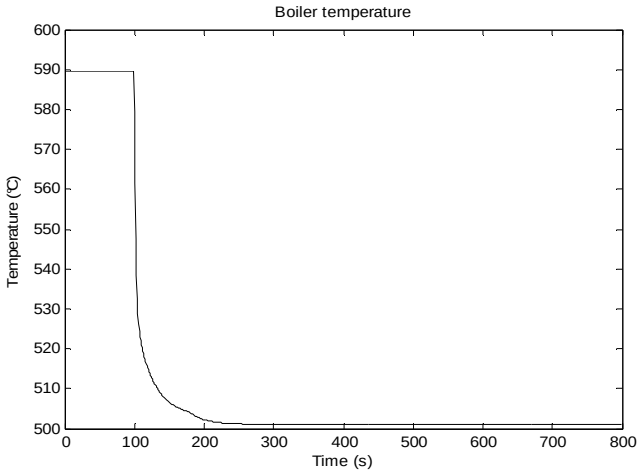

Figure 4.14: Boiler temperature response

From Figure 4.14 it can be seen that the temperature of the steam exiting the boiler settles just above $500\,℃$ at a mass flow rate of 5 kg/s. What can also be noted is the decrease in the temperature of the steam as the mass flow rate of the water increases. This is due to the residence time changing, which influences the heat transfer rate as the mass flow rate changes.

4.6 Conclusion

The methodology for successfully selecting and specifying the size of each component of the Rankine cycle so as to produce the same responses as that of the validated model was implemented by first obtaining the literature surrounding each component, followed by the implementation of the sizing of the component from the specifications. Finally the components were simulated to verify that it was correctly selected and sized.

Chapter 5: Combined cycle model integration

With the selecting, sizing, and verifying each of the components of both the Rankine and the Brayton cycle discussed in the previous chapters, the integration of these components to form a combined cycle Concentrated Solar Power (CSP) plant can be implemented. Chapter 5 discusses the integration process by first discussing the integration of the components of each cycle followed by the integration of the two cycles. To validate the model of the combined cycle plant, the major components are simulated with its results compared to that of the TRNSYS model.

5.1 Component integration

The process of integrating each of the different components to form both the Rankine as well as the Brayton cycle will now be discussed, starting with the Brayton cycle:

5.1.1 Brayton cycle component integration

The Brayton cycle, which forms the primary side of the plant, is developed by interconnecting each of the components selected and sized in Chapter 3. These components include: a Solar Collector Field (SCF), two gas turbines, a Thermal Energy Storage (TES) tank, a boiler, two compressors and a duct burner with its controller as seen in Figure 5.1.

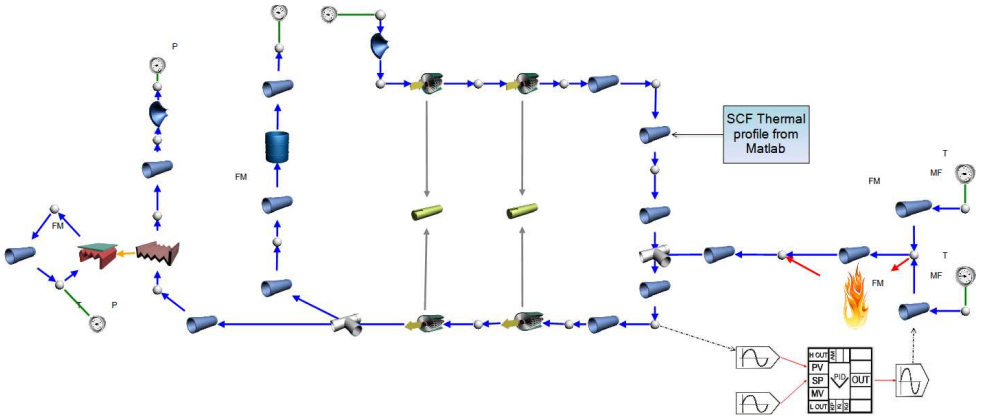

Figure 5.1: Brayton cycle

The selected fluid circulating through the cycle is mixed gasses, constituting both air as well as combustion gasses, with a mass flow rate set by adjusting the open/close position of the flow restrictor connected to the input of the upstream compressor. The verification of the cycle involves simulating the cycle with a step response in the mass flow rate of the mixed gasses flowing through the gas turbines, and measuring the resultant mechanical power output. Figure 5.2 illustrates the resultant power output of the gas turbines with a step response of 1.1 kg/s to 1.6 kg/s simulated.

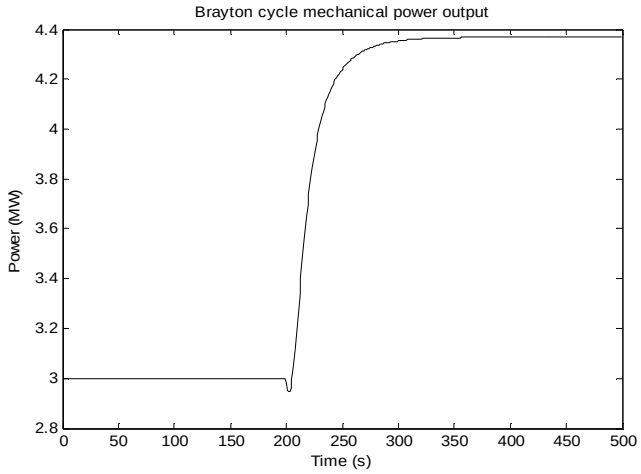

Figure 5.2: Brayton cycle mechanical power output step response

From Figure 5.2 it can be seen that the mechanical power output of the gas turbines, with a step response in the mass flow rate of the air flowing through the cycle simulated, forms a non-minimum phase response which is as expected.

5.1.2 Rankine cycle component integration

The Rankine cycle, which forms the secondary side of the plant, is developed by interconnecting each the components selected and sized in Chapter 4. These components include: an economiser, an evaporator, a super heater, low pressure- intermediate pressure- and high pressure- turbines, a condenser, and a boiler feed pump as seen in Figure 5.3:

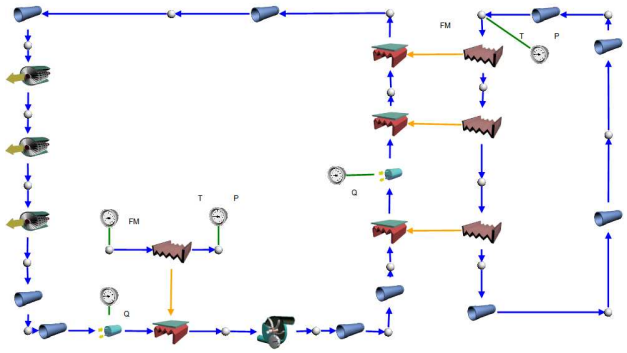

Figure 5.3: Rankine cycle

The selected fluid circulating through the cycle is water with its mass flow rate set by adjusting the speed (rpm) of the feed pump. The verification of the Rankine cycle involves simulating the cycle with a step response in the mass flow rate of the water flowing through the cycle, and measuring the resultant mechanical power output of the turbines.

The thermal energy source to the cycle, for this simulation purpose, is made by making use of a boundary condition, at the primary side of the boiler, specifying the temperature of the source to the cycle at $600\ ^{\circ}\mathrm{C}$. Figure 5.4 illustrates the resultant power output response of the cycle with a step in the speed of the feed pump simulated. The mass flow rate of the water flowing through the cycle is stepped from 0.01 kg/s to 0.2 kg/s.

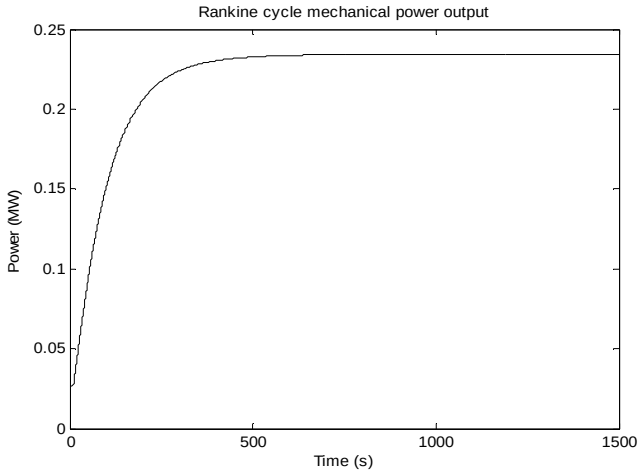

Figure 5.4: Rankine cycle mechanical power step response

From Figure 5.4 it can be seen that the power output of the steam turbines, with a step response in the mass flow rate of the steam flowing through the cycle, forms that of a over damped second order system which is as expected.

5.2 System integration

With each of the components of both the Rankine cycle as well as the Brayton cycle integrated and simulated with step responses so as to verify that both cycles perform as they ought to, the two cycles can be integrated to form the combined cycle model.

5.2.1 Combined cycle system integration

The integration of the two cycles involves replacing the Brayton cycle's heat exchanger, at the exhaust of the gas turbines, with the heat exchangers of the Rankine cycle with the primary side of the boiler connected to the gas turbine exhaust gasses. This process results in the Brayton cycle forming the source of thermal energy to the Rankine cycle. Figure 5.5 illustrates the resultant integrated model of the combined cycle CSP plant.

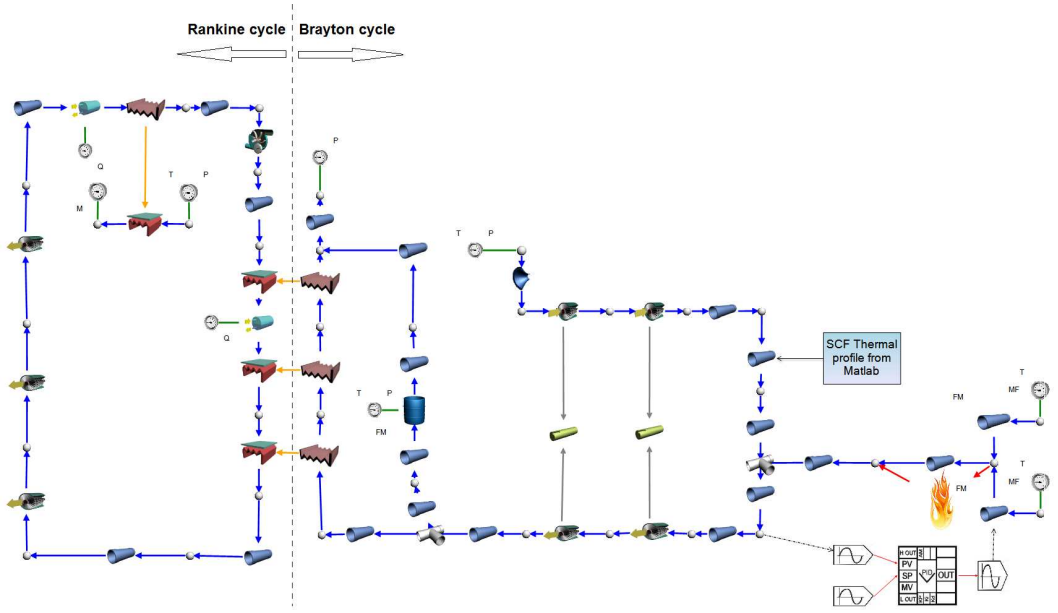

Figure 5.5: Flownex model of a combined cycle CSP plant.

From Figure 5.5 it can be seen that each of the components interconnected to each other forms both the primary side (right-side of the line) and the secondary side (left side of the line) of the plant. The power output of the plant is determined by the sum of all five turbines' mechanical power outputs.

To ensure that each of the components are interconnected correctly, and to ensure that the correct parametric values have been specified to each of the components a method of validation is required. The next section will discuss both the methodology as well as the implementation of validating the model.

5.3 Combined cycle model validation

The methodology used to validate the Flownex model constitutes using the bench mark (TRNSYS) model's responses as the desired responses which the Flownex model has to be able to produce with the same input signals specified. This is made possible due to the University of Stellenbosch's renewable energy division who helped provide the necessary information to produce the required responses.

To determine whether the responses are the same, the data of both the TRNSYS model as well as the Flownex model will be plotted on the same graph. This will serve the purpose of illustrating that the resultant responses match, which then ultimately represents the validation of the model.

In order to extract and plot the resultant responses, a series of simulations must be implemented to obtain the appropriate responses. The simulation responses of both models will be plotted by making use of Matlab®. This is done since Matlab® is capable of plotting two graphs over each other even if the lengths of the matrices differ due to different sampling rates used in both simulation platforms.

The next section discusses the validation of the developed model, but since the simulation results can only be compared if the same input signals are used, the input signals will first be defined and validated.

5.3.1 Model input signal validation

The input signals to a plant form an important aspect of the plant. This is since these signals are used to alter the dynamic responses of the plant. The main input signal used to alter the output responses of the plant include altering the mass flow rate of the fluids flowing through the various components. The next section will discuss the different input signals of the plant:

Input signal 1: Primary mass flow rate.

The first input signal simulated is the mass flow rate of the mixed gasses flowing through the gas turbines. This flow rate is the sum of the Heat Transfer Fluid (HTF), which is air, flowing through the compressor and the SCF, and the combustion gasses flowing into the system from the duct burner. The input signal is altered by either adjusting the position of the flow restrictor of the compressor or by adjusting the amount of fuel added to the system.

The mass flow rates selected is set to be the same as that of the TRNSYS model. Figure 5.6 illustrates the resultant input signal responses of the primary mass flow rate input signal:

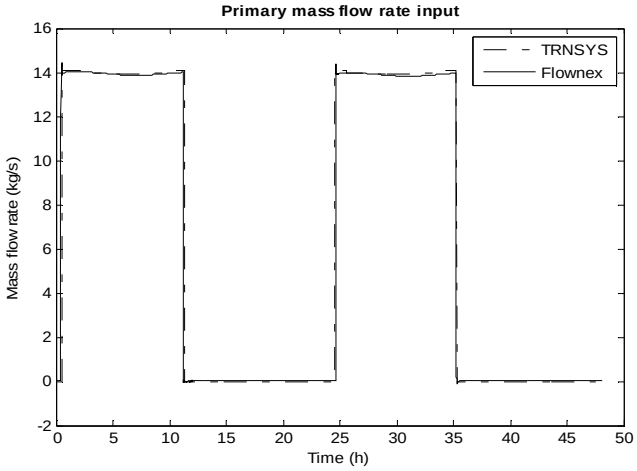

Figure 5.6: Primary mass flow rate input

As seen in Figure 5.6, both the mass flow rate inputs of the Flownex model as well as the TRNSYS model is satisfyingly close to each other. The difference in the magnitude between the two models is due to different controllers used to control the amount of fuel added to the system.

Input signal 2: TES mass flow rate.

The next input signal simulated is the mass flow rate of the mixed gasses flowing through the TES tank as the tank charges or discharges. This input is set by adjusting the flow rate of one of the inline pipes. The simulation of this input signal is made in such a way that the input signal of the Flownex model is as close as possible to that of the TRNSYS model. Figure 5.7 illustrates the resultant mass flow rate input signals of both models:

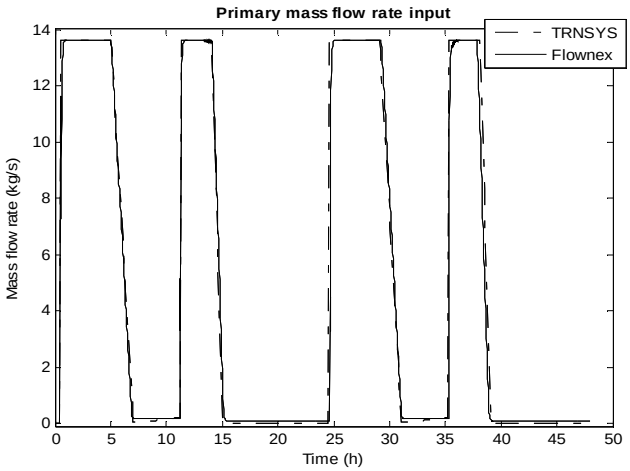

Figure 5.7: TES mass flow rate input

As seen in Figure 5.7 both the mass flow rate input signals of the Flownex model and the TRNSYS model correspond quite well.

Input signal 3: Secondary mass flow rate.

The third input signal simulated is the mass flow rate of the water flowing through the components of the Rankine cycle. This input is set by adjusting the speed of the boiler feed pump which

manipulates the flow rate. Figure 5.8 illustrates the resultant mass flow rate input signals of both the Flownex as well as the TRNSYS model.

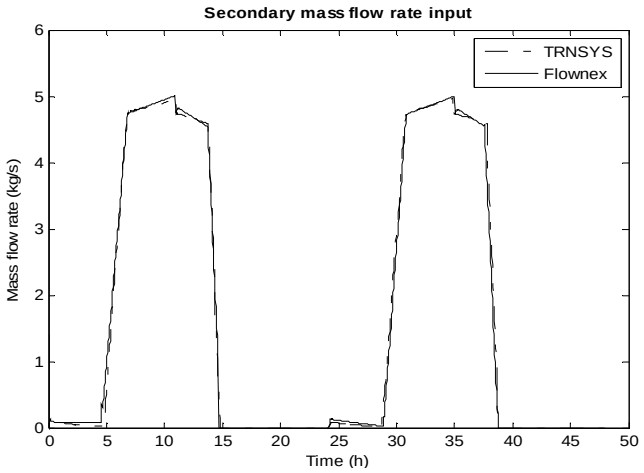

Figure 5.8: Secondary mass flow rate input

From Figure 5.8 it can be seen that the mass flow rates of both models are satisfyingly close.

The mass flow rate of the fluids flowing through each of the various components does not form the only input signals to the model. Another input signal includes the thermal energy input from the solar radiation absorbed by the SCF.

Input signal 4: Solar thermal energy profile.

The solar thermal energy input profile of the SCF forms the main thermal energy source to the entire plant. The response of this signal, which is a temperature response signal, is dependent on a large number of factors that influence its response as discussed in Chapter 2. The resulting SCF temperature profile, with the same mass flow rate and thermal energy input signals used, of both the TRNSYS as well as the Flownex model can be seen in Figure 5.9:

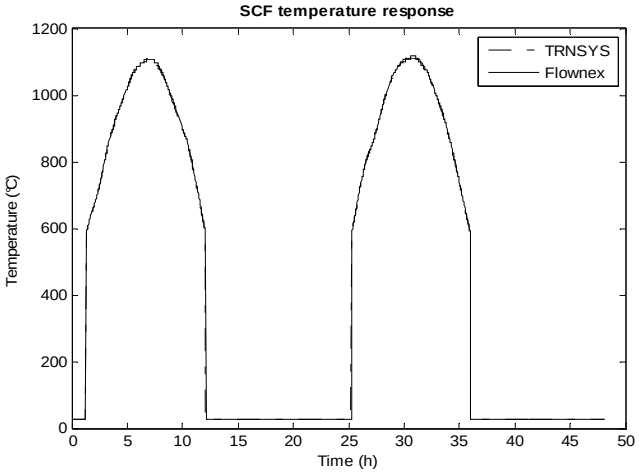

Figure 5.9: HCE temperature profile

From Figure 5.9 it can be seen that both models have their temperature profiles matching quite well.

With all the input signals to the plant defined and validated, the model itself can be validated by making use of the bottom-up process, discussed in Chapter 2, where validation of the components will first be implemented which is then followed by the validation of the model at system level. The next section will discuss the validation of each of the major components of the integrated plant model.

5.3.2 Component level validation

The validation of the model at component level constitute comparing the responses of the benchmark model (TRNSYS) to that of the Flownex model with the same input signals used for both models, as that which has been defined in the previous section.

The duct burner:

The first simulated component is the duct burner. The main prerequisite for the burner is that the output temperature of the HTF must be kept constant at $1500\,°C$ by controlling the amount of additional fuel added to the system while the sun is shining. If the sun is not shining, no additional amount of fuel is to be added to the system. Figure 5.10 illustrates the resultant temperature responses of the mixed gasses exiting the junction where the air from the SCF and the combustion gasses, from the duct burner, mix from both the TRNSYS model and the Flownex model.

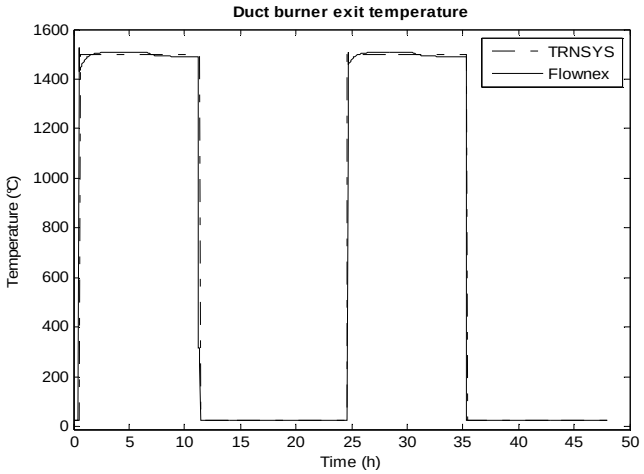

Figure 5.10: Temperature of the HTF exiting the burner

From Figure 5.10 it can be seen that the temperature response of the Flownex model has a good match to that of the TRNSYS model. The difference in the temperature is due to the different controllers used. The TRNSYS model makes use of an iterative feedback controller, whereas the Flownex model makes use of a Proportional Integral (PI) controller.

The gas turbines:

The next simulated components are the gas turbines of the Brayton cycle. The mixed gasses, from the duct burner and the SCF, flows through the turbines at a mass flow rate equal to that of the primary mass flow input signal. The validation of the gas turbines involves simulating the power output of the turbines as well as the output temperature response of the turbine since it forms the input to the downstream components. Figure 5.11 illustrates the power output of the gas turbines of both the TRNSYS and the Flownex model:

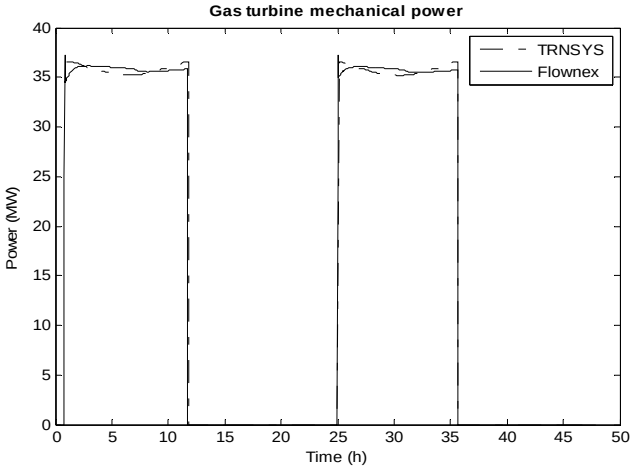

Figure 5.11: Gas turbine power output

From Figure 5.11 it can be seen that the Flownex model matches the power output responses of the TRNSYS model. The small difference in the responses, however, is due to the difference in both the gas temperature and mass flow rate between both models.

The next simulated response of the gas turbines is the temperature of the mixed gasses exiting the downstream gas turbine. The TRNSYS model specifies the temperature response to be at $600\ ^{\circ}C$ during the day, whilst the primary mass flow rate input is fully switched on, and $26\ ^{\circ}C$ during the night, when the primary mass flow rate input is fully switched off. Figure 5.12 illustrates the resultant temperature response of both the TRNSYS model and the Flownex model.

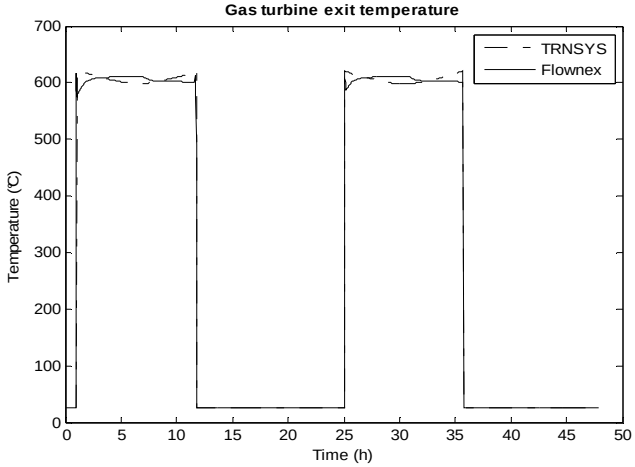

Figure 5.12: Gas turbine outlet temperature

In Figure 5.12 it can be seen that the temperatures of both models match, and the difference in the responses is due to the input temperature and mass flow rate differences.

The TES tank:

The next component validated includes the TES tank. The mixed gasses flow through the tank at a mass flow rate determined by the TES mass flow rate input signal. The temperature of the mixed gasses entering the tank is dependant of the temperature of the gasses exiting the downstream gas turbine during the day when the primary mass flow rate is on. Figure 5.13 illustrates the temperature response of the TES tanks of both the Flownex and the TRNSYS model:

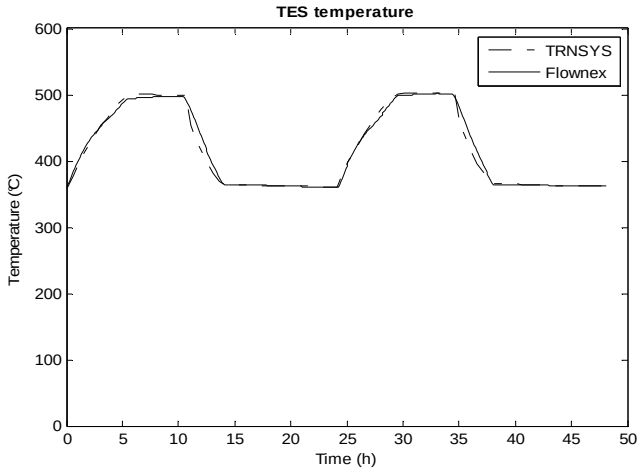

Figure 5.13: TES tank temperature

In Figure 5.13 it can be seen that both models produce the same temperature profile during both the charging and discharge cycles. What can be noted is the small difference in the temperature of the TES during its discharge phase.

The boiler:

The validation of the boiler is next. During the day, the boiler is supplied with thermal energy by the exhaust gasses of the gas turbines, and during the night, the boiler is supplied by the TES tank. The simulation of the boiler is implemented by measuring the temperatures of the superheated steam exiting the heat exchanger. Figure 5.14 illustrates the temperature response of the superheated steam exiting the boiler of both the Flownex and TRNSYS models.

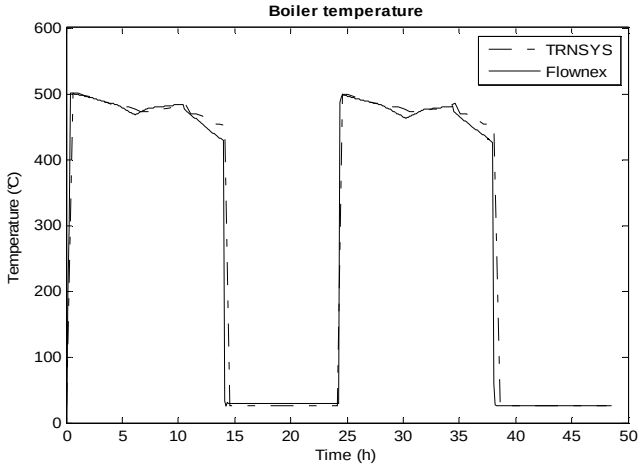

Figure 5.14: Boiler temperature response

From Figure 5.14 it can be seen that the temperature responses of both models match. The only part that does not fully match is when the temperature of the boiler decreases due to the TES tank temperature discharging.

The steam turbines:

The next components simulated are the steam turbines of the Rankine cycle. The steam exiting the boiler now enters the steam turbines at a mass flow rate equal to that of the secondary mass flow rate input signal. Figure 5.15 illustrates the combined mechanical power output of all three of the steam turbines of both the Flownex and the TRNSYS model.

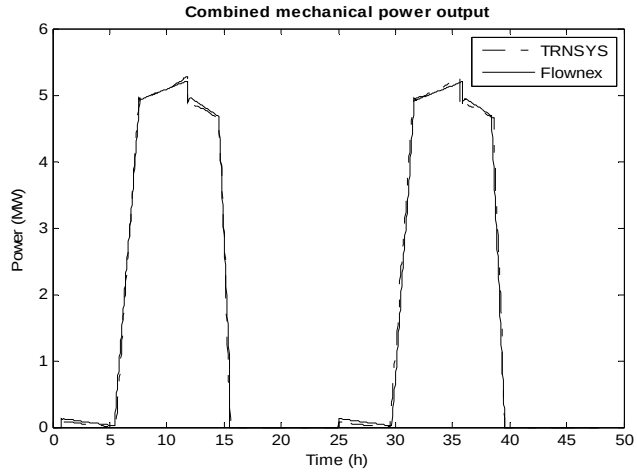

Figure 5.15: Combined steam turbine power output

As seen in Figure 5.15 the power outputs of both the models correspond quite well.

Boiler feed pump:

The last component validated is the boiler feed pump which circulates the water through the cycle. The validation of the boiler feed pump is implemented by simulating the pressure response of the pump. Figure 5.16 illustrates the pressure response of the water exiting the pump of both the Flownex and TRNSYS model:

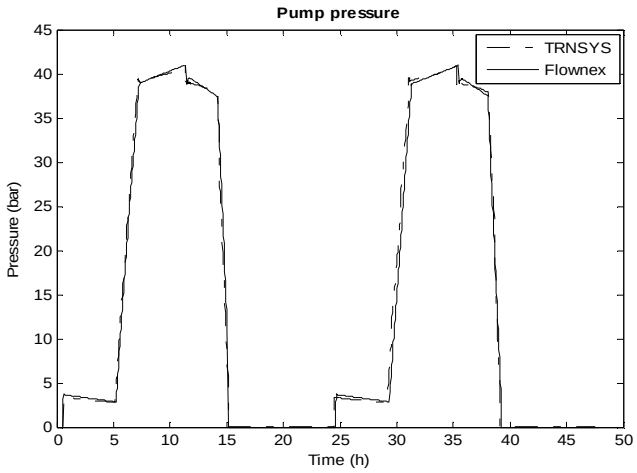

Figure 5.16: Pump pressure exit pressure

In Figure 5.16 it can be seen that the resultant pressure response of both the TRNSYS model as well as the Flownex model corresponds well.

5.3.3 System level validation

The validation of the model at a system level involves simulating the mechanical power output of all the turbines in the model and comparing the responses to that of the TRNSYS model. This includes the sum of the mechanical power output of all the turbines. Figure 5.17 illustrates the mechanical power output of both the TRNSYS and the Flownex model.

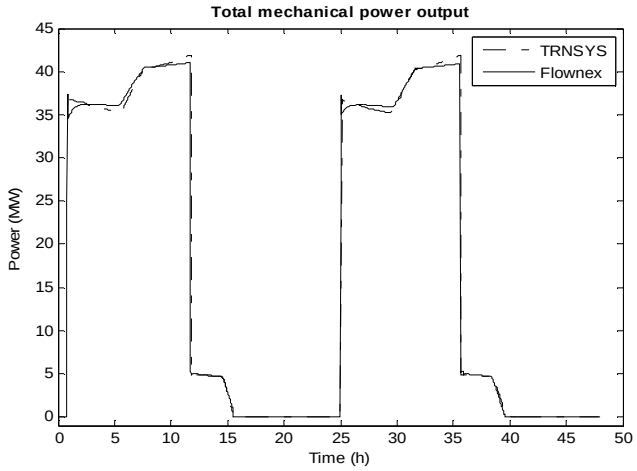

Figure 5.17: Combined cycle power output

The resultant power output seen in Figure 5.17 shows a close correlation between the responses of both the TRNSYS model as well as the Flownex model.

5.4 Conclusion

Based on Root Square Mean Error (RSME) calculations made for each of the measured responses of the Flownex and TRNSYS model, it can be concluded that an acceptable percentage deviation

between the two data sets (ranging between 1.78 and 6.1%) exist. The differences between the two models can however be explained. The largest cause of differences in the responses of the system can be assigned to the different controllers used between the models which controls the amount of fuel added to the system.

Chapter 6: Dynamic model characterisation

Now that a complete model of the Concentrated Solar Power (CSP) plant has been developed and validated, the process of characterising the plant, to gain insight in to the dynamic responses unique to that of a CSP plant, can be implemented. Before doing so, both the importance as well as the process of characterising the plant will be discussed.

6.1 Importance of CSP plant dynamic characterisation

The dynamic behaviour of a system provides us with important information concerning the system's reaction to certain changes made to its input signals. This information is important to understand, especially when developing a controller for the plant, which deals with the task of manipulating the behaviour of dynamical systems to satisfy certain desired responses from the system.

The capability of a power station being able to supply energy to match the ever-changing load demand is an example of why understanding the dynamics of a system is important. A typical load demand profile of the total energy consumed by all Eskom consumers throughout the day can be seen in Figure 6.1 [52].

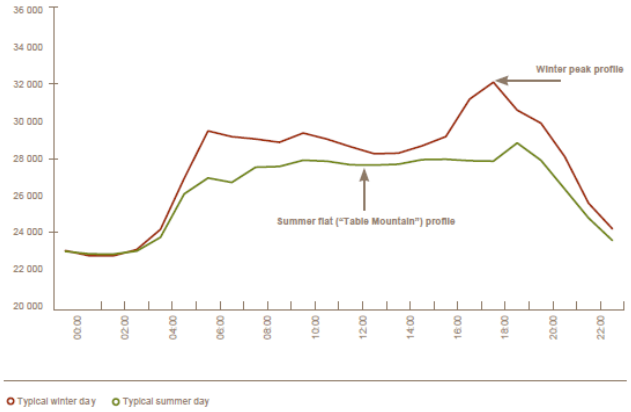

Figure 6.1: Eskom's typical load profile [52]

As seen in Figure 6.1, the load differs throughout the day as well as throughout the year as the seasons change (winter and summer loads), and a power station must thus be able to adjust its power delivery to the grid to sustain this demand. In a coal-fired power station, the power output of the plant is controlled by altering both the thermal energy input to the plant, as well as the mass flow rate of the fluids flowing through its turbines.

The difference however between a coal-fired power plant and a CSP plant lies within the primary energy source of thermal energy to the plant, when excluding the use of a duct burner. In a coal-fired plant the thermal energy can be altered by adjusting the amount of coal burnt according to the need. With a CSP plant the source of energy, although it is a variable input signal, cannot be changed [36]. This can be seen in Figures 6.2(a) and 6.2(b) where the thermal energy input during the day is limited to the available solar radiation from the sun, and at night where the thermal energy input to the plant is dependent on the amount of energy stored.

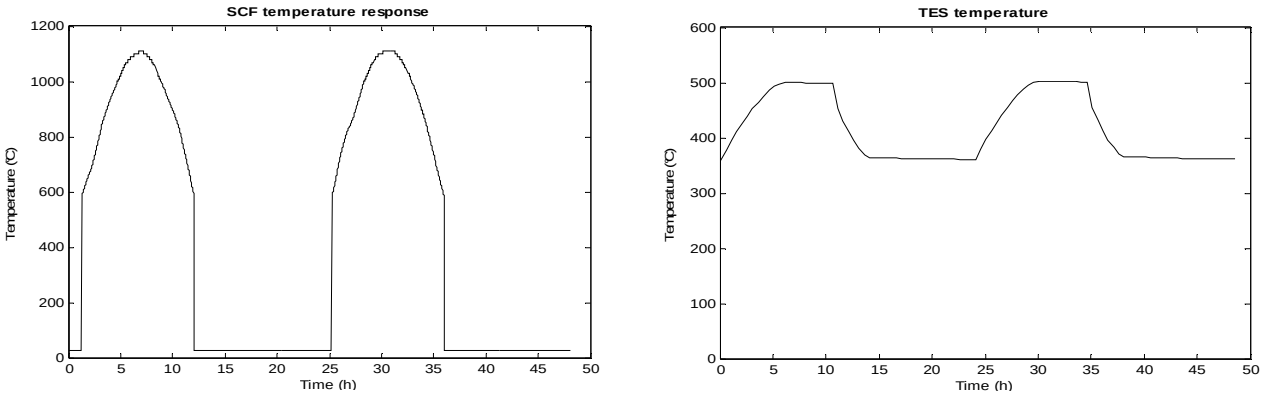

(a) Typical SCF temperature response

(b) Typical TES temperature profile

Figure 6.2: CSP thermal energy sources throughout the day

Due to these limitations, the operation of a CSP plant has to cope with issues that can be overcome by other power plants. Some subsequent issues include changing dynamics as the operating points of the plant change, and the existence of resonant and anti-resonant modes found within the control bandwidth of the plant, as discussed in chapter two [36].

Evaluating the influence that the major input signals have on the dynamic behaviour of the plant thus proves to be important. This is especially so if a controller for the plant is to be developed. The next section will discuss the characterisation process of the plant model.

6.2 CSP plant model characterisation

The two main factors influencing the dynamic responses of the entire plant include the temperature responses of its various components as well as the mass flow rate of the different fluids flowing through these components. Before discussing the process of evaluating the influence of these signals, a summarised overview of the operation of the plant is given.

6.2.1 Operation of the CSP plant

The entire operation of the plant is divided into two different operating scenarios that alter both the construction as well as the dynamics of the entire plant. These two operating scenarios include:

Operating scenario 1: Operation of the plant during the day

In the first operating scenario the Solar Collector Field (SCF) and the duct burner supplies thermal energy to the entire plant and all of its associated components. During this operating scenario, the power output of the plant is manipulated by altering the control variables, which include the mass flow rates of the fluid flowing through: the gas turbines, the steam turbines as well as the Thermal Energy Storage (TES) tanks.

This operating scenario can further be divided into various operating points, or regimes, at which the plant function. These operating points are defined as different thermal energy input levels of the SCF throughout the day.

Operating scenario 2: Operation of the plant during the night

In the second operating scenario, the TES supplies the Rankine cycle part of the plant with its thermal energy required to drive its turbines. During this operating scenario, the Brayton cycle part of the plant is isolated from the rest of the plant by shutting down both the duct burners' fuel supply as well as closing the control valve of the air entering the compressors. The power output of the plant is manipulated by altering the control variables, which include the mass flow rates of the fluid flowing through the steam turbines as well as the TES.

This operating scenario can further be divided into various operating points at which the plant function. These operating points are defined as different temperature levels of the TES during the night.

With the operation of the plant discussed, the process of characterising the plant, to gain insight into the dynamic behaviour of the plant, can be discussed.

6.2.2 The characterisation process

Evaluating the influence that the major input signals have on the dynamic behaviour of the various components of the plant, especially at its various operating scenario's operating points, can be implemented by evaluating the local linear models of the plant. By doing so, information such as the dominant dynamic behaviour, the change in the dynamic behaviour as the operating points change, and the presence of resonant and anti-resonant modes within the control bandwidth of the plant can be evaluated.

Since there are no local models that physically describe the dynamics of the developed plant, other than the Flownex model itself, and since most of the components are sized based on steady state equations, these local models need to be developed. In chapter 2 it was concluded that the use of Matlab® System Identification Toolbox™ would suffice in assisting the development of these local linear models of the plant by simulating each of the relevant input signals to the plant and evaluating its resultant responses.

To ensure that accurate local models are developed, which include all the dynamics of the plant, the evaluated input signals are simulated with pseudo random binary sequence (PRBS) excitation signals that oscillates between 1 and -1 at random frequencies.

The selected order at which the local linear models are to be specified at, includes both low- and high order models. The use of low-order models allows for the evaluation of both the change in the dynamic behaviour of the plant, by evaluating the dominant pole positions of the model, as well as the dominant dynamic behaviour of the plant, by evaluating the step responses of the dominant pole models. The use of high order models allows for the evaluation of the presence of resonant and anti-resonant modes found within the bandwidth of the local models, by evaluating the local model's bode plots [36, 37].

The selection of the order at which the local models are to be specified at is implemented by making use of Matlab®'s "Estimate order" functionality, which simulates the resultant responses with a series of pole/zero combinations. From this, the pole/zero combination that produces a high percentage fit can be selected for both a high- and a low-order model.

Evaluating the local linear models of the plant at each operating scenario and operating point would indicate the change in the dynamics of the plant as mentioned earlier. Selecting the operating points of the models to be at its maximum, average and minimum operating regimes can give a good overview of the change in the dynamics of the components, from minimum to maximum operating conditions.

Table 6.1 gives a summarised overview of the various local models that are to be developed and evaluated, based on the characterisation approach discussed above.

Table 6.1 CSP plant open loop local linear models

Scenario	Local models	Operating points	Description	Motivation
Operating scenario 1	$F1=\frac{T_{SCF}(s)}{Q_{\text{Pri\_MF}}(s)}$	$P_{SCF\_\max}$, $P_{\text{SCF\_med}}$, $P_{SCF\_\min}$	Evaluate the influence that the mass flow rate $\dot{m}_{\text{Pri\_MF}}$ of the mixed gasses flowing through the Brayton cycle has on the temperature response T_{SCF} of the SCF, at each operating point of the SCF.	The temperature response of the SCF forms an important input signal that influences the responses of all of its downstream components including the power output of the plant. This signal is a function of both the mass flow rate of the mixed gasses flowing through the Brayton cycle as well as the thermal energy input to the SCF.
	$F2=\frac{T_{SCF}(s)}{P_{SCF}(s)}$	$P_{SCF\_\max}$, $P_{\text{SCF\_med}}$, $P_{SCF\_\min}$	Evaluate the influence that the thermal energy input P_{SCF} to the SCF has on the temperature response T_{SCF} of the SCF, at each operating point of the SCF.	
	$F3=\frac{T_{TES}(s)}{Q_{\text{Pri\_MF}}(s)}$	$P_{SCF\_\max}$, $P_{\text{SCF\_med}}$, $P_{SCF\_\min}$	Evaluate the influence that the mass flow rate $\dot{m}_{\text{Pri\_MF}}$ of the mixed gasses flowing through the Brayton cycle has on the temperature response T_{TES} of the TES, at each operating point of the SCF.	The temperature response of the TES forms an important input signal that influences the responses of all its downstream components, and is a function of the mass flow rate of the mixed gasses flowing through the Brayton cycle.
	$F4=\frac{P_{system}(s)}{Q_{\text{Pri\_MF}}(s)}$	$P_{SCF\_\max}$, $P_{\text{SCF\_med}}$, $P_{SCF\_\min}$	Evaluate the influence that the mass flow rate $\dot{m}_{\text{Pri\_MF}}$ of the mixed gasses flowing through the Brayton cycle has on the mechanical power output P_{plant} of the entire plant, at each operating point of the SCF.	The power output response, which is controlled based on the load requirements of the system, is an important controlled variable. This response is a function of both the temperature responses of the SCF, the TES, as well as the mass flow rate inputs signals to the plant.
	$F5=\frac{P_{system}}{Q_{TES\_MF}}$	$P_{SCF\_\max}$,	Evaluate the influence that the mass flow rate $\dot{m}_{\text{TES\_MF}}$ of the mixed gasses flowing through the TES has on the	

		$P_{\text{SCF\_med}}$, $P_{SCF\_\min}$	mechanical power output P_{plant} of the entire plant, at each operating point of the SCF.	
	$F6 = \frac{P_{system}}{Q_{\text{Sec\_MF}}}$	$P_{SCF\_\max}$, $P_{\text{SCF\_med}}$, $P_{SCF\_\min}$	Evaluate the influence that the mass flow rate $\dot{m}_{\text{Sec\_MF}}$ of the steam flowing through the Rankine cycle has on the mechanical power output P_{plant} of the entire plant, at each operating point of the SCF.	
Operating scenario 2	$F7 = \frac{P_{system}}{Q_{TES\_MF}}$	$T_{TES\_\max}$, T_{TES_med}, $T_{TES\_\min}$	Evaluate the influence that the mass flow rate $\dot{m}_{\text{TES\_MF}}$ of the mixed gasses flowing through the TES has on the mechanical power output P_{plant} of the entire plant, at each operating point of the TES.	
	$F8 = \frac{P_{system}}{Q_{\text{Sec\_MF}}}$	$T_{TES\_\max}$, T_{TES_med}, $T_{TES\_\min}$	Evaluate the influence that the mass flow rate $\dot{m}_{\text{Sec\_MF}}$ of the steam flowing through the Rankine cycle has on the mechanical power output P_{plant} of the entire plant, at each operating point of the TES.	

6.3 CSP plant local linear models characterisation

The characterisation of each of the local linear models listed in Table 6.1 will now be implemented based on the approaches discussed in 6.2.2. In order to do so this section is divided into two subsections that include the local linear models present at operating scenario 1 and 2.

6.3.1 Model characterisation: Operating scenario 1

The characterisation of the plant during operating scenario 1 is implemented by evaluating the influence that both the mass flow rate of the fluids flowing through the various components, as well as the thermal energy input to the SCF, has on the responses of the plant at each operating point. Before doing so, the open loop structure of the plant along with the various operating points, during this operating scenario, will be discussed.

Plant control variables and operating points

The responses of the CSP plant, whether it is the temperature responses of the SCF or the TES, or whether it is the power output of the plant, is controlled by altering the mass flow rate of the fluids flowing through the various components. Figure 6.3 illustrates the open loop structure of the plant during operating scenario 1.

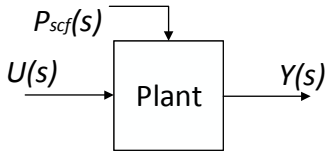

Figure 6.3: Plant open loop structure during operating scenario 1

In accordance with Figure 6.3, the relevant control variables for the open loop structure of the plant include:

$$\text{Outputs:}\quad Y(s) = T_{SCF}(s),\ T_{TES}(s),\ P_{plant}(s)$$
$$\text{Inputs:}\quad U(s) = Q_{\text{Pri\_MF}}(s),\ Q_{\text{Sec\_MF}}(s),\ Q_{\text{TES\_MF}}(s)$$
$$\text{Disturbance:}\quad P(s) = P_{SCF}(s)$$

The thermal energy input from the sun's solar radiation can be seen as a disturbance input to the plant due to its variable nature.

The different operating points, used for the characterisation of the plant, are selected based on the entire operating regimes of the plant. For this reason, these points are selected to be at its maximum thermal energy input ($P_{SCF\_\max}$) of 40 MW, its average thermal energy input ($P_{\text{SCF\_med}}$) of 25 MW, and at its minimum thermal energy input ($P_{SCF\_\min}$) of 10 MW.

Each input signal is perturbed with a PRBS signal with a magnitude of 5 % of its designed value. See Appendix B for the resulting PRBS signals along with the resultant responses of the plant for

each simulation. The local models of the plant at each operating point of this operating scenario, as defined in Table 6.1 will now be developed and evaluated:

6.3.1.1 Plant local models F1

Characterising the SCF temperature response, with respect to changes made to the mass flow rate of the mixed gasses flowing through the Brayton cycle, involves evaluating the local linear models $Y(s)/U(s) = T_{SCF}(s)/Q_{\text{Pri\_MF}}(s)$ at each of the different operating points defined in 6.3.1. The resultant low- and high order local models will now be discussed:

Low-order model evaluation:

In order to simplify identifying the dominant poles of the F1, the resultant low-order local linear models are shown in Table 6.2:

Table 6.2: Low-order local linear models F1

$F1 = \frac{T_{SCF}(s)}{Q_{\text{Pri\_MF}}(s)}$	$P1 = P_{SCF\_\max}$	$\frac{1.19\,s - 3.391}{s^2 + 0.6114s + 0.0258}$
	$P2 = P_{SCF\_\text{med}}$	$\frac{-2.394\,s - 0.03666}{s^2 + 0.03799s + 0.0003482}$
	$P3 = P_{SCF\_\min}$	$\frac{-5.46\,s - 0.2058}{s^2 + 0.1487s + 0.002655}$

The dominant dynamic response of F1 could be obtained by evaluating the poles situated closest to the origin (at s = 0), by zooming into the pole/zero diagram of each local model. Figure 6.4(a) illustrates the pole placement of the dominant poles at each of the operating points of F1. The pole/zero diagram illustrating the rest of the poles and zero's is included in Appendix B.

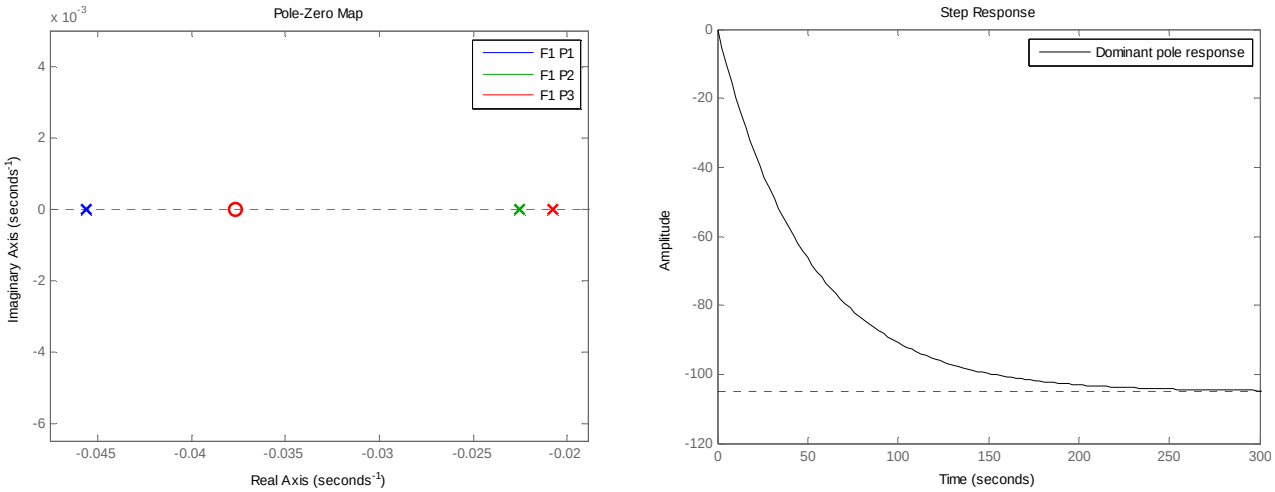

(a) Dominant pole plot **(b) Dominant pole model step response**

Figure 6.4: Dominant dynamic behaviour of models F1

From Figure 6.4(a) it can be seen that the dynamics of the plant changes from one operating point to the next with the dominant pole position changing. As the thermal energy input changes, so does the dynamic responses of the plant, with the system becoming faster and slower with an increase and decrease respectively in the thermal energy input to the SCF.

It can also be noted, from Figure 6.4(a), that both the bandwidth and the time constants of the models will not change linearly as the operating points change. This is due to the difference in the spacing between the dominant poles of the various models.

From Figure 6.5(b) it can be seen that the dominant behaviour of the temperature response of the SCF represents that of an over damped second order system with a negative gain.

High order model evaluation:

In order to evaluate the presence of resonant and anti- resonant modes, as well as to evaluate the difference between the responses of high order models and low-order models, the high order models are also developed. The resultant high order local linear models are shown in Table 6.3:

Table 6.3: High order local linear models F1

$F1$	$P1$	$\frac{-4.915s^5-1.453s^4-0.2895s^3-0.01667s^2-0.0002499s-8.504e-06}{s^6+0.3503s^5+0.07858s^4+0.009145s^3+0.0002767s^2+6.371e-06s+1.098e-07}$
	$P2$	$\frac{-7.566s^5-1.21s^4-0.0754s^3-0.002097s^2-4.092e-05s-6.449e-07}{s^6+0.2218s^5+0.01981s^4+0.0008856s^3+2.188e-05s^2+4.163e-07s+4.8e-09}$
	$P3$	$\frac{3.636s^5-3.018s^4-0.9081s^3-0.07405s^2-0.002298s-0.0001569}{s^6+0.9072s^5+0.2611s^4+0.03567s^3+0.001289s^2+8.047e-05s+1.488e-06}$

The high order models are evaluated by simulating and comparing the bode plots of F1 at each operating point, as well as step response of the high order model and dominant pole model:

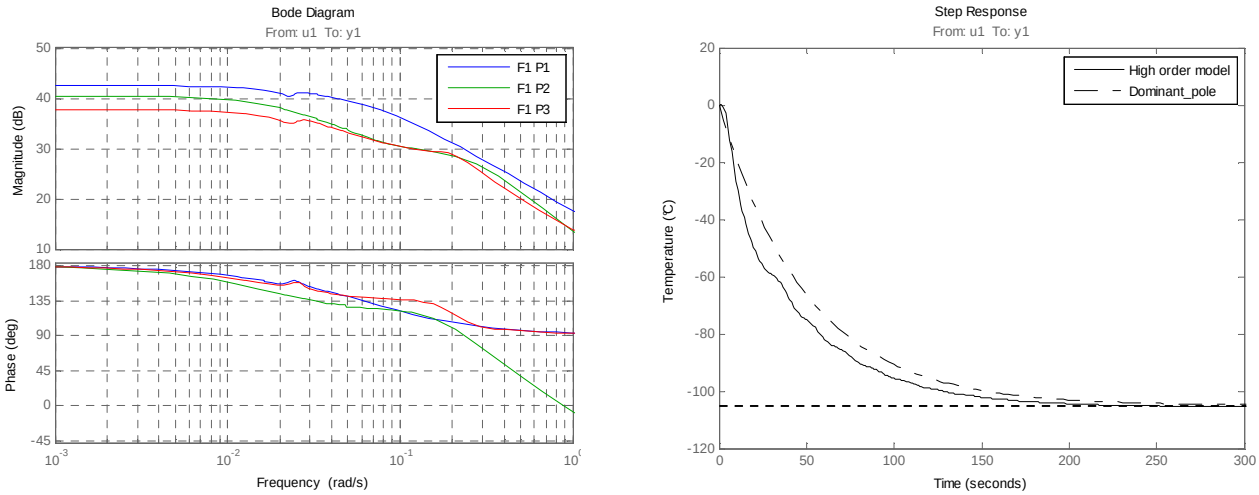

(a) Bode plot **(b) High/low-order model step response**

Figure 6.5: High order dynamic behaviour of models F1

From Figure 6.5(a) it can be seen that the frequency response of the models of F1 does contain resonant and anti-resonant modes. It is evaluated from Matlab® that the average bandwidth of the models is around 0.0488 rad/sec. With this in mind, it could then further be noted that resonant and anti-resonant modes are found within the bandwidth of the models.

The resonant and anti-resonant modes of operating point P3 can however not be seen as pronounced as the others, which could be due to a too short experiment taken or due to a too high PRBS signal amplitude used, which leads to a smoothing of the models frequency responses.

The correlation between the step response of the dominant pole response and the high order model response can be seen in Figure 6.5(b). From this figure it can be noted that both models differ slightly.

6.3.1.2 Plant local models F2

Characterising the SCF temperature response with respect to changes made to the thermal energy input signal to the SCF involves evaluating the local linear models $Y(s)/U(s) = T_{SCF}(s)/P_{SCF}(s)$ at each of the different operating points defined in section 6.3.1. The resultant low- and high order local models will now be discussed:

Low-order model evaluation:

The resultant low-order local linear models of F2 at each operating point are shown in Table 6.4:

Table 6.4: Low-order local linear models F2

$F2 = \frac{T_{SCF}(s)}{P_{SCF}(s)}$	$P1 = P_{SCF\_\max}$	$\frac{3.863e-05s^2+1.833e-05s+7.381e-07}{s^2+0.4918s+0.0109}$
	$P2 = P_{SCF\_\text{med}}$	$\frac{3.128e-05s^2+0.0001888s+6.462e-06}{s^2+5.617s+0.09522}$
	$P3 = P_{SCF\_\min}$	$\frac{2.421e-05s^2+1.79e-05s+5.521e-07}{s^2+0.6252s+0.00813}$

The dominant dynamic behaviour of these low-order models can be obtained by evaluating their dominant poles. Figure 6.6(a) illustrates the pole placement of the dominant poles at each operating point. The pole/zero diagram illustrating the rest of the poles and zero's is included in Appendix B.

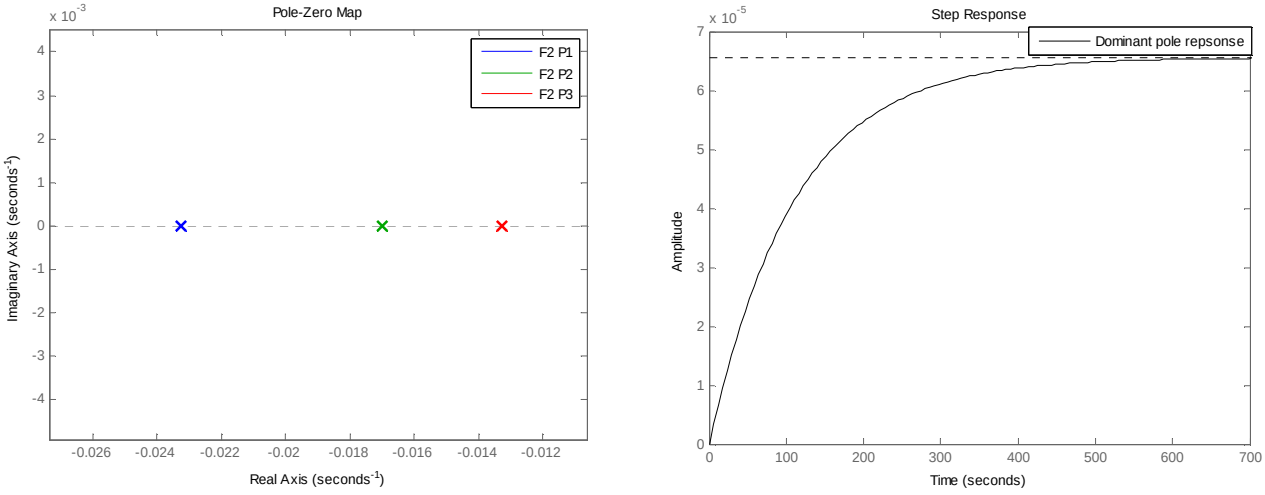

(a) Dominant pole plot **(b) Dominant pole model step response**

Figure 6.6: Low-order model responses of models F2

The change in the dynamics of the plant can also be seen from the positions of the dominating open-loop poles, in Figure 6.6(a), where the open-loop system becomes faster (poles move away from s = 0) as the thermal energy input increases. This results in the time responses, including the rise time and settling time of the system, to decrease as the thermal energy input to the SCF

increases. This then inherently also causes the bandwidth of the system to increase with an increase in the thermal energy input.

By evaluating the dominant pole response in Figure 6.6(b), it could be noted that the temperature response of the SCF with a step response in the thermal energy input to the SCF simulated, produces an over damped second order response.

High order model evaluation:

The resultant high order local linear models of F2, at each operating point, are shown in Table 6.5.

Table 6.5: High order local linear models F2

$F2$	$P1$	$\frac{3.907e-05s^{10}+1.71e-05s^{9}+4.486e-06s^{8}+7.202e-07s^{7}+8.667e-08s^{6}+7.134e-09s^{5}+4.796e-10s^{4}+1.631e-11s^{3}+4.883e-13s^{2}+4.574e-15s+1.316e-18}{s^{10}+0.5048s^{9}+0.1269s^{8}+0.02088s^{7}+0.002222s^{6}+0.00019s^{5}+1.04e-05s^{4}+3.523e-07s^{3}+8.776e-09s^{2}+6.723e-11s+1.886e-14}$
	$P2$	$\frac{3.067e-05s^{10}+5.044e-06s^{9}+1.246e-06s^{8}+1.273e-07s^{7}+1.389e-08s^{6}+8.889e-10s^{5}+4.625e-11s^{4}+1.856e-12s^{3}+3.575e-14s^{2}+8.812e-16s+6.642e-18}{s^{10}+0.1366s^{9}+0.03775s^{8}+0.003227s^{7}+0.0003958s^{6}+2.034e-05s^{5}+1.214e-06s^{4}+3.667e-08s^{3}+8.041e-10s^{2}+1.62e-11s+9.7e-14}$
	$P3$	$\frac{2.348e-05s^{10}+2.963e-06s^{9}+7.677e-07s^{8}+6.72e-08s^{7}+7.223e-09s^{6}+4.283e-10s^{5}+2.134e-11s^{4}+8.606e-13s^{3}+1.548e-14s^{2}+3.646e-16s+2.833e-18}{s^{10}+0.09578s^{9}+0.03003s^{8}+0.001979s^{7}+0.0002606s^{6}+1.103e-05s^{5}+6.966e-07s^{4}+1.885e-08s^{3}+4.014e-10s^{2}+7.378e-12s+4.144e-14}$

From these high order local linear models, the presence of resonant and anti-resonant modes along with the step response of the models can be evaluated by plotting both the frequency responses of the local models as well as the step response of a high order and a low-order model (dominant pole model):

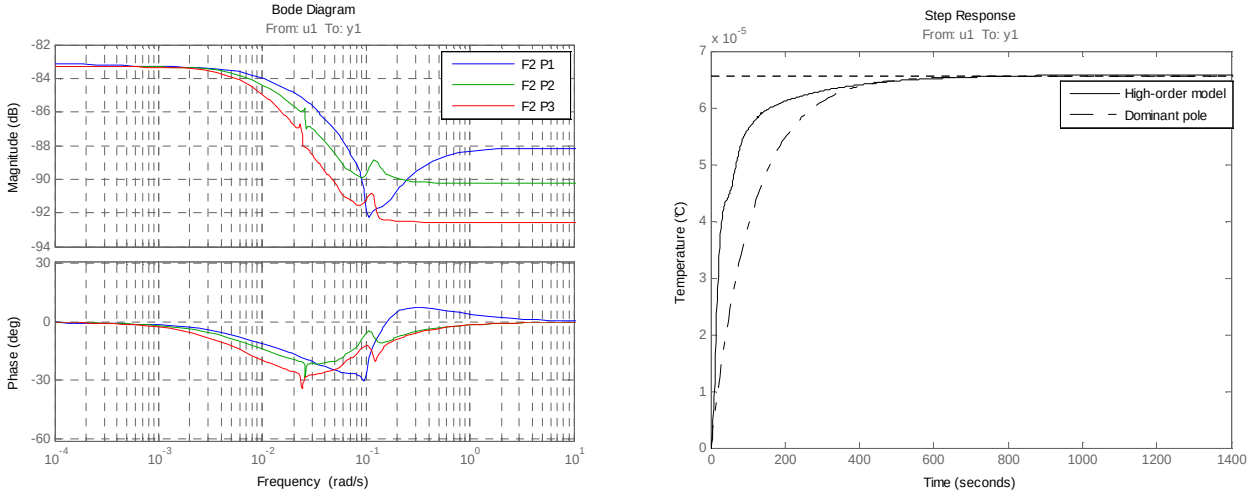

(a) Bode plot **(b) High/low-order model step response**

Figure 6.7: High order dynamic behaviour of models F2

From Figure 6.7(a) it can be seen that there does exist resonant and anti-resonant modes from the frequency responses of the models. The average bandwidth is calculated to be around 0.0365 rad/sec, which results in having the first resonant and anti-resonant modes falling within the bandwidth of the model. It can also be noted that the anti-resonant modes' frequency is slightly dependent on the operating point.

From Figure 6.7(b) it can be seen that there exists quite a large difference between the step response of the dominant pole model and the high order model. This is especially true when comparing the rise times of both models.

6.3.1.3 Plant local models F3

Characterising the TES temperature response, with changes made to the mass flow rate of the mixed gasses flowing through the Brayton cycle, involves evaluating the local linear models $Y(s)/U(s) = T_{TES}(s)/Q_{\text{Pri\_MF}}(s)$ at each of the different operating points defined in 6.3.1. The resultant low- and high order local models will now be discussed:

Low-order model evaluation:

The low-order local linear models of F3 simulated at each operating point, is shown in Table 6.6:

Table 6.6: Low-order local linear models F3

$F3 = \frac{T_{TES}(s)}{Q_{\text{Pri\_MF}}(s)}$	$P1 = P_{SCF\_\max}$	$\frac{\text{-0.03628 s - 2.293e-05}}{s^2 + 0.003208s + 4.27e-07}$
	$P2 = P_{SCF\_med}$	$\frac{\text{-0.03182 s - 2.012e-05}}{s^2 + 0.003214s + 4.036e-07}$
	$P3 = P_{SCF\_\min}$	$\frac{\text{-7.271 s - 0.1147}}{s^2 + 18.3s + 0.002383}$

Evaluating the dominant poles of these low-order models assists in obtaining the dominant dynamic behaviour of these models. Figure 6.8(a) illustrates the pole placement of the dominant poles at each operating point. Appendix B contains the pole/zero plot of all the poles and zero's of these models.

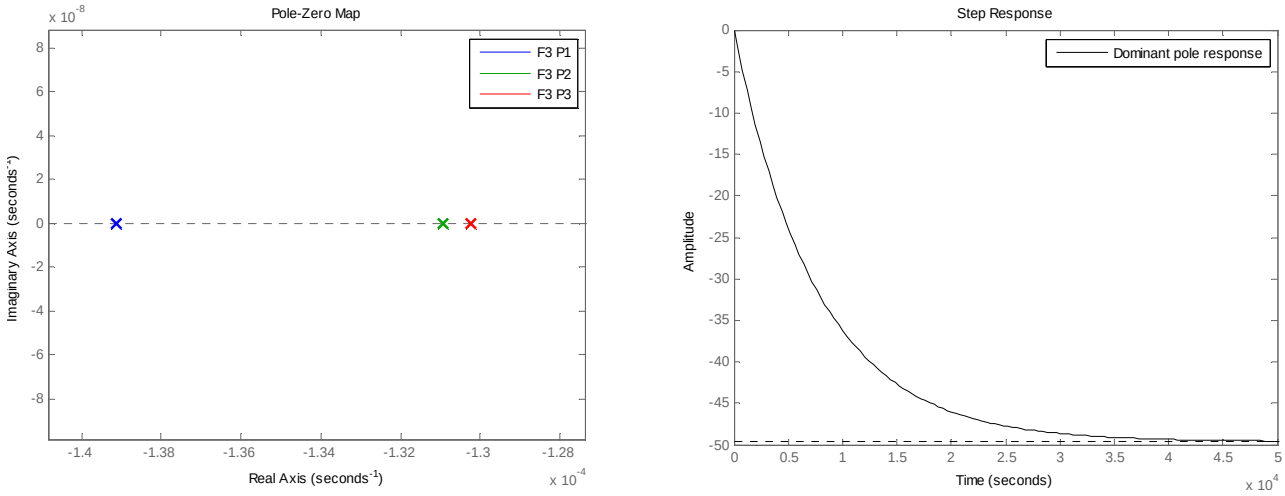

(a) Dominant pole plot **(b) Dominant pole model step response**

Figure 6.8: Dominant dynamic behaviour of models F3

By evaluating the pole position of the dominant poles of the plant in Figure 6.8(b), it can be noted that the dominant poles of the plant shifts as the operating point of the plant changes. This in turn results in the dynamic behaviour of the plant changing as the operating points change. The time

responses and the bandwidth of the models decrease and increase respectively as the thermal energy input to the plant increases with the poles moving away from s = 0.

Due to the difference in the spacing between the poles of the various operating points, it could be noted that the dynamic responses of the plant does not change linearly as the operating points change.

By evaluating the step response, in Figure 6.8(a), of one of the models' dominant poles, it could be noted that the temperature response of the TES, with a step response in the mass flow rate of the mixed gasses flowing through the Brayton cycle simulated, produces an over damped second order response with a negative gain.

High order model evaluation:

The high order local linear models of F3, simulated at each operating point are shown in Table 6.7.

Table 6.7: High order local linear models F3

$F3$	$P1$	$\frac{0.1338s^8+0.001306s^7+1.283e{-}06s^6+8.483e{-}09s^5-4.855e{-}11s^4-9.156e{-}14s^3-2.918e{-}16s^2-4.258e{-}19s-1.528e{-}22}{s^9+0.02599s^8+0.0002305s^7+1.293e{-}06s^6+5.197e{-}09s^5+1.352e{-}11s^4+2.431e{-}14s^3+3.712e{-}17s^2+2.528e{-}20s+2.871e{-}24}$
	$P2$	$\frac{0.1311s^8+0.0008775s^7+1.012e{-}06s^6+2.875e{-}09s^5-2.662e{-}11s^4-6.801e{-}14s^3-1.914e{-}16s^2-2.844e{-}19s-1.081e{-}22}{s^9+0.02563s^8+0.000217s^7+1.102e{-}06s^6+4.094e{-}09s^5+1.061e{-}11s^4+1.992e{-}14s^3+2.782e{-}17s^2+1.995e{-}20s+2.193e{-}24}$
	$P3$	$\frac{-0.003658s^8-3.125e{-}05s^7-2.138e{-}07s^6-1.07e{-}09s^5-2.929e{-}12s^4-9.09e{-}15s^3-1.097e{-}17s^2-1.146e{-}20s-5.298e{-}24}{s^9+0.006802s^8+5.255e{-}05s^7+2.034e{-}07s^6+6.541e{-}10s^5+1.552e{-}12s^4+2.068e{-}15s^3+1.97e{-}18s^2+1.087e{-}21s+1.098e{-}25}$

The bode plots of each of these high order local linear models along with the step response of a high order model compared to the step response of a dominant pole model can be seen in Figures 6.9(a) and 6.9(b):

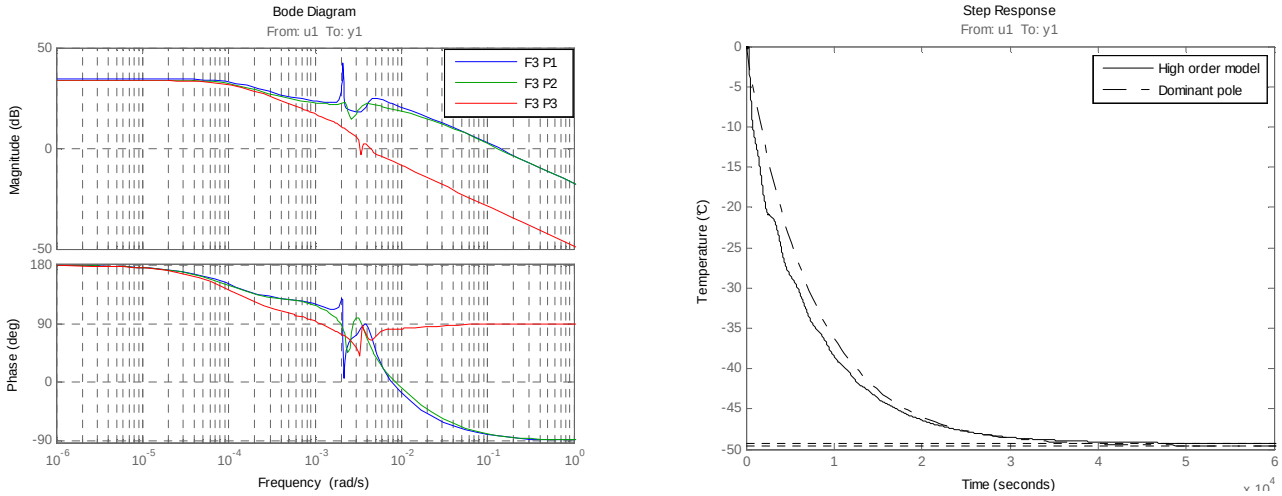

(a) Bode plot **(b) High/low-order model step response**

Figure 6.9: High order dynamic behaviour of models F3

From Figure 6.9(a) it can be seen that the frequency response of these models contain resonant and anti-resonant modes. It should also be noted that the frequency at which these modes are found in, are dependent on the operating point at which it is driven. The average bandwidth of

these models were found to be around 0.0004976 rad/sec, which results in the resonant and anti-resonant modes situated outside of the bandwidth of these models.

The difference in the step responses of both the high order model and the low-order model (dominant pole model), as seen in Figure 6.9(b), is significantly small.

6.3.1.4 Plant local models F4

Characterising the mechanical power output response of the plant, with respect to changes made to the mass flow rate of the mixed gasses flowing through the Brayton cycle, involves evaluating the local linear models $Y(s)/U(s) = P_{plant}(s)/Q_{\text{Pri\_MF}}(s)$ at each of the different operating points defined in 6.3.1. The resultant low- and high order local models will now be discussed:

Low-order model evaluation:

The resultant low-order local linear models of F4 at each operating point are shown in Table 6.8:

Table 6.8: Low-order local linear models F4

$F4 = \dfrac{P_{system}(s)}{Q_{\text{Pri\_MF}}(s)}$	$P1 = P_{SCF\_\max}$	$\dfrac{0.04273s^2 + 0.003924s + 2.681e-05}{s^3 + 0.5029s^2 + 0.01369s + 5.203e-05}$
	$P2 = P_{SCF\_med}$	$\dfrac{0.01278s^2 + 0.0008078s + 4.993e-06}{s^3 + 0.1195s^2 + 0.002769s + 1.036e-05}$
	$P3 = P_{SCF\_\min}$	$\dfrac{0.01061s^2 + 0.0001279s + 3.184e-07}{s^3 + 0.04515s^2 + 0.0003486s + 6.914e-07}$

The dominant dynamic behaviour of F4 could be obtained by evaluating the poles situated closest to the origin (at s = 0). Figure 6.10(a) illustrates the pole placement of the dominant poles at each operating point. The pole/zero diagram illustrating the rest of the poles and zero's is included in Appendix B.

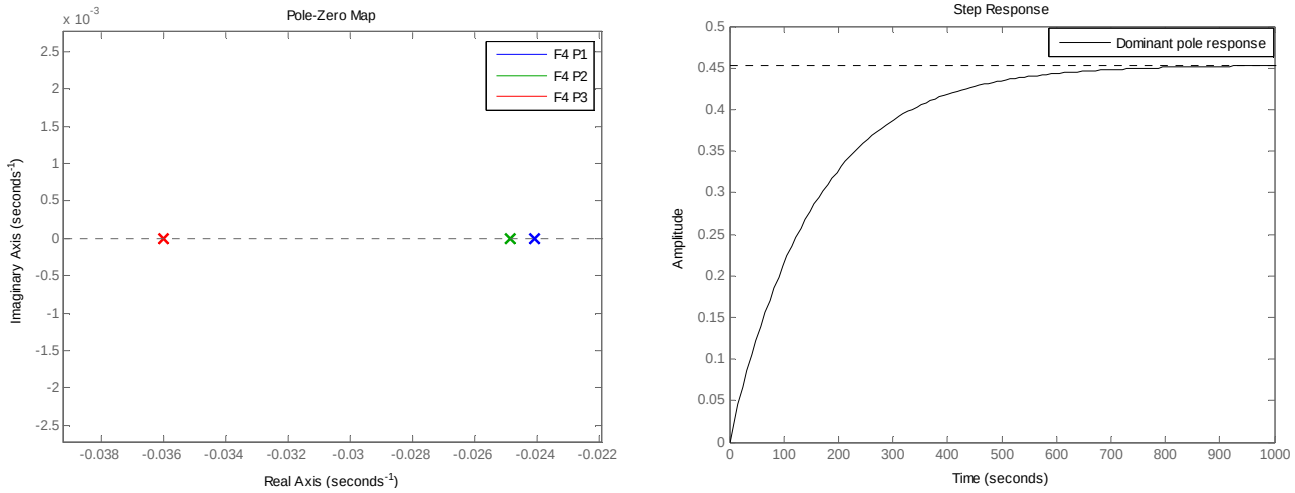

(a) Dominant pole plot **(b) Dominant pole model step response**

Figure 6.10: Dominant dynamic behaviour of models F4

Evaluating the pole position of the dominant poles in Figure 6.10(a) it can be noted that the pole position changes as the operating point of the plant changes. This in turn results in the dynamic behaviour of the plant changing as the operating points change. The direction at which these poles

are shifting does however differ from the other models since the system becomes slower as the thermal energy input increases, which results in a decrease in the models' bandwidth. It should further be noted that the dynamics of the plant does not change linearly as the operating points change.

Evaluating Figure 6.10(b), it can be noted that the temperature response of the SCF, with a step response in the mass flow rate of the mixed gasses flowing through the Brayton cycle simulated, produces an over damped second order response.

High order model evaluation:

The resultant high order local linear models of F4 are shown in Table 6.9:

Table 6.9: High order local linear models F4

$F4$	$P1$	$\frac{-0.09983s^{12}-0.009053s^{11}-0.0004022s^{10}+0.0003653s^{9}+0.0001384s^{8}+1.931e-05s^{7}+2.191e-06s^{6}+2.033e-07s^{5}+8.451e-09s^{4}+5.089e-10s^{3}+8.54e-12s^{2}+5.849e-14s+1.389e-16}{s^{12}+0.3824s^{11}+0.1183s^{10}+0.01992s^{9}+0.003235s^{8}+0.0002878s^{7}+2.958e-05s^{6}+1.433e-06s^{5}+7.708e-08s^{4}+2.316e-09s^{3}+2.825e-11s^{2}+1.479e-13s+2.761e-16}$
	$P2$	$\frac{-0.0574s^{13}+0.003631s^{12}+0.001688s^{11}+0.00101s^{10}+0.0002879s^{9}+4.924e-05s^{8}+8.059e-06s^{7}+8.753e-07s^{6}+8.156e-08s^{5}+6.01e-09s^{4}+2.872e-10s^{3}+1.39e-11s^{2}+1.671e-13s+6.249e-16}{s^{13}+0.3783s^{12}+0.1459s^{11}+0.03035s^{10}+0.006357s^{9}+0.0008361s^{8}+0.0001135s^{7}+9.443e-06s^{6}+8.408e-07s^{5}+4.2e-08s^{4}+2.225e-09s^{3}+5.585e-11s^{2}+4.872e-13s+1.312e-15}$
	$P3$	$\frac{-0.03061s^{12}+0.01429s^{11}+0.005028s^{10}+0.001361s^{9}+0.0002879s^{8}+3.76e-05s^{7}+4.074e-06s^{6}+3.316e-07s^{5}+1.232e-08s^{4}+4.315e-10s^{3}+4.341e-12s^{2}+1.737e-14s+2.551e-17}{s^{12}+0.3434s^{11}+0.1179s^{10}+0.02109s^{9}+0.003844s^{8}+0.0003897s^{7}+4.118e-05s^{6}+2.001e-06s^{5}+7.691e-08s^{4}+1.651e-09s^{3}+1.282e-11s^{2}+4.359e-14s+5.582e-17}$

The bode plots of each of these high order models, together with the step response of both a high order model and the dominant pole model will now be evaluated:

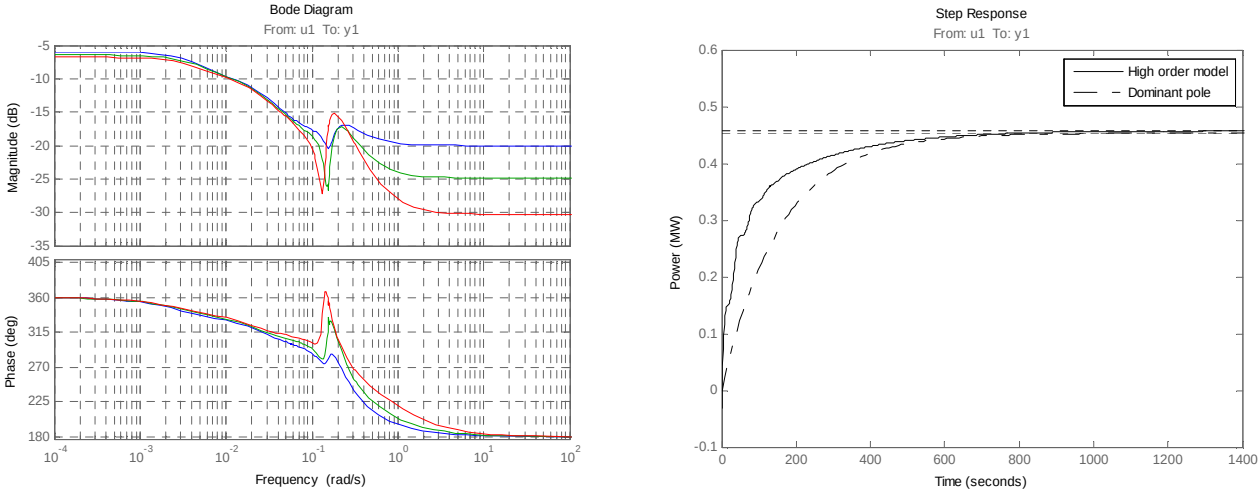

(a) Bode plot **(b) High/low-order model step response**

Figure 6.11: High order dynamic behaviour of models F4

From Figure 6.11(a) it can be seen that the frequency response of the local models does contain resonant and anti-resonant modes at frequencies dependent on the operating points of the models. The average bandwidth of these models was found to be around 0.0107 rad/sec. This results in having no resonant and anti-resonant modes found within the bandwidth of the models.

The step responses of both the high order model and the dominant pole model of F4 can be seen in Figure 6.11(b). From this figure it can be seen that there exists quite a large difference between the two models. This is especially the case when comparing the rise times of both models.

6.3.1.5 Plant local models F5

Characterising the mechanical power output of the plant, with respect to changes made to the mass flow rate of the mixed gasses flowing through the TES, involves evaluating the local linear models $Y(s)/U(s) = P_{plant}(s)/Q_{\text{TES\_MF}}(s)$ at each of the different operating points defined in 6.3.1. The resultant low- and high order local models will now be discussed:

Low-order model evaluation:

The low-order local linear models of F5, simulated at each operating point are shown in Table 6.10:

Table 6.10: Low-order local linear models F5

$F5 = \frac{P_{system}}{Q_{TES\_MF}}$	$P1 = P_{SCF\_\max}$	$\frac{\text{-0.00283 s - 0.0008097}}{\text{s + 0.00441}}$
	$P2 = P_{SCF\_med}$	$\frac{\text{-0.003996 s - 0.0006504}}{\text{s + 0.004383}}$
	$P3 = P_{SCF\_\min}$	$\frac{\text{-0.004343 s - 0.0005534}}{\text{s + 0.004327}}$

The dominant dynamic behaviour of these low-order models can be obtained by evaluating their dominant poles. Figure 6.12(a) illustrates the pole placement of the dominant poles at each operating point. The pole/zero diagram illustrating the rest of the poles and zero's is included in Appendix B.

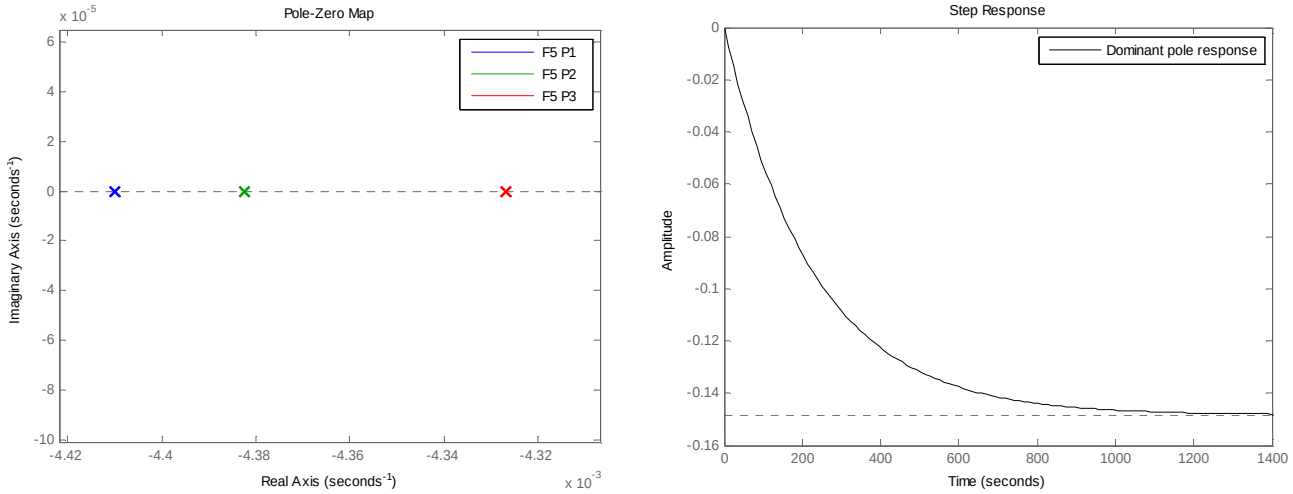

(a) Dominant pole plot **(b) Dominant pole model step response**

Figure 6.12: Dominant dynamic behaviour of models F5

Change in the dynamic behaviour of the plant can be seen from the positions of the dominating open-loop poles, seen in Figure 6.6(a), where the open-loop system becomes faster (poles move away from s = 0) as the thermal energy input increases. This results in the time responses, including the rise time and settling time, of the system to decrease as the thermal energy input to the SCF increases. This inherently also causes the bandwidth of the system to increase with an increase in the thermal energy input.

By evaluating the step response of the dominant pole model as seen in Figure 6.12(b), it could be noted that the power output response of the plant, with a step response in the mass flow rate simulated, produces an over damped second order response with a negative gain.

High order model evaluation:

The high order local linear models of F5, simulated at each operating point are shown in Table 6.11.

Table 6.11: High order local linear models F5

$F5$	$P1$	$\frac{-0.00813s^{10}-0.0007842s^{9}-0.0002875s^{8}-2.57e-05s^{7}-3.44e-06s^{6}-2.733e-07s^{5}-1.534e-08s^{4}-9.332e-10s^{3}-1.737e-11s^{2}-2.322e-14s-2.069e-16}{s^{10}+0.02453s^{9}+0.03337s^{8}+0.0007691s^{7}+0.0003616s^{6}+7.815e-06s^{5}+1.268e-06s^{4}+2.555e-08s^{3}+1.242e-10s^{2}+3.717e-13s+1.143e-15}$
	$P2$	$\frac{-0.007227s^{12}-0.001314s^{11}-0.0005111s^{10}-6.992e-05s^{9}-1.162e-05s^{8}-1.174e-06s^{7}-9.685e-08s^{6}-6.691e-09s^{5}-3.222e-10s^{4}-1.374e-11s^{3}-3.735e-13s^{2}-6.623e-15s-4.544e-17}{s^{12}+0.1121s^{11}+0.0529s^{10}+0.005313s^{9}+0.001239s^{8}+7.661e-05s^{7}+8.111e-06s^{6}+3.674e-07s^{5}+1.934e-08s^{4}+5.816e-10s^{3}+1.221e-11s^{2}+1.106e-13s+3.077e-16}$
	$P3$	$\frac{-0.005723s^{13}-0.00429s^{12}-0.001608s^{11}-0.0004446s^{10}-9.477e-05s^{9}-1.472e-05s^{8}-2.313e-06s^{7}-2.398e-07s^{6}-2.525e-08s^{5}-1.755e-09s^{4}-1.067e-10s^{3}-4.754e-12s^{2}-7.184e-14s-2.214e-16}{s^{13}+0.5412s^{12}+0.1916s^{11}+0.04637s^{10}+0.01026s^{9}+0.001434s^{8}+0.0001216s^{7}+1.95e-05s^{6}+2.318e-06s^{5}+1.055e-07s^{4}+8.444e-09s^{3}+1.585e-10s^{2}+9.388e-13s+1.742e-15}$

To illustrate whether or not resonant and anti-resonant modes exist within the bandwidth of the plant, as well as to illustrate the difference between a low- and a high order model, the bode plot of the high order models and the step response of both a dominant pole model and a high order model can be evaluated.

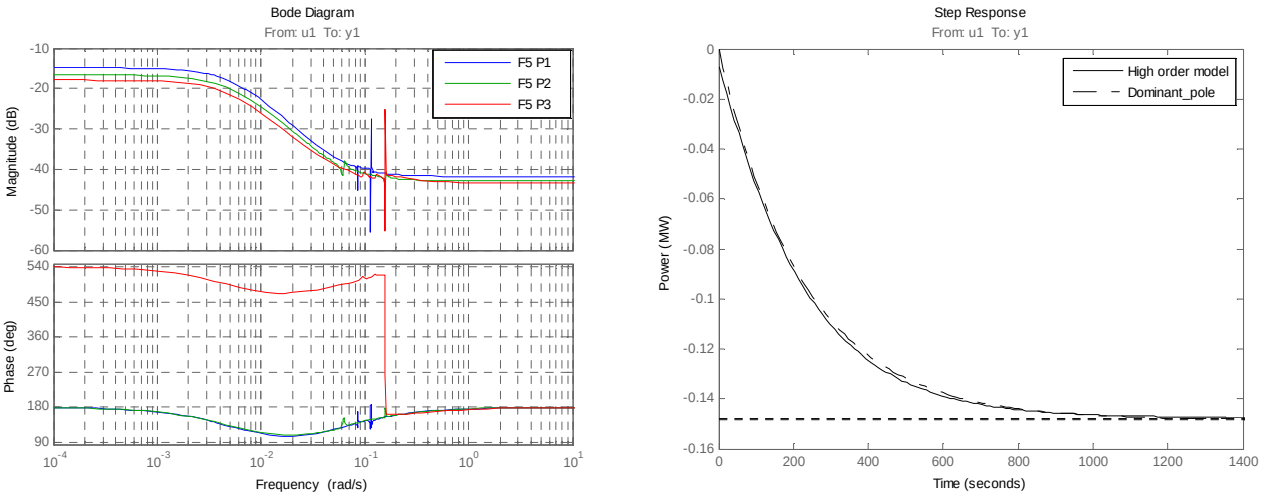

(a) Bode plot **(b) High/low-order model step response**

Figure 6.13: High order dynamic behaviour of models F5

From Figure 6.13(a) it can be seen that the frequency responses of F5 does contain resonant and anti-resonant modes. It was evaluated that the average bandwidth of the models is around 0.0047 rad/sec. With this in mind, it could then further be noted the resonant and anti-resonant modes fall outside the bandwidth of the models.

The correlation between the step response of the dominant pole model (low-order model) and the high order model of F5 can be seen in Figure 6.13(b). From this figure it can be noted that there is a high correlation between the high order local model and the dominant pole model.

6.3.1.6 Plant local models F6

Characterising the mechanical power output response of the plant, with changes made to the mass flow rate of the steam flowing through the Rankine cycle, involves evaluating the local linear models $Y(s)/U(s) = P_{\text{plant}}(s)/Q_{\text{Sec\_MF}}(s)$ at each of the different operating points defined in 6.3.1. The resultant low- and high order local models will now be discussed:

Low-order model evaluation:

The low-order local linear models of F6, simulated at each operating point are shown in Table 6.12:

Table 6.12: Low-order local linear models F6

$F6 = \frac{P_{system}}{Q_{\text{Sec\_MF}}}$	$P1 = P_{SCF\_\max}$	$\frac{0.02066\,s + 0.001078}{s^2 + 0.2156s + 0.002322}$
	$P2 = P_{SCF\_med}$	$\frac{0.02405\,s + 0.001311}{s^2 + 0.2622s + 0.002796}$
	$P3 = P_{SCF\_\min}$	$\frac{0.02041\,s + 0.001058}{s^2 + 0.2154s + 0.002245}$

The dominant dynamic behaviour of these low-order models can be obtained by evaluating their dominant poles. Figure 6.6(a) illustrates the pole placement of the dominant poles at each operating point. Appendix B includes the pole/zero plots of all the poles and zeros of these models.

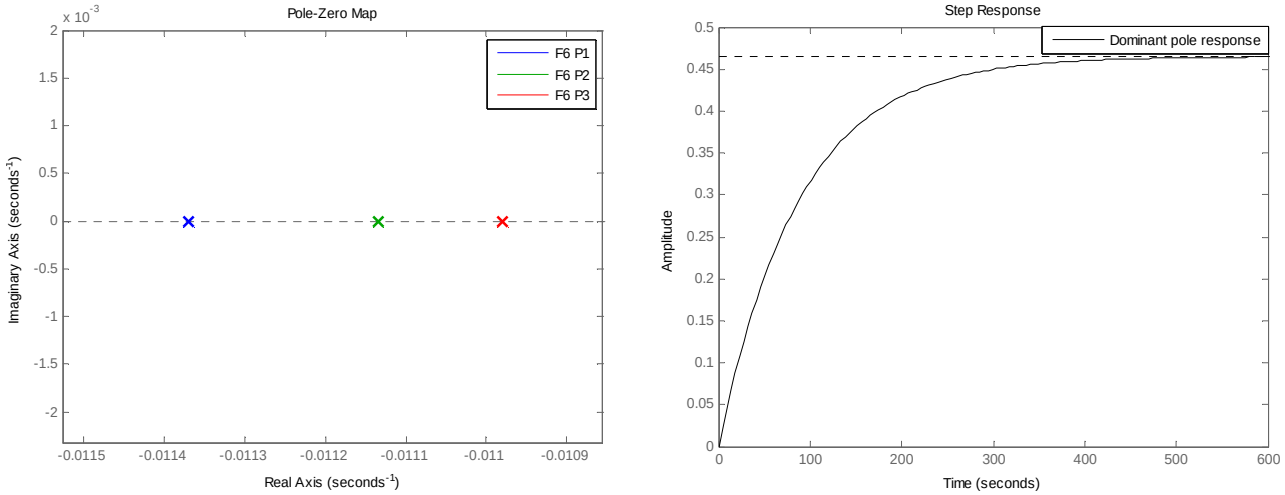

(a) Dominant pole **(b) Dominant pole model step response**

Figure 6.14: Dominant dynamic behaviour of models F6

The change in the dynamics of the plant can be seen from the positions of the dominating open-loop poles in Figure 6.14(a). As the thermal energy input increases, the open-loop system becomes faster (poles move away from s = 0). With the system becoming faster as the thermal energy increases, the time responses and the bandwidth of the plant decreases and increases accordingly.

Evaluating the step response of the dominant pole model, as seen in Figure 6.14(b), it can be noted that the power output response of the plant with a step response in the mass flow rate simulated, produces an over damped second order response.

High model order evaluation:

The high order local linear models of F6, simulated at each operating point are shown in Table 6.13.

Table 6.13: High order local linear models F6

$F6$	$P1$	$\frac{0.0007871s^7+0.001909s^6+0.0002599s^5+2.166e-05s^4+1.361e-06s^3+6.283e-08s^2+1.119e-09s+3.898e-11}{s^9+0.5872s^8+0.172s^7+0.03592s^6+0.003191s^5+0.0001914s^4+1.211e-05s^3+2.513e-07s^2+8.611e-09s+8.397e-11}$
	$P2$	$\frac{0.009899s^7+0.0019242s^6+0.0003823s^5+3.79e-05s^4+3.758e-06s^3+1.887e-07s^2+2.917e-09s+1.037e-10}{s^9+0.5853s^8+0.1712s^7+0.03513s^6+0.006671s^5+0.0003442s^4+3.64e-05s^3+6.618e-07s^2+2.301e-08s+2.199e-10}$
	$P3$	$\frac{0.2307s^7+0.07245s^6+0.02711s^5+0.007104s^4+0.0008888s^3+0.0001579s^2+7.641e-06s+2.121e-07}{s^9+1.178s^8+0.8191s^7+0.494s^6+0.09952s^5+0.0401s^4+0.003886s^3+0.0003837s^2+4.875e-05s+4.519e-07}$

From these high order local linear models, the presence of resonant and anti-resonant modes can be evaluated by plotting the frequency responses of the local models.

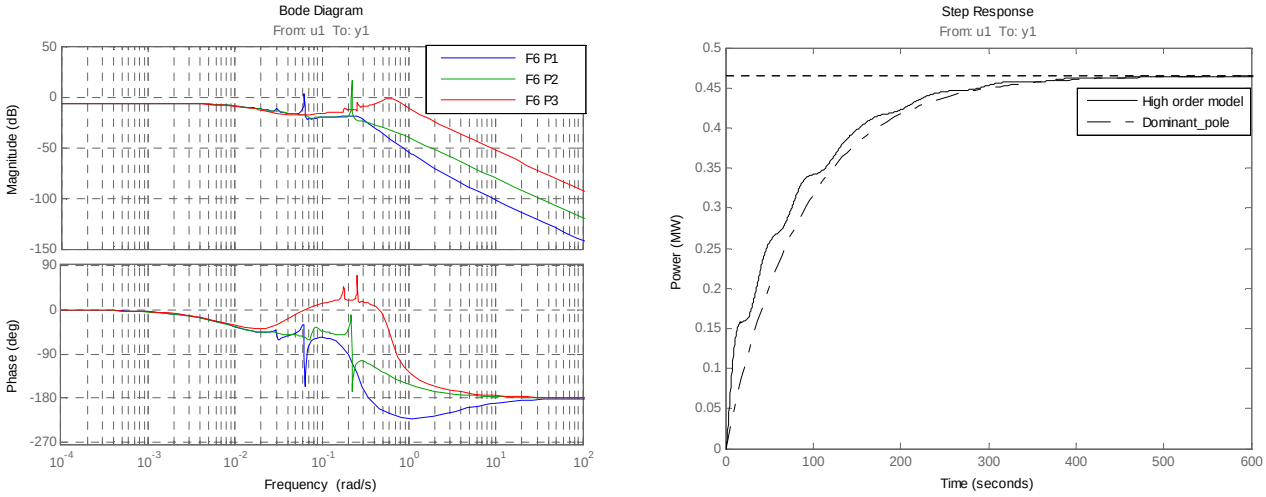

(a) Bode plot **(b) High/low-order model step response**

Figure 6.15: High order dynamic behaviour of models F6

From Figure 6.15(a) it can be seen that there does exist resonant and anti-resonant modes from the frequency responses of the models. The average bandwidth is calculated to be around 0.0121 rad/sec which results in having the resonant and anti-resonant modes falling just outside the bandwidth of the model.

From Figure 6.15(b) it can be seen that there exists only a relatively small difference between the low-order model (dominant pole model), and the high order model.

6.3.2 Model characterisation: Operating scenario 2

The characterisation of the plant during operating scenario 2 is implemented by evaluating the influence that the mass flow rate of the fluids flowing through the various components has on the responses of the plant at each operating point. Before doing so the open loop structure of the plant along with the various operating points during this operating scenario will be discussed.

Plant control variables and operating points

The responses of the CSP plant, whether it is the temperature responses of the components of the plant, or whether it is the power output of the plant, is controlled by altering the mass flow rate of the fluid flowing through its various components. Figure 6.16 illustrates the open loop structure of the plant during operating scenario 2.

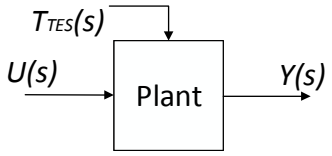

Figure 6.16: Plant open loop structure during operating scenario 2

In accordance with Figure 6.16 the relevant control variables for the open loop structure of the plant include:

$$\text{Outputs:} \quad Y(s) = P_{plant}(s)$$
$$\text{Inputs:} \quad U(s) = Q_{\text{Sec\_MF}}(s),\ Q_{\text{TES\_MF}}(s)$$
$$\text{Disturbance:} \quad T(s) = T_{TES}(s)$$

The temperature response of the TES is considered to be the disturbance input to the plant during this operating scenario due to its variable nature during the night.

The selection of the different operating points in which the plant will be characterised is selected to be at its maximum temperature input ($T_{TES\_\max}$) of 500 ℃, its average temperature input (T_{TES_med}) of 425 ℃, and at its minimum temperature input ($T_{TES\_\min}$) of 350 ℃. These points are selected based on the operating ranges for this CSP plant.

Each input signal is perturbed with a PRBS signal with magnitude of 5 % of its designed value. See Appendix B for the resulting PRBS signals along with the resultant responses of the plant for each simulation. The local models of the plant at each operating point of this operating scenario, will be developed and evaluated:

6.3.2.1 Plant local models F7

Characterising the mechanical power output response of the plant, with changes made to the mass flow rate of the mixed gasses flowing through the TES, involves evaluating the local linear models $Y(s)/U(s) = P_{plant}(s)/Q_{\text{TES\_MF}}(s)$ at each of the different operating points defined in 6.3.2. The resultant low- and high order local models will now be discussed.

Low-order model evaluation:

The low-order local linear models of F7, simulated at each operating point are shown in Table 6.14.

Table 6.14: Low-order local linear models F7

$F7 = \frac{P_{system}}{Q_{TES\_MF}}$	$T1 = T_{TES\_\max}$	$\frac{42.79\ s + 1.83}{s^2 + 3.298e05s + 1305}$
	$T2 = T_{TES\_med}$	$\frac{0.001436\ s + 4.775e\text{-}05}{s^2 + 9.768s + 0.03959}$
	$T3 = T_{TES\_\min}$	$\frac{0.0003368\ s + 2.657e\text{-}05}{s^2 + 8.336s + 0.03131}$

The dominant dynamic response of the models could be obtained by evaluating the poles situated closest to the origin (at s = 0) of each local model. Figure 6.17(a) illustrates the pole placement of the dominant poles at each operating point. The pole/zero diagram illustrating the rest of the poles and zero's is included in Appendix B.

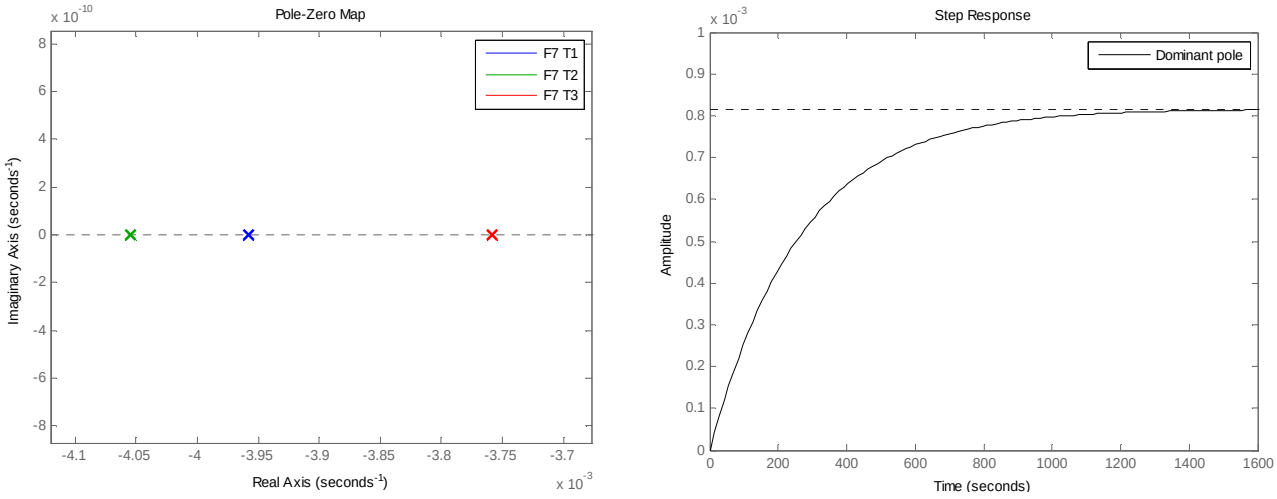

(a) Dominant pole **(b) Dominant pole model step response**

Figure 6.17: Dominant dynamic behaviour of models F7

By evaluating the pole position of the dominant poles of the plant seen in Figure 6.17(a), it can be noted that the poles position of the plant changes as the operating point of the plant changes. This in turn results in the dynamic behaviour of the plant changing as the operating points changes. What should be noted is that as the temperature of the TES decreases, the plant first becomes faster as the poles move away from the origin, and then becomes slower again with its poles moving to the right (towards s = 0). This then influences both the time responses as well as the bandwidth of the plant.

By evaluating Figure 6.17(b) it could be noted that the power output response of the plant with a step response in the mass flow rate of the mixed gasses flowing through the TES simulated, produces an over damped second order response.

High order model evaluation:

The high order local linear models of F7 are shown in Table 6.15:

Table 6.15: High order local linear models F7

$F7$	$P1$	$\frac{-2.044e-05s^7+1.918e-05s^6+2.387e-06s^5+4.335e-07s^4+3.122e-08s^3+1.337e-09s^2+3.538e-11s+1.47e-13}{s^9+9.049s^8+0.3822s^7+0.4925s^6+0.01303s^5+0.004488s^4+8.954e-05s^3+7.296e-06s^2+5.335e-08s+1.268e-10}$
	$P2$	$\frac{-0.0001126s^7+7.682e-06s^6-9.237e-07s^5+9.569e-08s^4+3.225e-09s^3+6.524e-11s^2+9.454e-13s+5.362e-15}{s^9+0.2223s^8+0.3536s^7+0.05607s^6+0.004821s^5+0.0005208s^4+9.57e-06s^3+2.04e-07s^2+1.468e-09s+3.997e-12}$
	$P3$	$\frac{3.913e-07s^7+8.747e-08s^6+8.416e-09s^5+1.455e-09s^4+3.741e-11s^3+3.049e-12s^2+4.645e-14s+4.977e-16}{s^9+0.05673s^8+0.03348s^7+0.001553s^6+0.0003082s^5+1.154e-05s^4+6.166e-07s^3+1.884e-08s^2+1.926e-10s+6.102e-13}$

The bode plots of each of these high order models will now be evaluated:

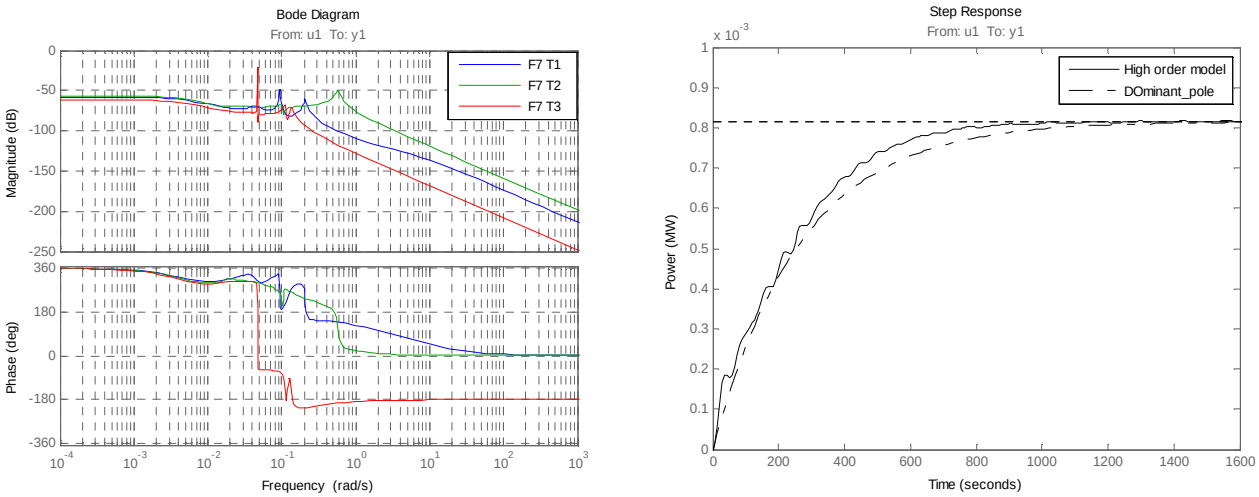

(a) Bode plot **(b) High/low-order model step response**

Figure 6.18: High order dynamic behaviour of models F7

From Figure 6.18(a) it can be seen that the frequency response of the local models does contain resonant and anti-resonant components at frequencies dependent on the operating points of the models. The bandwidth of these models was found to average around 0.0048 rad/sec. This results in having no resonant and anti-resonant modes found within the bandwidth of the models.

The step responses of both a high order model and a dominant pole model of F7 can be seen in Figure 6.18(b). From this figure it can be seen that the two models only differ slightly.

6.3.2.2 Plant local models F8

Characterising the mechanical power output response, with respect to changes made to the mass flow rate of the steam flowing through the Rankine cycle, involves evaluating the local linear models $Y(s)/U(s) = P_{plant}(s)/Q_{\text{Sec\_MF}}(s)$ at each of the different operating points defined in 6.3.2. The resultant low- and high order local models will now be discussed.

Low-order model evaluation:

The resultant low-order local linear models of F8 at each operating point are shown in Table 6.16.

Table 6.16: Low-order local linear models F8

$F8 = \frac{P_{system}}{Q_{\text{Sec\_MF}}}$	$T1 = T_{TES\_\max}$	$\frac{0.01065\,s + 0.0005584}{s^2 + 0.1466s + 0.001464}$
	$T2 = T_{TES\_med}$	$\frac{0.01111\,s + 0.0005823}{s^2 + 0.1487s + 0.001523}$
	$T3 = T_{TES\_\min}$	$\frac{0.01128\,s + 0.0006044}{s^2 + 0.1492s + 0.001569}$

The dominant dynamic behaviour of these low-order models can be obtained by evaluating their dominant poles. Figure 6.19(a) illustrates the pole placement of the dominant poles at each operating point. The pole/zero diagram illustrating the rest of the poles and zero's is included in Appendix B.

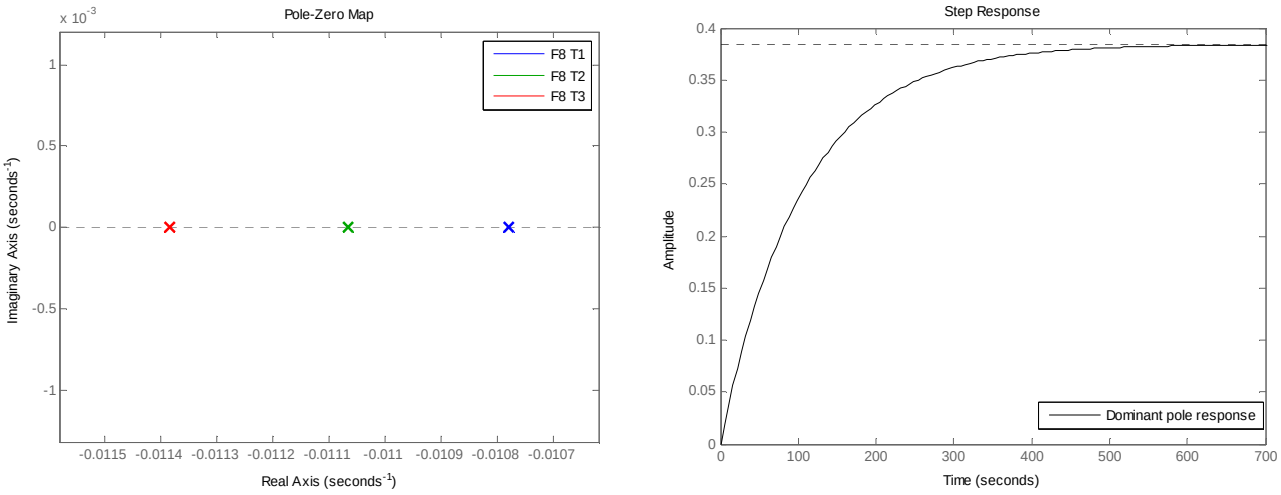

(a) Dominant pole **(b) Dominant pole model step response**

Figure 6.19: Dominant dynamic behaviour of models F8

The change in the dynamics of the plant can be seen from the positions of the dominating open-loop poles in Figure 6.19(a) that the open-loop system becomes faster (poles move away from s = 0) as the temperature of the TES decreases. This results in the time responses, including the rise time and settling time, of the system to decrease as the temperature response of the TES decreases. This then inherently then also causes the bandwidth of the system to increase with a decrease in the temperature response.

By evaluating Figure 6.19(b) it is noted that the power output response with a step response in the mass flow rate simulated, produces an over damped second order behaviour.

High order model evaluation:

The resultant high order local linear models of F8 at each operating point are shown in Table 6.17.

Table 6.17: High order local linear models F8

$F5$	$P1$	$\frac{-2.044e-05s^7+1.918e-05s^6+2.387e-06s^5+4.335e-07s^4+3.122e-08s^3+1.337e-09s^2+3.538e-11s+1.47e-13}{s^9+9.049s^8+0.3822s^7+0.4925s^6+0.01303s^5+0.004488s^4+8.954e-05s^3+7.296e-06s^2+5.335e-08s+1.268e-10}$
	$P2$	$\frac{-0.0001126s^7+7.682e-06s^6-9.237e-07s^5+9.569e-08s^4+3.225e-09s^3+6.524e-11s^2+9.454e-13s+5.362e-15}{s^9+0.2223s^8+0.3536s^7+0.05607s^6+0.004821s^5+0.0005528s^4+9.57e-06s^3+2.04e-07s^2+1.468e-09s+3.997e-12}$
	$P3$	$\frac{3.913e-07s^7+8.747e-08s^6+8.416e-09s^5+1.455e-09s^4+3.741e-11s^3+3.049e-12s^2+4.645e-14s+4.977e-16}{s^9+0.05673s^8+0.03348s^7+0.001553s^6+0.0003082s^5+1.154e-05s^4+6.166e-07s^3+1.884e-08s^2+1.926e-10s+6.102e-13}$

From these high order local linear models, the presence of resonant and anti-resonant modes can be evaluated be plotting the frequency responses of the local models.

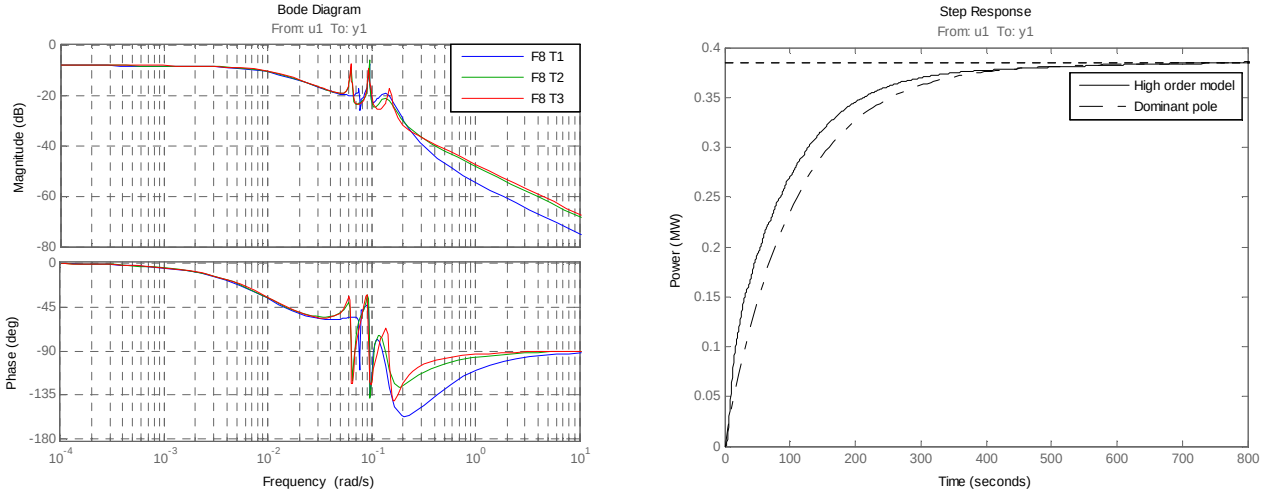

(a) Bode plot **(b) High/low-order model step response**

Figure 6.20: High order dynamic behaviour of models F8

From Figure 6.20(a) it can be seen that there does exist resonant and anti-resonant modes from the frequency responses of the models. The average bandwidth is calculated to be around 0.0118 rad/sec which results in having no resonant and anti-resonant modes falling within the bandwidth of the model.

From Figure 6.20(b) it can be seen that there exists a large correlation between the low-order model (dominant pole model), and the high order model.

6.4 Conclusion

The process of characterising the dynamic responses associated with that of a CSP plant, by evaluating the local linear models of the plant, could successfully be implemented by using system identification procedures. The use of pseudorandom binary sequence excitation signals helped capture all of the important dynamic responses of the plant, and the use of low- as well as high order models helped identify these responses.

From these simulations, it is evident that the dynamic behaviour of the local models of the plant changes as the operating points of the plant changes, for both the operation of the plant during the day, as well as during the night. The characterisation process of the plant also illustrated the presence of resonant and anti-resonant modes in the temperature responses of the SCF, and for this reason should be controlled by making use of high order models, although there was a high correlation between the step response of a low-order model and a high order model.

The power output response of the plant illustrated no resonant and anti-resonant modes found present within the bandwidth of the plant. The use of low-order local linear models for the control of the power output response of the plant would thus suffice.

It should be noted that although the low and high order models, derived from system identification procedures, have a high correlation between both models' step responses; in some cases the phases of both the models do however differ which influences the selection of a controller for the model. This could be as a result of the specific system identification software selected not being capable of deriving the local linear models as accurately as expected, or it could be that the low order models derived leave out important information concerning phase of the local model which is included in the high order model.

Chapter 7: Conclusions and recommendations

This chapter includes all the conclusions and recommendations made throughout this study, based on the methodologies used to both develop and characterise a model of a combined cycle concentrated solar power (CSP) plant.

7.1 Conclusions

The development and characterisation of a combined cycle CSP plant, to obtain a deeper understanding of the influence that the input signals of the plant have on its dynamic responses, was successfully implemented. The next few sections will discuss some of the conclusions made for both the development as well the characterisation of the CSP plant:

7.1.1 CSP plant model development

The development of a systems computational fluid dynamics (Flownex®) model of a combined cycle CSP plant proved to provide an accurate model that represents all the important dynamics of the plant. The successful development of the model could be implemented by following a two-stage approach:

Stage 1: Methodological implementation study

The first stage of developing the model included conducting a study on the selection of the model development approach, followed by the methodology of selecting and sizing the various different components of the plant. Flownex®, which is a simulation platform based on a pre-programmed model development approach, was the selected platform to use for this study due to both its

availability as well as its advantages. Developing the model of the plant based on this approach allowed for the accurate development of a model that represents all the important dynamics of the associated components without having to go through tedious development procedures.

Some of the challenges faced with this approach included issues concerning both the availability and functionality of some of the Flownex® components. One of the availability issues faced, was the absence a component representing that of a solar collector field (SCF) from the Flownex® component library. This issue was resolved after a model of the SCF was developed which produced the required dynamic behaviour of a SCF.

One of the functional issues that were faced, during the development of the evaporator and condenser, included the operation of the evaporator component from the Flownex® library which could not simulate any phase changes. Fortunately, this was resolved by consulting with M-Tech Industrial regarding this issue.

Stage 2: Model development

The second stage of developing the model involved the selection, sizing and integration of each of the components that constitute that of a combined cycle CSP plant.

The use of schematic diagrams, responses of the benchmark model (TRNSYS model), and supporting literature which included the mathematical expressions describing each of the components allowed for successfully selecting and sizing each of the components in the model. This approach proved to work effectively, and any issues with the sizing of the components due to the unavailability of some responses from the benchmark model could be overcome by making use of informed assumptions.

After selecting and sizing each of the components of the plant, verification in the form of simulations was implemented to verify that the components performed as it was intended to. The use of seed independence verification worked effectively, by illustrating whether the responses matched that of the literature.

The validation of the model, by making use of a bottom-up validation procedure, which is based on a model comparison approach, proved to work well. This is since simulating the model, at both a component level as well as at a system level, with the same input signals, allowed for the system to be validated on both levels.

7.1.2 CSP plant model characterisation process

The use of open loop local linear models, to identify and evaluate the dynamic responses unique to that of a CSP plant, could successfully be implemented by making use of Maltab's system identification (SID) toolbox. This allowed for the successful development of local models

representing important dynamic responses of a CSP plant, which further helped comment on the design of a controller for the plant.

The use of Pseudorandom Binary Sequence excitation signals, to simulate the Flownex components, helped in identifying the important dynamics of the plant. The use of both low-order as well as high order models, which were selected based on the orders suggested by Matlab®'s SID toolbox, allowed for the successful identification of the important associated dynamic responses.

Evaluating the dominant pole positions of the low-order models at each operating point, allowed for the identification of the dominant dynamic behaviour as well as the change in the dynamics of the models as the operating points changed. The use of high order models allowed for the identification of the resonant and anti-resonant modes of the models, by evaluating the bode plots of these models.

The dominant dynamic behaviour of the plant, from the derived local models, represents that of an over damped second order system with either a positive or a negative gain, depending on the evaluated models. The study of these models also illustrated a change in the dynamic behaviour of the plant with most of the local models of the plant becoming faster as the thermal energy input to the plant increases. This results in the time responses and the bandwidth of the plant to decrease and increase respectively as the thermal energy input to the plant increases.

It could further be noted that the models also illustrated the presence of resonant and anti-resonant modes within the control bandwidth of the plant. These modes were however only found within the bandwidth of the SCF temperature response, and not in the other measured responses.

7.2 Future work

7.2.1 CSP plant modelling

The developed model of the CSP plant still has room for improvements. Some of the future work includes improvements on the CSP components (SCF and TES) as well as the operating philosophies of the plant.

The current model of the SCF illustrates all the required dynamics, but the current design of the SCF only allows for the resultant thermal energy input to the model to be specified. Ideally, one wants to specify other input variables such as the direct normal irradiance, the efficiency, and the structural design of the SCF. In order to improve on the model, it is therefore important to further develop the model of the SCF to allow the user to be able to substitute these values into the model.

The Thermal Energy Storage (TES) model of the plant also needs to be revised, due to the fact that the component library of Flownex® limits the design of the TES to a direct active heat storage type of design. The use of such a design is not ideal since gasses generally do not have high thermal capacitance, which results in the design to be less efficient. To improve on the design a passive heat storage design should rather be considered.

Currently the operating philosophy for the plant includes the Rankine cycle side of the plant only functioning during peaking conditions, and at night when the TES supplies the plant with thermal energy until it reaches its minimum temperature level. Due to both the financial- and time constraints associated with the start-up and shutdown process of the Rankine cycle, operating the plant in such a manner is not practical and feasible. The operation of the plant should thus be revised to allow for the Rankine cycle part of the plant to be operated continuously.

The current methodology used to alter the power output of the plant is of an open loop nature, and thus requires human input. To improve on the model, a controller must be developed which automatically alters the relevant mass flow rates so as to change the power output to match the load requirements.

7.2.2 CSP plant model characterisation process

The process of identifying the dynamic responses, unique to that of a CSP plant, which utilises solar power tower technologies, did illustrate the presence of resonant and anti-resonant modes within the bandwidth of some of the models, along with changes in the dynamic responses of the plant. Since the literature included a study on the presence of these phenomena of distributed solar collector field connected plants , a comparison study must be made, where the existing structure of the plant is used, but with different SCF technologies (solar power tower vs. distributed SCF) selected.

7.3 Closure

The problem statement in Chapter 1 could thus be addressed successfully by breaking down the study into two subsections:

The model of the combined cycle CSP plant was developed based on a pre-programmed model development approach, and was verified and validated in order to ensure that the responses obtained from the model represent the comparative simulated dynamics of such a plant as well as to ensure that the responses are according to specification.

The characterisation, with the intent of obtaining an understanding of the dynamic behaviour of such a plant could be achieved by evaluating the local linear models of the plant. To obtain these

models, the use of both an accurate model of a CSP plant as well as system identification software assisted in the characterisation process.

References

[1] “Renewable energy,” Atoms for Peace: Nuclear energy for the twenti-first century, 2003. [Online]. Available: http://www.ifpaenergyconference.com/Renewable-Energy.html. [Accessed 2012].

[2] Müller-steinhagen, H. and Trieb, F. “A review of the technology,” *Concentrating solar power,* p. 8, 2004.

[3] http://www.sciencedaily.com/releases/2009/11/091117133504.htm {ScienceDaily, “Fossil Fuel Carbon Dioxide Emissions Up by 29 Percent Since 2000”, ScienceDaily (Nov. 17, 2009)}

[4] Power, C. S., Province, N. C., Africa, S., Africa, S., Government, S. A., Paper, W., Energy, R., et al. (n.d.). CONCENTRATING SOLAR POWER (CSP). Revision, 2-4.

[5] E. M. van Voorthuysen, “The promissing perspective of Concentrating Solar Power (CSP),” no. 2, p. 7.

[6] Quaschning, V. (2004). Technical and economical system comparison of photovoltaic and concentrating solar thermal power systems depending on annual global irradiation. Solar Energy, 77(2), 171-178. doi:10.1016/j.solener.2004.04.011.

[7] K. Lovegrove and W. Stein, “ Principles, Development and Applications,” *Concentrating Solar Power Technology,* no. 21, p. 2, 2012.

[8] Newton, M., Sen, P. K., & Member, S. (2007). Bulk Power Energy Storage and Concentrated Solar Power : Is there a Future in USA ? Engineer.

[9] Patnode, A. M., & Science, M. O. F. (2006). Simulation and Performance Evaluation of Parabolic Trough Solar Power Plants by.

[10] Heller, L. (2012). INVESTIGATION OF THE THERMAL STORAGE SYSTEM FOR A 5 MW EL CONCENTRATED SOLAR POWER (CSP) PILOT PLANT.

[11] “Solar Power Tower,” Electrical Engineering Portal, 15 Dec 2010. [Online]. Available: http://electrical-engineering-portal.com/solar-power-tower. [Accessed 2013].

[12] Powell, K. M., & Edgar, T. F. (2012). Modeling and control of a solar thermal power plant with thermal energy storage. Chemical Engineering Science, 71, 138-145. Elsevier. doi:10.1016/j.ces.2011.12.009.

[13] Y. A. Cengel and R. H. Turner, Fundamentals of thermal-fluid sciences, 2nd ed. New York, America: McGraw-Hill, 2005.

[14] Birnbaum, J., Eck, M., Fichtner, M., Hirsch, T., Lehmann, D., & Zimmermann, G. (2010). A Direct Steam Generation Solar Power Plant With Integrated Thermal Storage. Journal of Solar Energy Engineering, 132(3), 031014. doi:10.1115/1.4001563

[15] Stabat, P., & Marchio, D. (2004). Simplified model for indirect-contact evaporative cooling-tower behaviour, 78, 433-451. doi:10.1016/j.apenergy.2003.09.004.

[16] Plants, L. C. (2006). Power cycles Principles of combustion cycles and efficient concepts This contribution is based on the EC BREF- document Reference Document on Best Available Techniques for, (July), 1-34.

[17] Schwarzbo, P., Buck, R., Sugarmen, C., Ring, A., Altwegg, P., & Enrile, J. (2006). Solar gas turbine systems : Design , cost and perspectives, 80, 1231-1240. doi:10.1016/j.solener.2005.09.007

[18] M. Anheden, “Analysis of Gas Turbine Systems for Sustainable Energy Conversion,” Stocholm, Sweden, 2000.

[19] Sánchez, C., Juárez, R., Sanz, J., & Perlado, M. (2013). Design and analysis of helium Brayton power cycles for HiPER reactor. Fusion Engineering and Design. Elsevier B.V. doi:10.1016/j.fusengdes.2012.12.007

[20] Kribus, A., Zaibel, R., Carey, D., Segal, A., & Karni, J. (1998). A SOLAR-DRIVEN COMBINED CYCLE POWER PLANT, 62(2), 121-129.

[21] Vahidi, B., Member, S., Reza, M., Tavakoli, B., & Gawlik, W. (2007). Determining Parameters of Turbine ’ s Model Using Heat Balance Data of Steam Power Unit for Educational Purposes, 22(4), 1547-1553.

[22] Limon, D., Alvarado, I., Alamo, T., Ruiz, M., & Camacho, E. F. (2008). Robust control of the distributed solar collector field ACUREX using MPC for, 958-963.

[23] Regin, A. F., Solanki, S. C., & Saini, J. S. (2009). An analysis of a packed bed latent heat thermal energy storage system using PCM capsules : Numerical investigation. Renewable Energy, 34(7), 1765-1773. Elsevier Ltd. doi:10.1016/j.renene.2008.12.012

[24] Reza, M., Tavakoli, B., Vahidi, B., Member, S., & Gawlik, W. (2009). An Educational Guide to Extract the Parameters of Heavy Duty Gas Turbines Model in Dynamic Studies Based on Operational Data, 24(3), 1366-1374.

[25] Lee, Y.-ren, Kuo, C.-ron, & Wang, C.-chuan. (2012). Transient response of a 50 kW organic Rankine cycle system. Energy, 1-7. Elsevier Ltd. doi:10.1016/j.energy.2012.10.029

[26] O. M. Bamgbopa, “Modeling and performance evaluation of an organic Rankine cycle (ORC) with R245FA as working fluid,” Middle East Technical University, 2012.

[28] H. Price, “A Parabolic Trough Solar PowerPlant Simulation Model,” in *International Solar Energy Conference*, Hawaii, 2003.

[29] Kelly, B. (2006). Nexant Parabolic Trough Solar Power Plant Systems Analysis Task 1 : Preferred Plant Size Nexant Parabolic Trough Solar Power Plant Systems Analysis Task 1 : Preferred Plant Size January 20 , 2005 — December 31 , 2005, (July).

[30] Seidel, W. (2010). Model Development and Annual Simulation of the Supercritical Carbon Dioxide Brayton Cycle for Concentrating Solar Power Applications by.

[31] Maruta, I., & Sugie, T. (2013). Systems & Control Letters Projection-based identification algorithm for grey-box continuous-time models. Systems & Control Letters, 62(11), 1090-1097. Elsevier B.V. doi:10.1016/j.sysconle.2013.08.006

[32] “CSP plant modelling: Pinpointing output and revenue forecasts,” CSP today, 28 April 2011. [Online]. Available: http://social.csptoday.com/technology/csp-plant-modelling-pinpointing-output-and-revenue-forecasts. [Accessed 2013].

[33] J. Hillston, “Model Validation and Verification,” 2003.

[34] Tummescheit, H. (n.d.). Design and Implementation of Object-Oriented Model Libraries using Modelica.

[35] Sargent, R. G. (2011). Proceedings of the 2011 Winter Simulation Conference S. Jain, R.R. Creasey, J. Himmelspach, K.P. White, and M. Fu, eds., 183-198.

[36] Camacho, E. F., Rubio, F. R., & Berenguel, M. (2007). A survey on control schemes for distributed solar collector fields . Part I : Modeling and basic control approaches. Solar Energy, 81, 1240-1251. doi:10.1016/j.solener.2007.01.002

[37] Johansen, T. A., Hunt, K. J., & Petersen, I. (2000). Gain Scheduled Control of a Solar Power Plant 1 Introduction. Structure, (1), 1-24.

[38] Johansen, T. A., Hunt, K. J., & Petersen, I. (2000). Gain Scheduled Control of a Solar Power Plant 1 Introduction, (1), 1-24.

[39] Arbor, A., & Lacy, S. L. (2005). Sequential Multisine Excitation Signals for System Identification of Large Space Structures The University of Michigan. *Distribution*, *298*(0704).

[40] Philipps, S P & Peharz, G (2010). Solar Energy Materials & Solar Cells Energy harvesting efficiency of III – V triple-junction concentrator solar cells under realistic spectral conditions. Solar Energy Materials and Solar Cells, vol. 94, Issue.

[41] Duffie, John A., and Beckman, William A. Solar Engineering of Thermal Processes. 2nd edition. New York: John Wiley and Sons, Inc., 1991.

[42] Hurlbut, David J (2009). Colorado ' s Prospects for Interstate Commerce in Renewable Power Prepared for the Colorado Governor ' s Energy Office , Renewable Energy Development Infrastructure (REDI) Colorado ' s Prospects for Interstate Commerce in Renewable Power Prepared for the Colorado Governor ' s Development Infrastructure (REDI). Contract (December).

[43] Group, S. P. (n.d.). Integrating Steam Generation from Concentrating Solar Thermal Collectors to Displace Duct Burner Fuel in Combined Cycle Power Plants Andrew McMahan. *Design*, 1-19.

[44] Quoilin, S., Aumann, R., Grill, A., Schuster, A., & Lemort, V. (2011). Dynamic modeling and optimal control strategy of waste heat recovery Organic Rankine Cycles. Applied Energy, 88(6), 2183-2190. Elsevier Ltd. doi:10.1016/j.apenergy.2011.01.015

[45] Bari, P. D. I. (2011). PERFORMANCE OF A 50 MW CONCENTRATED SOLAR POWER PLANT.

[46] Chaibakhsh, A., & Ghaffari, A. (2008). Simulation Modelling Practice and Theory Steam turbine model, 16, 1145-1162. doi:10.1016/j.simpat.2008.05.017

[47] T, A. Z. W., & Newman, J. (2005). Modeling gas-phase flow in porous media B. International Communications in Heat and Mass Transfer, 32, 855-860. doi:10.1016/j.icheatmasstransfer.2004.08.026

[48] P. Kundur, “Chapter two: Fundamentals of Steam Power,” in *Power System Stability and Control*, pp. 35-84.

[49] Quaschning, V. (2004). Technical and economical system comparison of photovoltaic and concentrating solar thermal power systems depending on annual global irradiation. Solar Energy, 77(2), 171-178. doi:10.1016/j.solener.2004.04.011.

[50] Spelling, J. D. (2011). Steam Turbine Optimisation for Solar Thermal Power Plant Operation. Stockholm, Sweden.

[51] R. K. Shah and D. P. Sekulic, “Heat exchangers,” in *Delphi Harrison Thermal Systems*, Lockport, New York, pp. 17.1-17.169.

[52] “ Leading and partnering to keep the lights on load profiles,” Eskom Holdings SOC Limited Interim Integrated Report, 30 September 2013. [Online]. Available: http://integratedreport.eskom.co.za/iir2014/per-leading.php. [Accessed 2014].

Appendix A

A.1 Burner temperature control

Controlling the HTF temperature entering the turbine:

The temperature of the mixed gasses entering the gas turbines are influenced by both the thermal energy input of the solar collector field (SCF) as well as the amount of fuel burnt by the duct burner which can be manipulated by making use of a controller. Proportional Integral (PI) control meets the control needed for this problem since it is one of the most used control schemes in the industry and since this problem is only a single loop problem with only one measured variable (temperature) and one control variable (fuel flow rate) [45].

The most used method of constructing a PI controller without making use of its transfer function to solve for its gains is to make use of the Ziegler-Nichols method. This method makes use of empirical values to derive the control parameters and is used primarily for single loop control applications [45]. The method makes use of a simulated step response to determine its resultant gain values which controls the system. The response obtained from any given system can be represented by [28]:

$$\frac{Y(s)}{U(s)} = \frac{Ae^{-st_d}}{t_{s+1}} \tag{A.1}$$

where t_d is the time delay, A is the steady state value (reference value), and t is the time.

In order to determine the values of the proportional, integral and differential gains needed to have a stable controller; Ziegler and Nichols derived the following equation [28]:

$$D_c(s) = k_p(1 + \frac{1}{T_I s} + T_D s) \tag{A.2}$$

where k_p is the proportional gain value, T_I is the integral gain value and T_D is the differential gain value.

One of the two methods used to determine the gains of the controller based on the Ziegler-Nichols method is to simulate a step response to the system and set all the gains to zero. After this is done the proportional gain is increased until the resulting output response is an oscillating response as seen Figure A.1 [28].

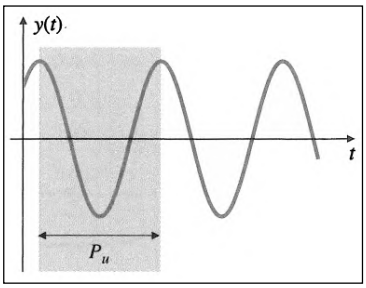

Figure A.1: Oscillating output [28]

The resulting gain is known as the ultimate gain of the system and is represented by K_u. P_u which is the ultimate period of the oscillating output can then further be determined from the resultant waveforms period. By making use of Table A.1, the rest of the gains can be calculated [28]:

Table A.1: Ziegler-Nichols tuning method [28]

Ziegler–Nichols Tuning for the Regulator $D_c(s) = k_p(1 + 1/T_I s + T_D s)$, Based on the Ultimate Sensitivity Method

Type of Controller	Optimum Gain
P	$k_p = 0.5K_u$
PI	$\begin{cases} k_p = 0.45K_u \\ T_I = \frac{P_u}{1.2} \end{cases}$
PID	$\begin{cases} k_p = 1.6K_u \\ T_I = 0.5P_u \\ T_D = 0.125P_u \end{cases}$

After each of the gains have been calculated the gains must be changed one by one as to determine whether or not the integral or differential gains are needed. If the gains improve the output of the system, then they should be added otherwise not. Once all the most important gains are included then fine-tuning can be implemented for optimal control.

Appendix B

B.1 System identification data

The simulated data used to develop the local linear models of the Flownex plant model, for characterisation purposes, which were not included in Chapter 6, are shown and discussed next, for operating scenario 1 and 2. Note that the data shown is only included for one operating point per local linear model, except for the pole zero plot of each model at each operating point.

B.1.1 Operating scenario 1

Open loop local linear models: F1P2

The excitation signal (at operating point P2 of local model F1) used to specify the mass flow rate of the mixed gasses flowing through the Brayton cycle, along with the temperature response of the SCF, is shown in Figure B.1.

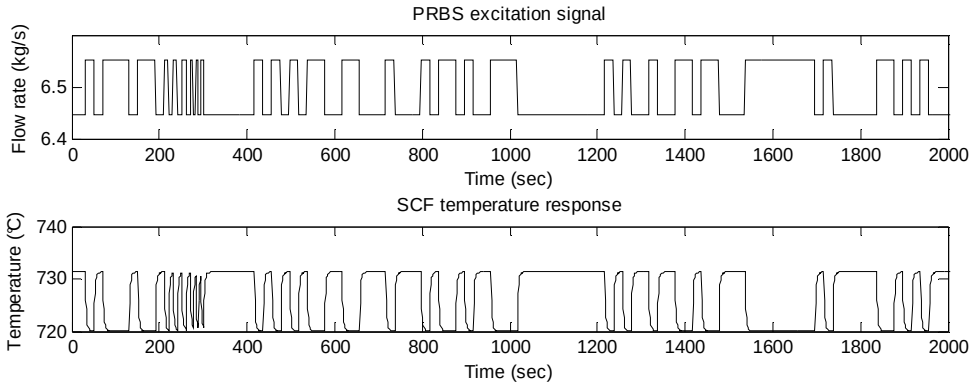

Figure B.1: Simulated input/output data of F1P2

The selected low-order local linear models' model fit along with the pole/zero plot of these models can be seen in Figure B.2 (a) and (b):

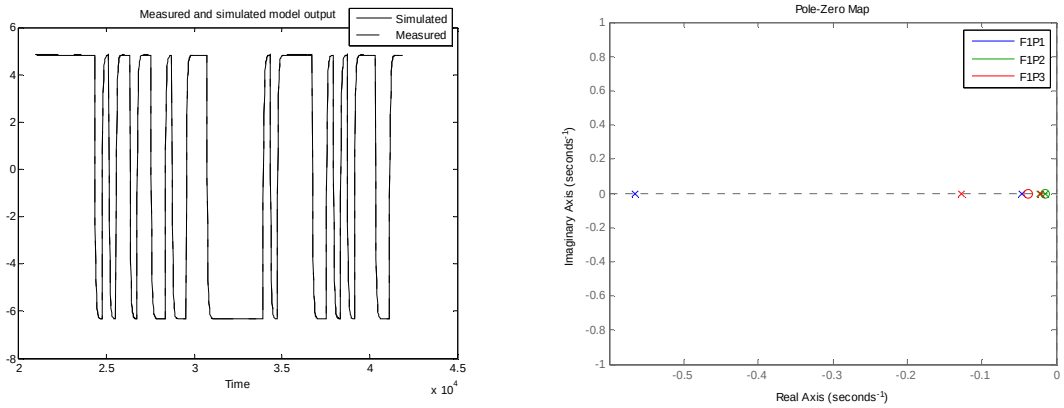

(a) Model fit **(b) Pole/Zero plot**

Figure B.2: Local linear model results: F1

Figure B.2 (a) illustrates a high percentage model fit between both the simulated data of the local linear model, as well as the measured data of the developed Flownex model. The pole zero diagram of models F1 can be seen in Figure B.2 (b), accept for the zero situated at s = 3, which is removed in order to see the other poles and zeros better.

Open loop local linear models: F2P2

The excitation signal (at operating point P2 of local model F2) used to specify the thermal energy input signal to the SCF, along with the temperature response of the SCF is shown in Figure B.3.

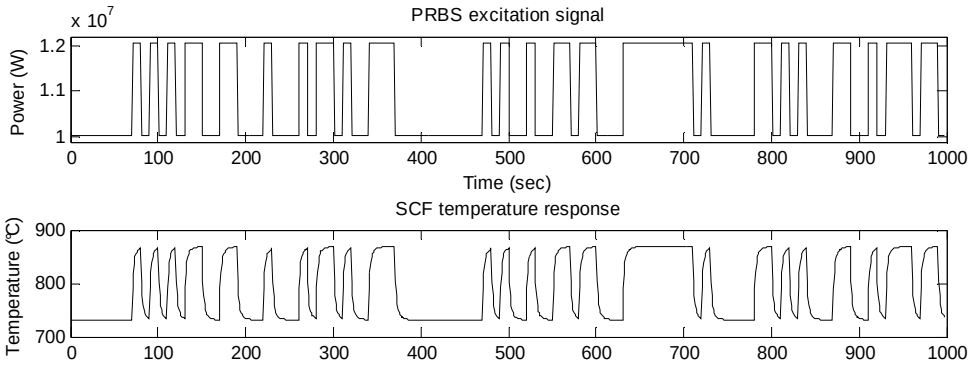

Figure B.3: Simulated input/output data of F2P2

The selected low-order local linear models' model fit along with the pole/zero plot of these models can be seen in Figure B.4 (a) and (b):

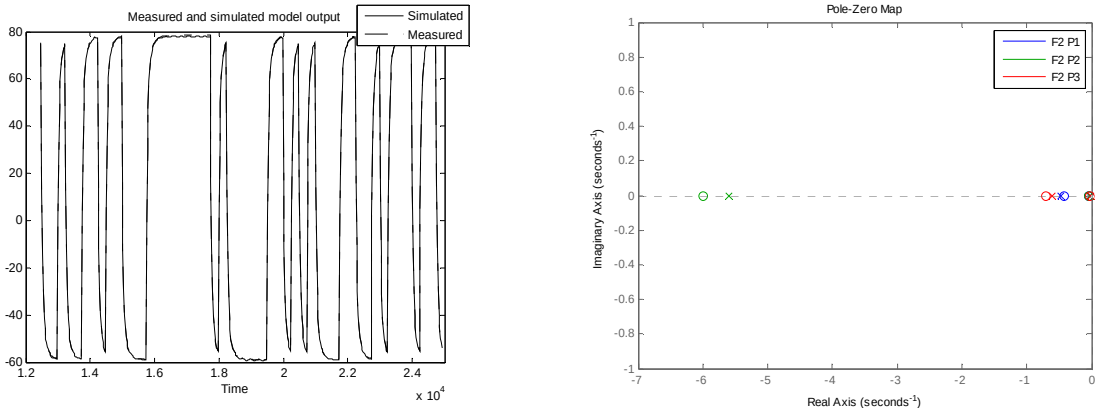

(a) Model fit **(b) Pole/Zero plot**

Figure B.4: Local linear model results: F2

Figure B.4 (a) illustrates a high percentage model fit between both the simulated data of the local linear model, as well as the measured data of the developed Flownex model.

Open loop local linear models: F3P2

The excitation signal used (at operating point P2 of local model F3) to specify the mass flow rate of the mixed gasses flowing through the Brayton cycle along with the temperature response of the TES is shown in Figure B.5.

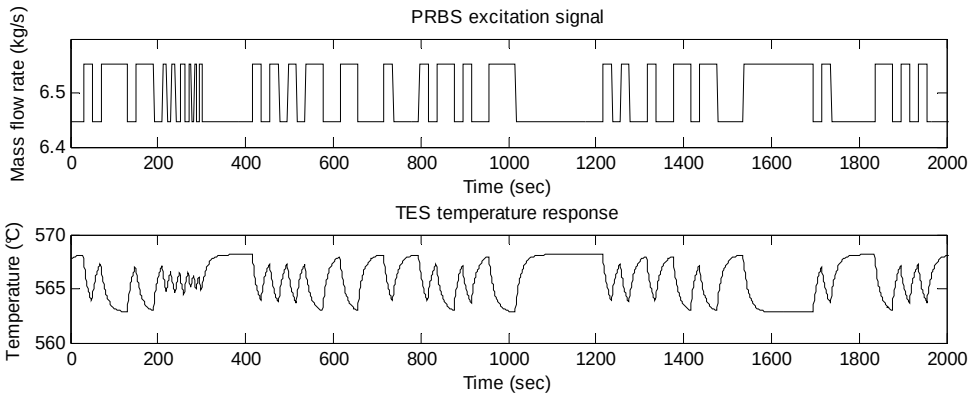

Figure B.5: Simulated input/output data of F3P2

The selected low-order local linear models' model fit along with the pole/zero plot of these models can be seen in Figure B.6 (a) and (b):

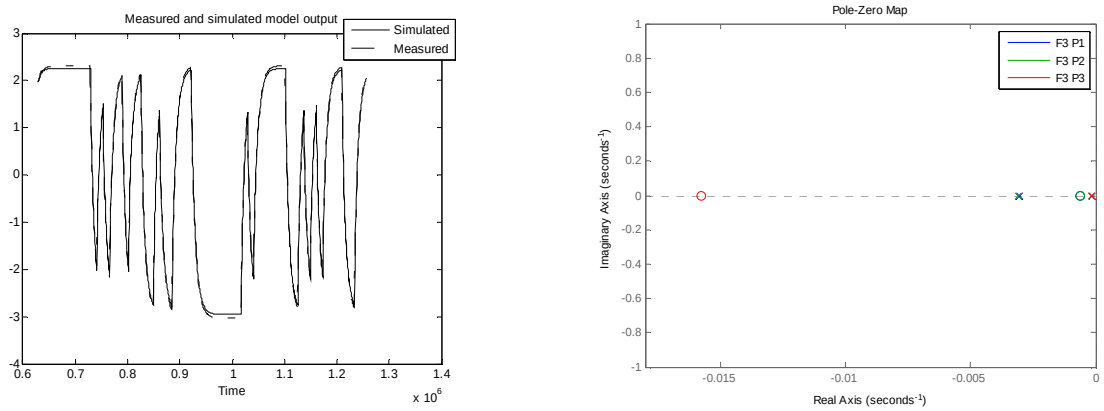

(a) Model fit **(b) Pole/Zero plot**

Figure B.6: Local linear model results: F3

Figure B.6 (a) illustrates a high percentage model fit between both the simulated data of the local linear model, as well as the measured data of the developed Flownex model. The pole zero diagram of models F3 can be seen in Figure B.6 (b), accept for the pole situated at s = -18, which is removed in order to see the other poles and zeros better.

Open loop local linear models: F4P2

The excitation signal used (at operating point P2 of local model F4) to specify the mass flow rate of the mixed gasses flowing through the Brayton cycle along with the mechanical power output response of the plant is shown in Figure B.7.

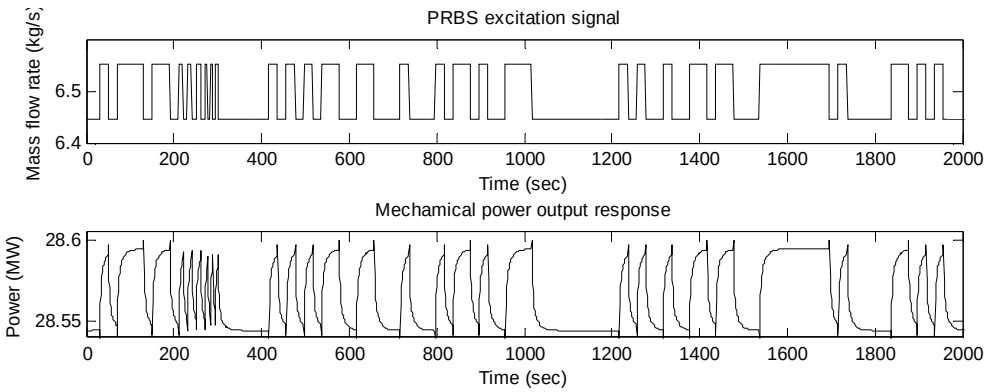

Figure B.7: Simulated input/output data of F4P2

The selected low-order local linear models' model fit along with the pole/zero plot of these models can be seen in Figure B.8 (a) and (b):

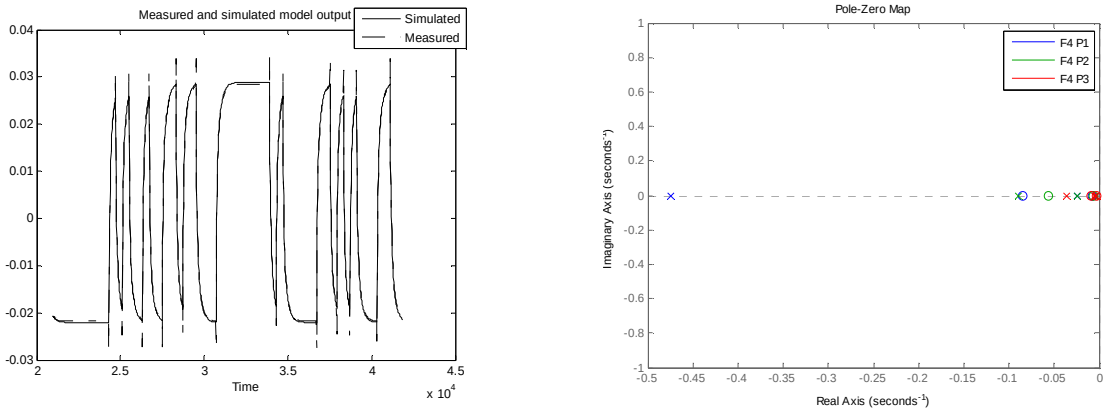

(a) Model fit **(b) Pole/Zero plot**

Figure B.8: Local linear model results: F4

Figure B.8 (a) illustrates a high percentage model fit between both the simulated data of the local linear model, as well as the measured data of the developed Flownex model.

Open loop local linear models: F5P1

The excitation signal used (at operating point P1 of local model F5) to specify the mass flow rate of the mixed gasses flowing through the TES along with the mechanical power output response of the plant is shown in Figure B.9.

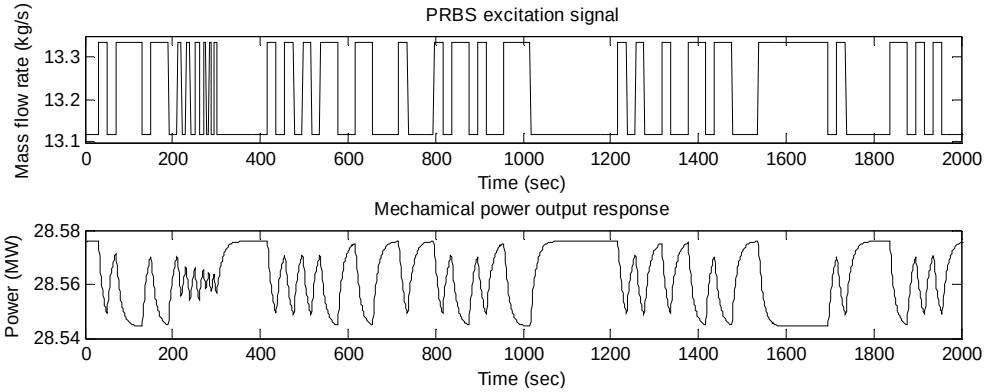

Figure B.9: Simulated input/output data of F5P1

Figure B.10 (a) illustrates a high percentage model fit between both the simulated data of the local linear model, as well as the measured data of the developed Flownex model.

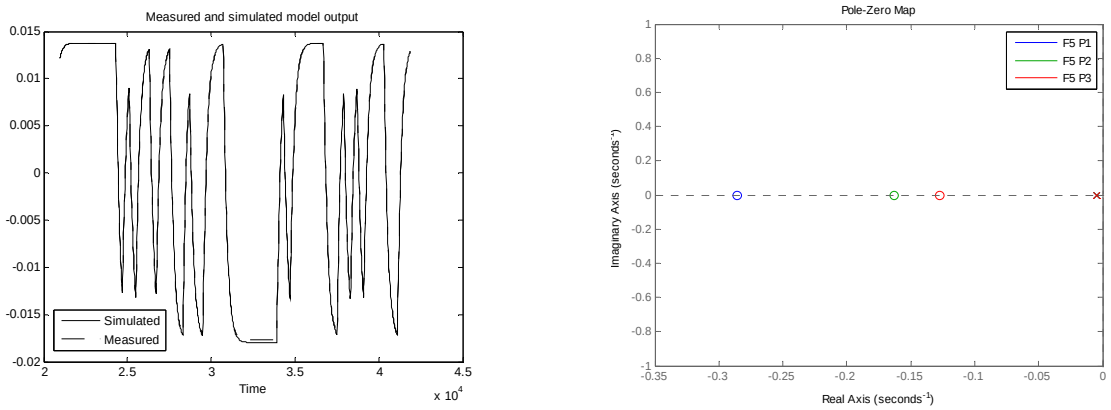

(a) Model fit **(b) Pole/Zero plot**

Figure B.10: Local linear model results: F5

Figure B.10 (a) illustrates a high percentage model fit between both the simulated data of the local linear model, as well as the measured data of the developed Flownex model.

Open loop local linear models: F6P2

The excitation signal used (at operating point P2 of local model F6) to specify the mass flow rate of the steam flowing through the Rankine cycle along with the mechanical power output response of the plant is shown in Figure B.11.

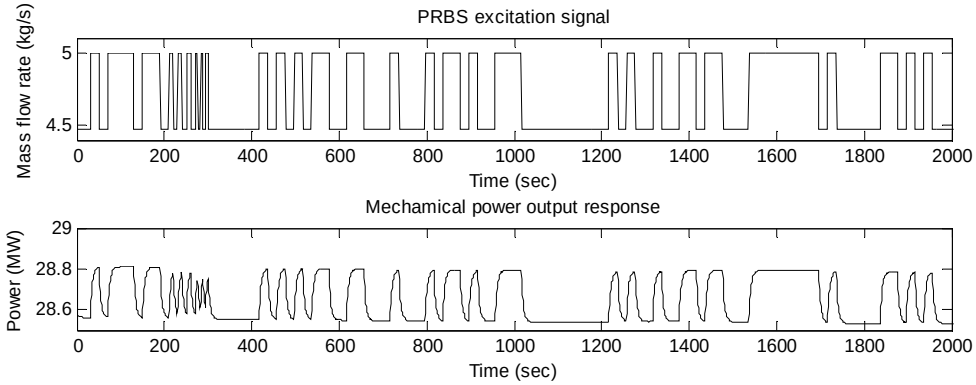

Figure B.11: Simulated input/output data of F6P2

Figure B.12 (a) illustrates a high percentage model fit between both the simulated data of the local linear model, as well as the measured data of the developed Flownex model.

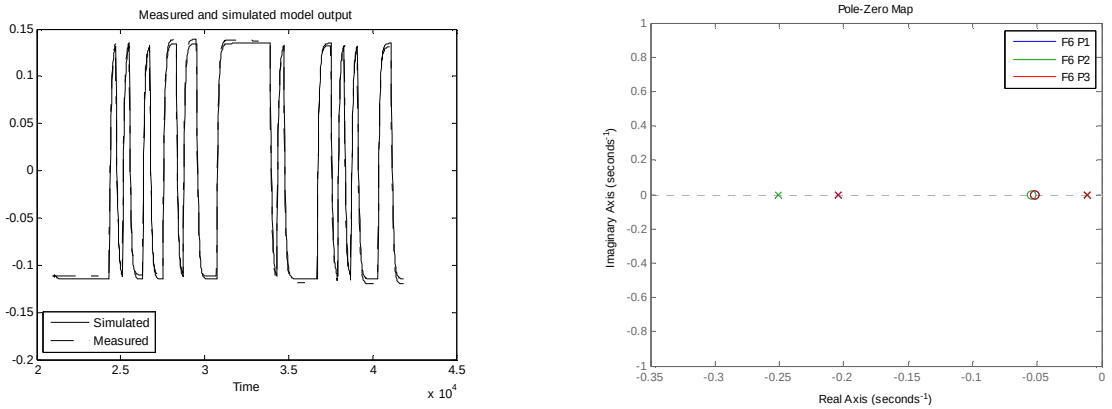

(a) Model fit **(b) Pole/Zero plot**

Figure B.12: Local linear model results: F6

Figure B.12 (a) illustrates a high percentage model fit between both the simulated data of the local linear model, as well as the measured data of the developed Flownex model.

B.1.1 Operating scenario 2

Open loop local linear models: F7P1

The excitation signal used (at operating point P1 of local model F7) to specify the mass flow rate of the mixed gasses flowing through the TES along with the mechanical power output response of the plant is shown in Figure B.13.

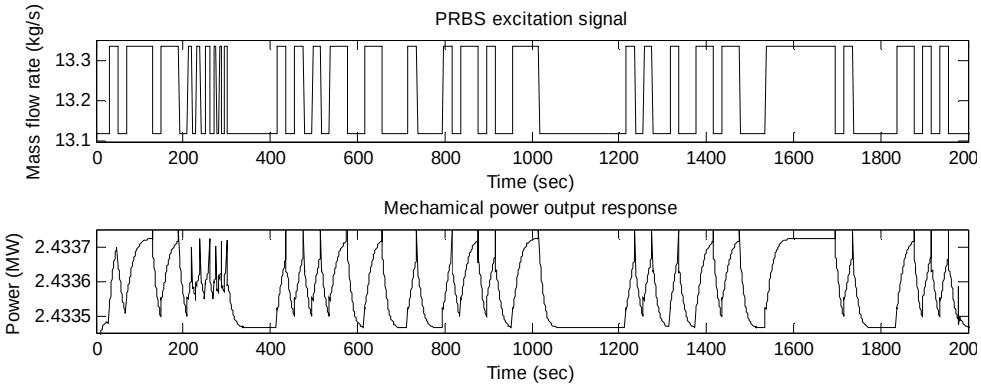

Figure B.13: Simulated input/output data of F7P1

Figure B.14 (a) illustrates a high percentage model fit between both the simulated data of the local linear model, as well as the measured data of the developed Flownex model.

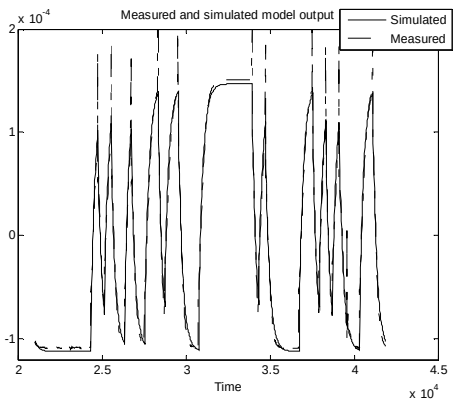

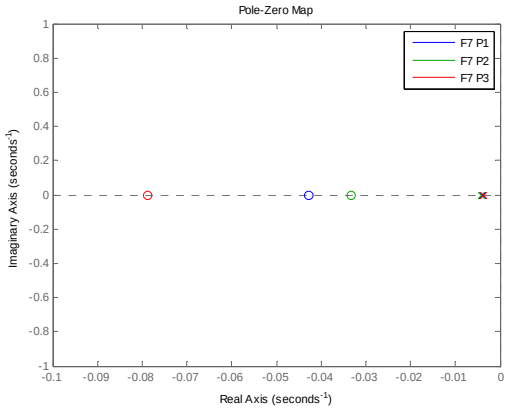

(a) Model fit **(b) Pole/Zero plot**

Figure B.14: Local linear model results: F6

Figure B.14 (a) illustrates a high percentage model fit between both the simulated data of the local linear model, as well as the measured data of the developed Flownex model.

Open loop local linear models: F8P2

The excitation signal used (at operating point P2 of local model F8) to specify the mass flow rate of the steam flowing through the Rankine cycle along with the mechanical power output response of the plant is shown in Figure B.15.

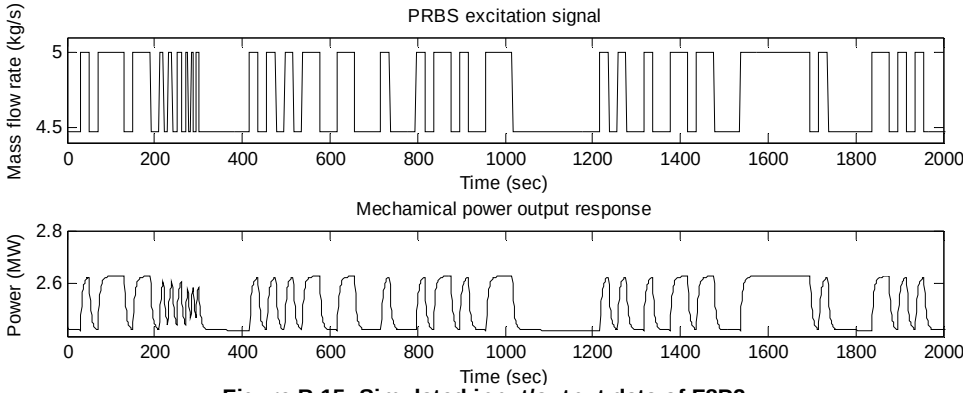

Figure B.15: Simulated input/output data of F8P2

Figure B.16 (a) illustrates a high percentage model fit between both the simulated data of the local linear model, as well as the measured data of the developed Flownex model.

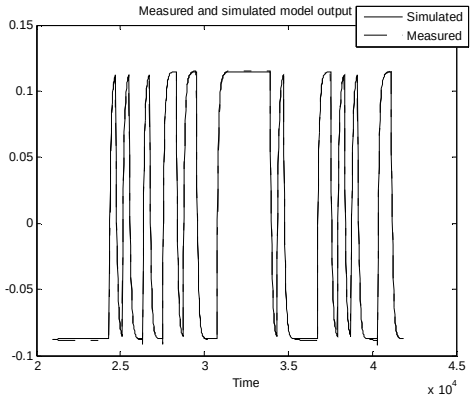

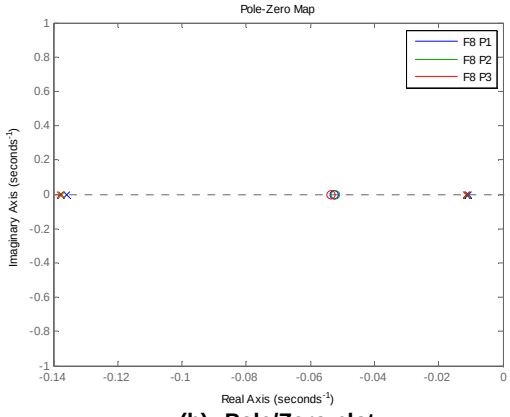

(a) Model fit **(b) Pole/Zero plot**

Figure B.16: Local linear model results: F8